THE SIGNALING OF RETINAL GANGLION CELLS IN THE MOUSE RETINA

WANG QIN

PhD

The Hong Kong Polytechnic University

2022

The Hong Kong Polytechnic University

School of Optometry

The Signaling of Retinal Ganglion Cells in the Mouse Retina

WANG Qin

A thesis submitted in partial fulfilment of the requirements for the degree of Doctor of Philosophy

July 2021

CERTIFICATE OF ORIGINALITY

I hereby declare that this thesis is my own work and that, to the best of my knowledge and belief, it reproduces no material previously published or written, nor material that has been accepted for the award of any other degree or diploma, except where due acknowledgement has been made in the text.

_____ (Signed)

Wang Qin (Name of student)

Abstract

Purpose

Retinal ganglion cells (RGCs) are the output neurons of the retina. All our visual experiences derive from signals generated from RGCs traveling down through the optic nerves. This thesis aims to investigate the signaling of RGCs in both physiological and pathological conditions. Our first aim was to characterize the morphology of amacrine cells coupled with alpha RGCs (αRGCs). As myopia is a prevalent abnormal eye conditions and defocus is the main trigger factor, our second aim was to investigate the effect of focused/defocused image projection on the signaling of αRGCs. As atropine is widely used to control myopic progression in children, our third aim was to explore the effect of low-does atropine on the signaling of αRGCs. Retinitis pigmentosa is a blinding neurodegenerative disease. The fourth aim was to explore the unmasking effect of PTX on signaling of αRGCs in rd10 mouse. The last part focused on glaucoma, the leading cause of visual loss. We aimed to characterize the effect of elevated IOP on αRGCs activities in the mouse model.

Methods

Wild-type C57BL/6 mice, the KCNG-YFP mice, rd10 mice, and/or Cx36-knockout mice were used in the study. Dye-injection (Neurobiotin and 594 mixed with Popro1) and confocal microscopy were used to investigate the morphology of neurons in the mouse retina. For electrophysiology, spikes or current responses of RGCs were recorded. Either 525nm full-field light or pattern light projected by an Organic Light-Emitting Diode (OLED) micro-display was used as light stimulation.

Results

Study 1. The ON and OFF αRGCs, which were fluorescence-labeled in the KCNG-YFP mice, were coupled with at least two types of ACs. Most coupled ACs were wide-field ACs.

Study 2. Custom-made light patterns were projected as focus/defocused images onto the retina, resulting in generation of different defocused statuses. Light-evoked current responses of αRGCs were recorded by patch clamp. Myopic and hyperopic defocus led to a decrease of the light-evoked current response in αRGCs.

Study 3. Approximately 2 μM atropine was detected in the retina after external application of 800 μM (equal to 0.05% topical application) atropine. Low-dose atropine (1 μM) did not change the morphology of the αRGCs. Most physiological properties were unchanged after 0.05-10 μM atropine application. However, ON responses were induced in OFF αRGCs by the low to high concentrations of atropine, which might block the GABA pathway and affect the signaling of the retina.

Study 4. The morphology of αRGCs in P46 rd10 and wide-type mice did not show significant difference. PTX increased the excitatory postsynaptic current and decreased the inhibitory postsynaptic currents of αRGCs. PTX induced light-evoked spike responses in 47.5% of tested αRGCs, mainly by blocking the $GABA_A$ receptors. Glycine and dopamine receptor antagonists could not induce light-evoked spike responses. PTX application could improve the ERG and optokinetic responses in P41 rd10 mice.

Study 5. The high IOP mouse model was produced by anterior injection of 1 μm and 6 μm microbeads mixtures. The IOP was increased by 3.28 ± 1.41 mmHg 7 days after injection, and this elevation could persist for up to 28 days after injection. RGC number decreased, and light sensitivity of OFF αRGCs increased under 4-week IOP elevation.

Conclusion

Alpha RGCs are coupled with wide-field ACs. Electrical activities of RGCs could reflect

different pathological conditions. Defocused stimuli decreased the inputs of αRGCs to inhibit the firing, which might be the first step of the retina sensing the defocus, providing clues to prevent myopia in electrophysiology. The mild change of atropine on αRGCs signaling might suggested the mechanisms of side effects in clinical administration. Removing inhibition unmasked light responses of αRGCs derived from retained cones, suggested a therapeutic clue for RP and other neurodegenerative diseases. Enhanced excitability hypothesized in our glaucomatous model suggested an early change before RGCs degeneration.

Overall, these observations of signaling of RGCs in physiological and pathological conditions have important consequences for our understanding of the neural information processing in the retina. The RGCs signaling suggested very early pathological changes and mechanisms in myopia, RP, and glaucoma, providing us biophysical mechanisms to target in exploring preventive strategies for these eye diseases.

Publications

Wang, Q., Banerjee, S., So, C., Qiu, C., Lam, H. C., Tse, D., Volgyi, B. & Pan, F. (2020). Unmasking inhibition prolongs neuronal function in retinal degeneration mouse model. *FASEB J, 34*(11), 15282-15299.

Wang, Q., Banerjee, S., So, C.H., Qiu, C. T., Sze, Y. H., Lam, T. C., To, C. H. & Pan, F. (2021). The effect of low dose atropine on alpha ganglion cell signaling in the mouse retina, *Frontiers in Cellular Neuroscience*, 15(129).

Banerjee, S., **Wang, Q.**, So, C. H., & Pan, F. (2020). Defocused images change multineuronal firing patterns in the mouse retina. *Cells*, 9(3). (co-first author)

Banerjee, S., **Wang, Q.**, Zhao, F.X., Tang, G., So, C.H., Tse, D., To, C.H., Feng, Y., Zhou, X.T., Pan, F. (2020). Increased connexin36 phosphorylation in AII amacrine cell coupling of the mouse myopic retina. *Frontiers in Cellular Neuroscience* 14: 124. (co-first author)

Banerjee, S., **Wang, Q.**, Tang, G., So, C.H., Shan, S.W., Li, K.K., Do, C.W., Pan, F. (2021). Functional connexin36 increased in the myopic chicken retina. *Visual Neuroscience, 38*: E008.

Conference presentations

"Low-dose atropine might affect alpha ganglion cell signaling in the mouse retina" at ARVO 2021 as a poster presentation

"Prolong neuronal function in retinal degeneration mouse model by unmasking inhibition" at Congress on Ocular Pharmacology & Therapeutics (AOPT) 2021 as a poster presentation

Acknowledgements

Close to completion of this dissertation, the three-year PhD is fast when looking back, but it is also a long journey. I have got so much support and encouragement along the way.

First, I would like to thank my supervisor Dr Feng PAN. He is the most important role in this journey to give me opportunities, show me the path, give me strength, support, and courage. He taught me to face the tasks with tough and confident characteristics, which has gone far beyond the experiments.

Thanks to Seema BANERJEE, led me through the toughest beginning time in the lab, with tremendous patience. Thanks to Chung-him SO, Chun-ting QIU, and Ting ZHANG. They have given me countless support and inspiration in work, study, and life. I couldn't feel more fortunate to have them as groupmates.

Thank Dr Chi-wai DO as my co-supervisor, providing me support from the beginning. I also would like to thank other professors: Dr Bin LIN, Dr Chea-su KEE, Dr Dennis TSE, Dr Thomas LAM, Dr Henry CHAN, Dr Chi-ho TO. Special thanks to Dr Maureen BOOST for modifying this thesis.

Thanks to my senior colleagues or peers who provided lots of help in conducting experiments or completion of the thesis: King Kit LI, Bing ZUO, Christie LAM, Hoi Lam LI, Samantha SHAN, Li PAN, Wei YANG, Yammunadevi LAKSHMANAN, Andes SZE.

Thanks to my other colleagues and friends helped and accompanied me in our department: Mei ZHAO, Kirk PATRICK, Ya-jing YANG, Shashi CHAUDHARY, Jing ZHANG, Da-qian LU, Jimmy CHEUNG, Lydia YU, An-qi LYU, An-qi LIN, Fang-yu XU, Mezbah UDDIN, Samuel ABOKYI, Jeremy KANG, Ben CHAN, Jennifer BIAN, Ying-kun CUI, Ying ZHU, Wen-qiu ZHANG, Elie DELESTRANGE, Jeffery LEUNG, Ella GUO, Kit Ying CHOY, Kai Yip CHOI, Sonal VYAS.

Thanks to Alice AU and other Centralised Animal Facilities staff.

Special thanks to Meng CHENG, Rong LI, and Yuanyuan LIANG, who have supported me and kept me company throughout the three years.

Thanks to my friends, who have given me indispensable mental support.

Thanks to my mom Ai-ni WANG, dad Zhong-sheng WANG, and my family. The love they give is my first and last motivation.

Thank you all!

Table of Contents

List of Figures

List of Abbreviations

Abbreviation	Explanation
AC	Amacrine cell
ACh	Acetylcholine
BC	Bipolar Cell
CCF	Cross-Correlation Function
ChAT	Choline Acetyltransferase
CNS	Central Nervous System
DBCs	Depolarized Bipolar Cells
Ec	Equilibrium potential of cation
Ecl	Equilibrium potential of chloride
EPSCs	Excitatory Postsynaptic Currents
ERG	Electroretinogram
GABA	Gamma-Aminobutyric Acid
GCL	Ganglion Cell Layer
HBC	Hyperpolarized Bipolar Cell
HC	Horizontal Cell
INL	Inner Nuclear Layer
IOP	Intra Ocular Pressure
IPL	Inner Plexiform Layer
IPSCs	Inhibitory Postsynaptic Currents
ISI	Inter-spike Interval
LCA	Leber Congenital Amaurosis
ONL	Outer Nuclear Layer
OPL	Outer Plexiform Layer
PDE	Phosphodiesterase
PhNR	Photopic Negative Response
PSTH	Peristimulus Histogram
PTX	Picrotoxin
RGC	Retinal Ganglion Cell
RP	Retinitis Pigmentosa
SEM	Standard Error of the Mean
WT	Wide type
αRGC	Alpha Retinal Ganglion Cell
λ	Wavelength

Chapter 1 Introduction

1. Retina

The retina is a neural tissue that lines the back of the eye. It senses light signals from environments and transfers these to the brain for further processing. About 80 percent of the information from human perception of the world comes from vision. Any insult to the retina can impact on vision or even cause permanent blindness, which would bring devastating physiological, psychological, and economic burdens to the patients and their families.

1.1 Retinal structure

The retina is considered a part of the central nervous system (CNS) from its developmental background and has a sandwich-like structure. The detailed morphology of the retinal neurons was first revealed by Cajal in 1892. Photoreceptors, horizontal cells, bipolar cells, amacrine cells, and ganglion cells are the main types of neurons in the vertebrate retina (Masland, 2012a). **Fig 1.1** shows the retinal "sandwich-like" structure stained with DAPI, a nuclear dye.

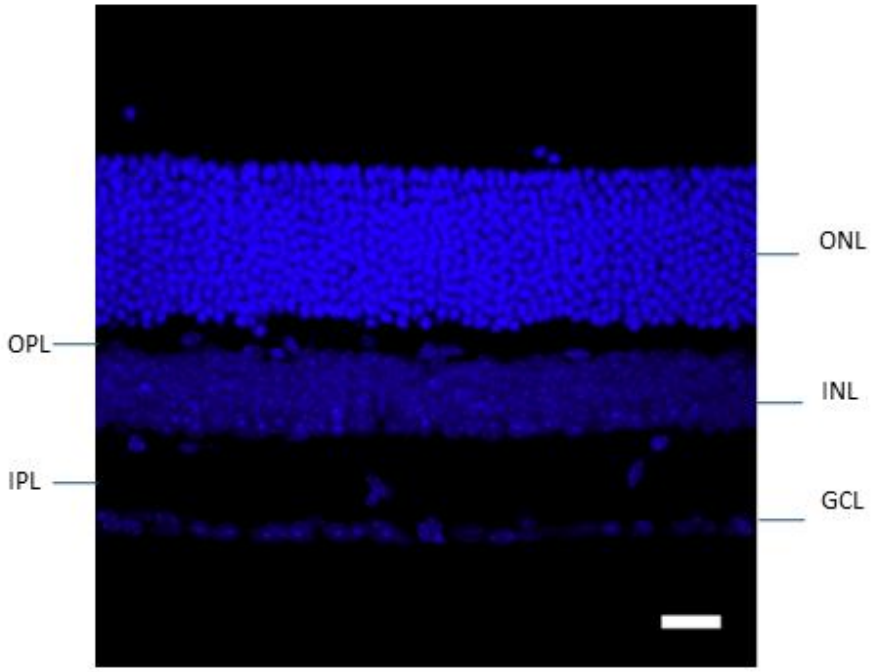

Figure 1.1 Cross-section of C57BL/6J mouse retina.

The retina was stained with DAPI (4′,6-diamidino-2-phenylindole). Scale bar is 20μm.

1.1.1 Photoreceptors

Photoreceptors are located in the outer layer of the retina, where the light signals are transferred into electrical-chemical signals. Photoreceptors are consisted of outer segments, inner segments, cell bodies, and axon terminals. They are classified into rods and cones, based on the spectral sensitivity and shapes of outer segments. Rods are sensitive to dim light and responsible for scotopic vision, while cones are sensitive to bright light and responsible for photopic vision. Rods make up approximately 95%, whereas cones comprising only 5% of the photoreceptors in the human retina. Mice as nocturnal animals have a higher percentage of 97% rods and 3% cones (Jeon et al., 1998a).

Function of photoreceptors is accomplished through phototransduction. Photopigments, comprised of opsin and retinal, are located in the outer segments and absorb photons. Altered cellular protein activate phosphodiesterase (PDE) that hydrolyze cyclic guanosine monophosphate (cGMP). Ion channels permeable to Na^+ and Ca^{2+} are closed due to decreases of cGMP, which hyperpolarize cells. This leads to the electrical behavior that photoreceptors depolarize in the dark and hyperpolarize under light in the vertebrate retina.

In humans and other trichromatic animals, cones are classified into three types based on the different opsin molecules sensitive to the different light spectrums for red, green, and blue wavelengths. In mice and other dichromatic animals, long-wavelength cones are absent so that they are not sensitive to red light (Applebury et al., 2000). Thus, red light can be used in dark-adaptation experiments for mice. However, any insults to photoreceptors cause abnormal phototransduction, leading to pathological conditions including color blindness and retinitis pigmentosa.

1.1.2 Bipolar cells

Bipolar cells (BCs) are located in the inner nuclear layer (INL) and transfer signals from photoreceptors to retinal ganglion cells (RGCs). There are more than ten types of cone BCs, but only one type of rod BCs in the mouse retina (Boycott & Wassle, 1991). The synapses between photoreceptors and BCs are of two types, invaginating and flat synapses. Invaginating synapses usually use inhibitory metabotropic glutamate receptors (mGluR), specifically mGluR6, while the flat synapses use excitatory ionotropic AMPA-kainate glutamate receptors (iGluR). Thus, the BCs with mGluR are classified as depolarized bipolar cells (DBCs) and BCs with iGluR are hyperpolarized bipolar cells (HBCs) according to their different responses to light. This property also underlies the splitting of ON and OFF pathways: DBCs are ON BCs and HBCs are OFF BCs. In mouse retina, BCs connected to rods are all DBCs, while those connected to cones are of both types.

1.1.3 Horizontal cells

Horizontal cells (HCs) are located in the INL of the retina. Their dendrites and axons both connect with photoreceptors. HCs have wide-spread coupling by gap junctions. There is only one type of HCs in the mouse retina, which are coupled by Cx57. HCs are depolarized by glutamate and provide feedback inhibition to photoreceptors and feedforwards inhibition to BCs to form the central-surround organization of receptive field. These functions contribute to the contrast enhancement and light adaptation of the retina (Demb & Singer, 2015).

1.1.4 Amacrine cells

Amacrine cells (ACs), which are located in INL, are neurons that receive signals from BCs or other ACs, and transfer these to RGCs. More than 60 subtypes of ACs have been identified in the mouse retina (Yan et al., 2020). ACs, which have a variety of morphologies, can be divided into small-, medium-, or wide-field ACs according to their dendritic fields (Kolb et al., 1981).

The glycinergic ACs are usually small-field ACs, such as AII, which occupy several strata vertically but extend short distances horizontally. The wide-field ACs usually emit GABA as a neurotransmitter. The functions of ACs are diverse, providing inhibitory GABAergic and glycinergic input to RGCs and shaping these cells to have concentric receptive fields and transient responses (Lagnado, 1998). AII ACs are responsible for transmitting rod signals to RGCs. Some types of ACs release neuromodulators, such as dopamine, acetylcholine, or nitric oxide to modulate neuronal activity (Masland, 2012b). ACs are also responsible for the object motion detection of RGCs, corresponding to the movement of a stimulus relative to the background (Masland, 2012a).

1.1.5 Ganglion cells

Retinal ganglion cells (RGCs), located in the ganglion cell layer (GCL), are the output neurons encoding visual signals to the brain. Axons of RGCs terminate in the lateral geniculate nucleus of the thalamus, the superior colliculus, the pretectum and the hypothalamus, finally project to the visual cortex. They play important roles in signal transmission and vision formation.

1.2 Retinal synapse

The synapses between neurons can be classified into chemical and electrical synapses. The normal activities in the synapses modulate and maintain the physiological function of the retina.

1.2.1 Chemical synapses

Chemical synapses are the classical synapses that are present in all types of neurons in the retina. The signal pathways connected by chemical synapses operate in three directions (Wu, 2010). The radial direction is observed in photoreceptors which synapse with BCs, which then synapse onto RGCs. Glutamate is the neurotransmitter in this pathway. The lateral and feedback directions include HCs making synapses to BCs or photoreceptors, and ACs making synapses to BCs, ACs, or RGCs. GABA and glycine are the main inhibitory neurotransmitters in the lateral pathway.

1.2.2 Electrical synapses

Gap junctions exist in almost all tissues of animals. They are composed of two hemichannels, which enable direct communication between adjacent cells. A hemichannel is composed of six connexins which have approximately 20 isoforms. Their structural properties allow small molecules up to 1000 Da (Dalton) to go directly through the gap junction. The effects of gap junctions have been well-studied in many systems, including embryonic and tissue development, cell death, tissue restructure, cardiac muscle contract (Nielsen et al., 2012). Recently, the gap junction blocker, Meclofenamate (MFA), has been used in an ongoing clinical pilot trial to treat brain metastases (Aasen et al., 2019).

The gap junctions in the nervous system are also called electrical synapses. Because of the nature of these gap junctions, signal transmission via electrical synapses is much faster than via chemical synapses. Thus, they are involved in rapid responses, such as the escape reflex and visual response. There are various methods to study gap junction, including

electrophysiological recording, tracer assays, and hybrid methods (Dong et al., 2018). Blocking the gap junctions seems to provide neuroprotection in neuronal system diseases such as brain ischemia, epilepsy, and neurodegeneration (Takeuchi & Suzumura, 2014), but the effect is controversial (Nakase & Naus, 2004).

The retina is an ideal place to investigate the diversity of gap junctions. Cx57 or Cx50 gap junctions have been identified between HCs, whereas Cx45 are located in bistratified RGCs and heterotypic gap junctions between RGCs and ACs (Bloomfield & Volgyi, 2009). Cx36 is a widely distributed connexin in the retina, mainly in photoreceptors, AII ACs, and RGCs (Bloomfield & Volgyi, 2009). The properties of gap junction channels differ according to the connexin component present. For example, Cx50 is a relatively large conductance located between HCs to adapt receptive field expansion. In contrast, Cx36 and Cx45 are the small-channel connexins to support multiple physiological properties. Electrical synapses are highly plastic and can be regulated by environmental light and neuromodulators (O'Brien & Bloomfield, 2018). Blocking gap junctions could provide a protective effect to RGCs under high intraocular pressure (Akopian et al., 2014; Akopian et al., 2017).

1.3 Major neurotransmitters in the retina

1.3.1 Glutamate

Glutamate is the major excitatory neurotransmitter in the retina. It is released by photoreceptors and BCs. Glutamate receptors (GluRs) are classified as either ionotropic or metabotropic GluRs. There are three main groups of post-synaptic ionotropic GluRs based on their response to glutamate agonists: (1) α-amino-3-hydroxy-5-methyl-4-isoxazolepropionic acid (AMPA) receptors including GluR1-4, (2) kainite (KA) receptors including GluR5-7, KA1, and KA2, (3) *N*-methyl-D-aspartate (NMDA) receptors including NR1, NR2A, NR2B, NR2C, and NR2D

(Monaghan et al., 1989). Eight distinct metabotropic GluRs (mGluR1-8) have been identified in vertebrates, which can be subdivided into three groups based on differences in their pharmacological profiles (Conn & Pin, 1997; Duvoisin et al., 1995). Group-I receptors, mGluR1, and mGluR5, are coupled to the stimulation of phospholipase C. Group-II (mGluR2 and mGluR3) and Group-III (mGluR4, mGluR6, mGluR7, and mGluR8) receptors are coupled to the inhibition of adenylyl cyclase. Metabotropic receptors affect ion channels via intracellular second messenger cascades. In the retina, ionotropic glutamate receptors are excitatory to glutamate, make cells hyperpolarize to light, locate on OFF BCs. Metabotropic glutamate receptors (mGluR6) are inhibitory to glutamate, make cells depolarize to light, locate on ON BCs. 2-amino-4-phosphobutyric acid (APB, also called L-AP4) is the agonist for sign-inverting Group-III receptors (Ferraguti & Shigemoto, 2006; Quraishi et al., 2007). mGluR6 is located on DBCs (ON BCs) and application of APB can selectively block the ON pathway in the retina (Slaughter & Miller, 1981). Excessive glutamate leads to excitotoxicity of neurons, which relates to Alzheimer's disease and glaucoma.

1.3.2 Gamma-Aminobutyric acid (GABA)

GABA is the main inhibitory neurotransmitter in the retina. It is released and used in the lateral pathway by ACs and HCs. Vesicular GABA transporters are present in ACs and HCs (Cueva et al., 2002). GABA receptors include GABA-A/B/C subtypes. $GABA_A$ and $GABA_C$ receptors are ligand-gated chloride channels, which can elicit fast and transient responses, while $GABA_B$ receptors belong to the G-protein coupled receptor superfamily and mediate slow and sustained responses (Marc et al., 2004). GABA receptors are present on cones (Picaud et al., 1998), HCs (Dong et al., 1994; Paik et al., 2003), BCs (Shields et al., 2000), as well as ACs and RGCs (Popova, 2015; Yang, 2004). GABAergic inhibition contributes to the centre-surround receptive field (Flores-Herr et al., 2001), directive selection (Auferkorte et al., 2012), and light sensitivity of RGCs (Pan et al., 2016). Picrotoxin (PTX) is a nonspecific GABA receptor

antagonist. $GABA_A$ receptor blockers include Gabazine (SR 95531) and bicuculline, while $GABA_B$ receptors can be blocked by saclofen. $GABA_C$ receptor blockers include (1,2,5,6-Tetrahydropyridin-4-yl) methylphosphinic acid (TPMPA). GABA has been associated with myopia development (Stone et al., 2003), and glaucoma (Moreno et al., 2008).

1.3.3 Glycine

Glycine is another inhibitory neurotransmitter, expressed by small-field ACs. Compared with wide-field GABAergic ACs, glycinergic ACs are mainly involved in local interaction across the IPL. Glycine receptors are ligand-gated chloride channels, composed of α and β subunits. Glycine receptors are found on BCs, ACs, and RGCs (Wässle et al., 2009) and may be blocked by strychnine. Homomeric-α glycine receptors can be blocked by PTX (Pribilla et al., 1992). $GABA_A$ receptor antagonists were also shown to inhibit glycine receptors (Wang & Slaughter, 2005). Glycinergic synapses affect retinal signals by inhibiting inner retinal function and exciting the outer retina. The dual function of glycine is related to different chloride electrical-chemical gradient potentials (Shen & Jiang, 2007). Glycine and GABA also play roles in the interaction of ON and OFF pathways (Popova, 2014).

1.3.4 Acetylcholine

Acetylcholine (ACh) is a well-known excitatory neurotransmitter in the peripheral nervous system, but studies have suggested its role is more as a neuromodulator in the CNS and retina (Picciotto et al., 2012). ACh is released by starburst ACs in the retina. ACh receptors are classified into ionotropic nicotinic acetylcholine receptors (nAChRs) and metabotropic muscarinic acetylcholine receptors (mAChRs). The nAChRs are ligand-gated ion channels, comprised of different α/β subunits and are classified into five subtypes, M1-M5. The nAChRs and mAChRs are present in BCs, ACs, and RGCs (Liu et al., 2009; Strang et al., 2010) and RGC responses can be affected by mAChRs (Strang et al., 2010). ACh has a close relationship

with other neurotransmitters. ACh was shown to induce A17 ACs to release GABA via nAChR (Elgueta et al., 2015). Most mAChR-expressing ACs also express GABA (Strang et al., 2010). Mixed ACh/GABA transmission underlies the direction coding of RGCs (Sethuramanujam et al., 2016). The effect of retarding myopia by atropine has been suggested to involve mACh receptors (Arumugam & McBrien, 2012).

1.3.5 Dopamine

Dopamine is a neuromodulator released by dopaminergic ACs, which account for less than 1% of all ACs (Popova, 1995). There are two types of dopamine cells, of which type 1, also known as the A18 cell of the Golgi descriptions (Kolb et al., 1981), has soma located in the INL and a dense dendritic matrix located in the strata 1 of the IPL, which can be stained by tyrosine hydroxylase (TOH). In rabbit and macaque monkey retinas, the dendrites and axon-like processes can reach the OPL (Dacey, 1990; Witkovsky, 2004). Type 2 dopamine cells were identified in transgenic mice with their dendrites stratified into strata 3 of the IPL (Zhang et al., 2004; Zhang et al., 2007). The release of dopamine is under circadian control and is at high levels during the day and absent at night (Witkovsky, 2004). There are five types of dopamine receptors, D1-D5, which are all G-protein coupled receptors. They can be classified into D1-class (D1 and D5) and D2-class (D2-D4). D1-class receptors stimulate the production of cyclic adenosine monophosphate (cAMP) from adenylyl cyclase. cAMP promotes protein kinase A (PKA), resulting in phosphorylation of DARPP32, which inhibits protein phosphatases-1. In contrast, D2-class receptors inhibit the production of cAMP and decrease of PKA activity (Beaulieu & Gainetdinov, 2011). D2-class receptors are mainly located in photoreceptors and ACs, while D1-class are present in HCs, BCs, and RGCs. Agonists and antagonists for D1-class are SKF38393 and SCH23390 respectively and those for D2-class are quinpirole and eticlopride respectively.

Dopamine adjusts the gap junction between HCs, ACs (Mills & Massey, 1995), and RGCs

(Mills et al., 2007). Dopamine and its secondary messenger, cAMP, effectively reduces AII/AII coupling. It also modulates other neurotransmitters, including GABA (Contini & Raviola, 2003; Travis et al., 2018). Dopamine affects the light sensitivity of retinal neurons by suppressing rod-driven signals in bright light and enhancing light sensitivity in dim light (Herrmann et al., 2011; Li & Dowling, 2000). Dopamine is also suggested to act as a retarding signal for myopia progression (Feldkaemper & Schaeffel, 2013; Zhou et al., 2017).

1.4 Rod/cone pathway

The retina can sense a large range of light intensity. Rod and cone photoreceptor signaling enables the retina to respond over the range of ~10 log units of light encountered between night and day. Rod and cone pathways play an important role in this process.

There are three pathways for rod signals. The primary pathway is rods transfer the signals they receive to the depolarized rod BCs, which connect to AII ACs. AII ACs make a sign-inverting chemical synapse with OFF cone BCs, and a sign-conserving electrical synapse with ON cone BCs, which connect with corresponding RGCs. The second pathway involves the rods making gap junctions with cones, which delivers the rod signals directly to the cone pathway. The tertiary pathway comprises rods making synapses onto a unique type of OFF or ON BCs. The three rod pathways are shown in **Fig 1.2** (Pan et al., 2016).

Cones receive the signal and transfer these to cone BCs, of which there are around 10 types, classified according to their glutamate receptors and light response into ON and OFF types. The ON cone BCs make synapses with ON RGCs and OFF cone BCs synapse onto OFF RGCs. As it is shown in **Fig 1.2** and **Fig 1.3**, the cone pathway is more direct than the rod pathway.

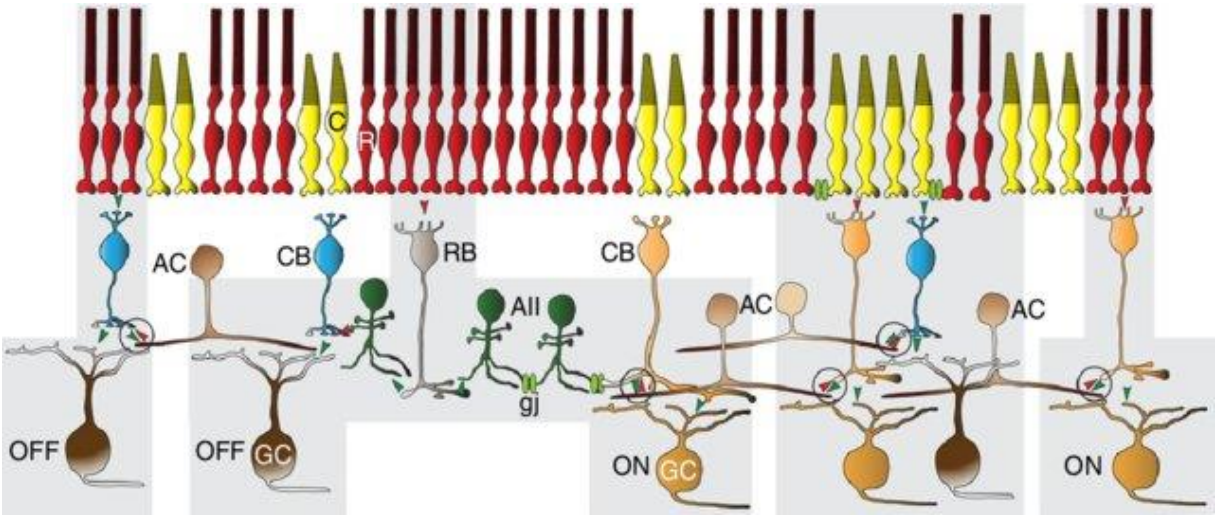

Figure 1.2 Three rod pathways

The primary rod pathway is composed of rods - RB - AII AC - CB - RGC. The second pathway is rods - cones - CB - RGC. The tertiary pathway is rods - CB - RGC. CB: cone bipolar cell; RB: rod bipolar cell.

The picture is adapted from (Pan et al., 2016).

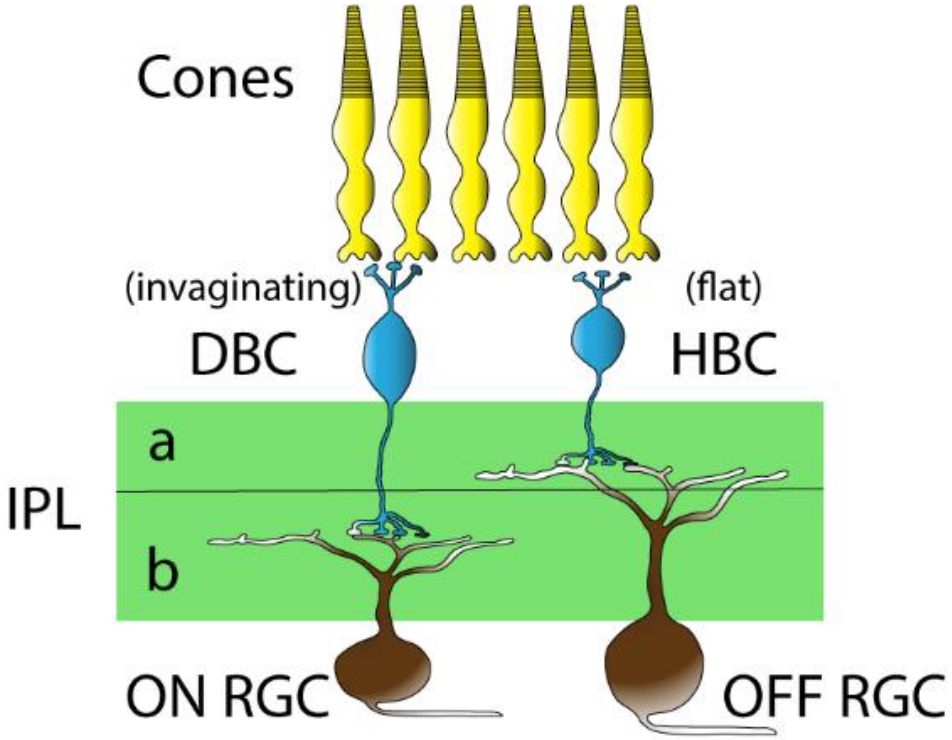

Figure 1.3 Cone pathways

Cones make invaginating synapses with DBC (depolarized bipolar cell), and flat synapses with HBC (hyperpolarized bipolar cell). The DBC and HBC connect with ON RGC and OFF RGC, respectively.

2. Retinal Ganglion Cells (RGCs)

RGCs are the output neurons of the retina, which receive information transmitted from the other four types of neurons and transfer these to the CNS. Therefore, RGCs play an essential role in vision processing. RGCs in the mouse retina can be classified into more than 40 types, based on their morphological and physiological properties (Baden et al., 2016; Sanes & Masland, 2015), as well as transcriptome variability (Rheaume et al., 2018).

2.1 Morphology of RGCs

Since Cajal described retinal neuron morphology one hundred years ago (Ramon y Cajal, 1933), a variety of methods have been used to show the morphology of RGCs, including microinjection, genetically encoded protein, photofilling, and gene gun. To date, morphological classification of RGCs has been published for several vertebrate animals, including zebrafish (Mangrum et al., 2002), rabbit (Rockhill et al., 2002), mouse (Volgyi et al., 2009), rat (Sun et al., 2002), and ferret (Isayama et al., 2009).

The basic structure of RGC is soma, axon, and dendrite. The axons of RGCs make up the optic nerve, which transmits signals from the retina to the CNS. RGC somas are present in the GCL, stratifying dendrites in the various sublamina of the IPL, which is closely related to its function (Famiglietti & Kolb, 1976; Hoshi et al., 2009). IPL can be divided functionally into ON and OFF halves (Famiglietti & Kolb, 1976). The ON half responds to stratum 3-5 (sublamina b), and the OFF half refers to stratum 1-2(sublamina a). ON BCs make ribbon synapses on ON RGCs in sublamina b, while OFF BCs terminate in sublamina b to OFF RGCs (Nelson et al., 1978). The ON and OFF halves of IPL can be distinguished by immunohistochemistry staining of starburst ACs. The band of ON starburst ACs was about 40% depth from the GCL, between S3(40%-60%) and S4(20%-40%) of IPL, and the band of OFF starburst ACs was fallen in 77% depth from GCL, between S1(80%-100%)-S2(60%-80%) of IPL (Li et al., 2016).

2.2 Inputs of RGCs

2.2.1 Chemical synapse

RGCs receive excitatory synapses from BCs with glutamate. The NMDA and non-NMDA glutamate receptors are located on RGCs. Excessive glutamate leads to excitotoxicity in RGCs via NMDA receptors (Sucher et al., 1997).

RGCs also receive inhibitory synapses from ACs with GABA or glycine. The direct inhibition from ACs is termed feedforward inhibition to RGCs. In parallel, ACs give inhibitory synapses to BCs, and other ACs, which also affect RGCs. The indirect inhibition is termed feedback inhibition to RGCs. $GABA_A$ receptors are located on RGC dendrites, as well as on ACs dendrites and BCs axon terminals. $GABA_C$ receptors are distributed on BCs axon terminals. Thus, $GABA_A$ receptors mediate feedforwards and feedback inhibitions, while $GABA_C$ receptors only mediate feedback inhibition. Acetylcholine receptors are also found on RGCs.

2.2.2 Electrical synapse

RGCs make gap junctions with ACs and/or other RGCs. Using retrograde labeling, 11% of displaced ACs and 4% of conventional ACs were found to be coupled to RGCs in the mouse (Pang et al., 2013). It was found that ON αRGCs only coupled to displaced ACs, while OFF αRGCs coupled to conventional ACs and homologous OFF RGCs. ACs coupled to RGCs displayed either polyaxonal or wide-field morphologies (Volgyi et al., 2009).

The gap junctions of RGCs were shown to consist of Cx36 and Cx45 (Pan et al., 2010; Schubert et al., 2005b). A higher Cx36 mRNA level was revealed in OFF αRGCs (Volgyi et al., 2013). Following the ablation of Cx36, half of the homologous coupling between RGCs and almost all heterologous coupling between RGCs and ACs were lost (Pan et al., 2010). Cx36 was revealed to be necessary for all heterologous couplings of OFF αRGCs (Volgyi et al., 2005), while there was a discrepancy about homologous OFF RGCs coupling (Schubert et al., 2005a).

It was believed that OFF αRGCs use Cx36 to make heterologous gap junctions with ACs rather than homologous gap junctions with each other (Volgyi et al., 2013). Therefore, it is estimated that Cx36 makes up the gap junction between OFF αRGCs and ACs, while the components of gap junctions between OFF RGCs homologous coupling and ON RGCs coupling are not confirmed.

The gap junction between RGCs and ACs underlies the concerted activity of RGCs (Volgyi et al., 2013). Their synchronous activity is believed to play an important role in the detection and transduction of visual information (Usrey & Reid, 1999).

2.3 Outputs of RGCs

RGCs, as the last neuron of the retina, can collect the signals from the retinal outer layers and transfer these to the CNS. The information it codes are spikes, which are further described in the following section.

2.3.1 Spikes and postsynaptic currents

Spikes, also known as action potentials, are dramatic changes of membrane potential (Hodgkin & Huxley, 1952). Spikes occur in both axons and dendrites to transfer electrical signals. The inducement of an action potential depends on the membrane potential (postsynaptic potential) reaching the threshold, and the work of voltage-gated sodium and potassium channels (Barnett & Larkman, 2007).

Neurotransmitters in the synapses bind to receptors and affect postsynaptic current and potential. The excitatory postsynaptic current (EPSC) is derived from inflowing of cation which depolarizes the neuron, while the inhibitory postsynaptic current (IPSC) is inflowing of chloride and hyperpolarizes the neuron ("Postsynaptic Currents (EPSCs and IPSCs) or Potentials (EPSPs and IPSPs)," 2009). The EPSCs and IPSCs can be examined in neurons by applying excitatory or inhibitory receptor blockers (Nanou et al., 2018; Potapenko et al., 2011).

The excitatory and inhibitory inputs of neurons can also be assessed by clamping the membrane potential at chloride equilibrium potential (E_{Cl}) or cation equilibrium potential (Ec) to negate corresponding effect. Holding the membrane potential at E_{Cl} allows the excitatory postsynaptic currents to be assessed. Similarly, Cl^--mediated inhibition can be accessed by holding the potential at Ec. The E_{Cl} and Ec for RGCs are -60mV and 0mV, respectively (calculated from the Nernst equation). In this way, the light-evoked postsynaptic current can directly show the inputs of RGCs from BCs and ACs respectively (Pang et al., 2002; Pang et al., 2004). The light-evoked postsynaptic current has been used as the criteria to classify RGCs in salamanders (Wang et al., 2016). It was also used to study the inhibitory surround of RGCs receptive fields (Flores-Herr et al., 2001).

2.3.2 Light-evoked response

ON and OFF response polarity is the most important aspect of the physiology of RGCs, as it helps to form the basis of visual contrast. RGCs respond to light in three main modes - ON, OFF, or ON-OFF. It was first described in cold-blooded vertebrates (Hartline, 1938), and became the most significant subdivision among vision features of RGCs. RGCs have been referred to as “feature detectors” since then (Lettvin et al., 1959). This feature was confirmed in the retinas of other vertebrates (Amthor et al., 1989; Nelson et al., 1978; Peichl & Wassle, 1981). ON ganglion cells spike when the light is turned on, and OFF ganglion cells spike when the light is turned off.

The response polarity of RGCs comes from the ON and OFF circuitry of the retina. Bright and dark information is separated into ON and OFF pathways in the invaginating or flat synapse BCs make with photoreceptors. The ON and OFF BCs transmit the signal to the RGCs.

2.3.3 Concerted activity

Concerted activity means that two or more neurons fire simultaneously by more than chance.

Half of the retinal spike activity underlies concerted firing of RGCs. Correlated firing is thought to contribute to efficient transmission, increase of the bandwidth of the optic nerve (Meister et al., 1995), and global vision detection (Roy et al., 2017).

RGC concerted spontaneous spike activity can be analyzed via cross-correlation functions (CCFs) fitted with a Gaussian function, characterized by amplitude and width. Concerted RGC correlation can be separated into narrow, medium, and broad CCF profiles. Broad correlation is correlated with chemical and electrical synapses, while narrow and medium profiles are only correlated to the electrical synapse. OFF αRGCs show spike synchrony, but only with superposition of narrow and medium correlation. It has been demonstrated that narrow spike correlations are mediated by RGC-RGC coupling and medium correlations by RGC-AC coupling (Volgyi et al., 2013).

2.4 Alpha (α) RGCs

Alpha RGCs is a well-identified cell type, which has the largest soma and stout dendrites, and regularly spaces in the retina (Peichl, 1991). They were first identified in cats (Boycott & Wassle, 1974), and conserve similar morphological properties in different species, suggesting the fundamental tasks of αRGCs may take in visual processing.

Alpha RGCs are positioned semi-regularly forming a mosaic in the retina (Krieger et al., 2017). There are several physiological properties shared by αRGCs. They have short response latency, fast conducting axons, and concentric and nonlinear receptive fields arising from the effect of BCs and ACs. Alpha RGCs are not color and direction coded. In mice, αRGCs can be classified into ON and OFF types according to their light response (Volgyi et al., 2005), and further categorized into sustained or transient response time (Krieger et al., 2017). Axons of αRGCs project to deep layers in the superior colliculus and lateral geniculate nucleus (Martersteck et al., 2017). Therefore, their function may relate to visual-motor guidance and visual perception.

Because of the distinct morphological properties and typical ON and OFF light responses, αRGCs could be easily targeted in electrophysiological recording and represent the basic properties of RGCs in the retina.

3. Myopia

Myopia is a common vision disorder rapidly increasing in prevalence and affecting a significant proportion of young adults (Morgan et al., 2012). It has been reported that more than 70% of school children are myopic in East Asia (Grzybowski et al., 2020). Although myopia can be corrected by various optical methods, so far there is no effective way to reverse myopia.

3.1 Myopia etiology

Myopia colloquially termed "nearsightedness", is characterized by elongated axial length. Both genetic and environmental factors are believed to contribute to the development of myopia (Cooper & Tkatchenko, 2018; Morgan et al., 2012). Human epidemiological studies have indicated that environmental factors include outdoor activity, near-work activity, and education. Among the environmental factors, the blurred and defocused image caused by accommodation lag may be the key factor. Defocus means the image converted by optical components cannot be precisely projected to the retina. If the light is projected behind the retina, it is called hyperopic defocus. If the image is projected before the retina, it is myopic defocus.

Animal studies have demonstrated that eye growth is influenced by optical defocus. The axial length becomes longer when exposed to hyperopic defocus, while the axial length is shorter if exposed to myopic defocus (Smith Iii & Hung, 1999). Studies on humans also suggest the effect of defocus on eye growth. After short-term application of a plus or minus lens, significant and compensating changes were found in the axial length of young adults (Read et al., 2010). Similar effects were also reported in choroidal thickness of presbyopic subjects (Chiang et al., 2018), particularly with a local regional effect (Hoseini-Yazdi et al., 2019). Electroretinograms (ERG) showed sign-dependent changes with short-term defocus in adults, with positive defocus resulting in increases of amplitude, while negative defocus leads to decreased amplitude (Ho et al., 2012). Long-term studies have also suggested that myopic defocus contributes to reducing myopia progression in children (Berntsen et al., 2013; Phillips, 2005).

The above studies suggest that hyperopic defocus could be a causal reason for myopia. However, the mechanism of myopia development involves not only hyperopic defocus. The myopic defocus produced in myopia does not make the development a self-limiting process. Whilst spectacle visual correction to eliminate the myopic defocus has been proven to be safe (Ma et al., 2015), myopic defocus produced by optical under-correction leads to a faster progression in children (Chung et al., 2002). The paradox between hyperopic and myopic defocus may be attributable to different sensitivity to defocus through refractive development (Rose et al., 2016), but the specific mechanism behind these phenomena is not clear. However, these studies still suggest that defocus can trigger myopia progression, via poorly understood mechanisms.

The retina, as the sensing tissue of the eye, is responsible for receiving environmental signals and transmitting these to the CNS, so it is crucial to determine if the retina can sense defocus (Schaeffel & Wildsoet, 2013). Animal studies have demonstrated that myopia can still develop even after section of the optic nerve (Troilo et al., 1987), and regional elongation of the eyeball could be induced by local blur (Rada et al., 2006). These findings suggest that the retina can sense and transfer signals to initiate the remodeling. Human ERGs showed sign-dependent results to myopic and hyperopic defocus (Chin et al., 2015; Ho et al., 2012). Myopic progression was also associated with a decrease of central inner retinal activity (Li et al., 2017). However, how the retina senses defocus remains elusive (Burge & Geisler, 2011; Hung & Ciuffreda, 2007). It has been shown that ablation of the ON pathway increases susceptibility to myopia (Chakraborty et al., 2015). Pharmacological inhibition of ON or OFF responses led to a sign-dependent compensation of refractive error (Crewther & Crewther, 2003). ON delayed RGCs could help to encode images of high spatial frequency (Mani & Schwartz, 2017). A previous study revealed that defocused images changed multi-neuronal firing patterns and signaling of RGCs in mice (Banerjee et al., 2020). These findings all indicate that the electrical

signaling of the retina plays an important role in detecting defocus and myopia inducement, but the specific mechanism of myopia induction remains elusive.

3.2 Myopia control

Myopia usually develops during school age, progressing at 0.6-0.7 Diopter per year. The risks of ocular pathologies including retinal detachment and macular diseases increase with the extent of myopia (Haarman et al., 2020). Therefore, controlling myopia progression is important to both reduce myopia and prevent severe pathologies. The methods to control myopia involved optical interventions, increased outdoor activities, and pharmaceutical interventions.

3.2.1 Optical intervention

Single vision lenses are used to correct the refractive error and improve the vision of myopes. As the role of defocus was revealed in myopia etiology, a variety of optical interventions based on spectacles to control myopia were extensively studied. The results of the Correction of Myopia Evaluation Trial (COMET) studies which used multifocal lenses to reduce accommodation lag to decrease hyperopic defocus, were statically significant(Correction of Myopia Evaluation Trial 2 Study Group for the Pediatric Eye Disease Investigator, 2011). Spectacle and contact lenses designed to correct central vision and reduce periphery hyperopia were shown to have a significant control effect on myopic progression in children (Sankaridurg et al., 2010). Dual power lenses simultaneously projecting myopic and hyperopic or plano defocus were shown to slow ocular growth in animals (Arumugam et al., 2014; McFadden et al., 2014; Tse & To, 2011). The dual power contact lens (Anstice & Phillips, 2011), Defocus Incorporated Multiple Segments (DIMS) spectacle lenses (Lam et al., 2020), and Defocus Incorporated Soft Contact (DISC) lenses (Lam et al., 2014), which aimed to provide simultaneous clear vision and myopic defocus were proven to be effective in retarding myopia

progression. In contrast to the various lenses based on the manipulation of the defocus, orthokeratology lens uses physical strength to flatten the cornea and improve the vision temporarily. Several studies have confirmed that orthokeratology lenses had a significant control effect on myopic progression (Lee & Cho, 2010; Santodomingo-Rubido et al., 2012).

3.2.2 Pharmaceutical interventions

Compared with the wide variety of lenses for optical interventions to control myopia, only one pharmaceutical intervention, atropine, is effective in clinical trials (Ganesan & Wildsoet, 2010; Wu et al., 2019).

The use of atropine to slow myopia progression was initially based on its effect of paralyzing presumed excessive accommodation. Although this cycloplegic effect was excluded by later animal experiments, the effects of atropine on reducing myopia progression were confirmed by subsequent clinical trials (Huang et al., 2016; Song et al., 2011). Recent studies also indicated that atropine provided additive effects with orthokeratology on myopia control (Kinoshita et al., 2020; Tan et al., 2020).

However, various side effects were reported associated with the use of atropine, including photophobia, poor near vision, and allergy. These side effects are mainly due to the dilation of the pupil and paralysis of accommodation. It was reported that the percentage of subjects reporting side effects was dependent on the concentration of atropine (Gong et al., 2017). The highest concentration that did not induce clinical symptoms was reported to be 0.02% (Cooper et al., 2013).

The concentration of atropine used in clinical trials has varied from 0.01%-1%. The use of 1% atropine was demonstrated to have a good effect on slowing myopia progression. Early studies reported that a decrease of concentration led to a decrease in the control effect (Shih et al., 1999). However, a recent meta-analysis demonstrated that there was no significant difference

in the effect associated with the concentration of atropine (Gong et al., 2017). ATOM2 study reported that a concentration as low as 0.01% atropine could be effective and reported there was comparable efficacy with higher concentrations (Chia et al., 2012). However, caution should be applied in drawing conclusions as the significant result was presented as cycloplegic refractive error rather than the effect on axial elongation (Cooper & Tkatchenko, 2018).

Although the efficacy of atropine on retarding myopia is undoubted, exploration of the mechanism of the effect is still ongoing. Previous animal experiments excluded the involvement of accommodation effect in this process, based on results of the efficacy of atropine in animals that do not have accommodation (Schaeffel et al., 1990) and with the section of optic nerve (Troilo et al., 1987), as well as regional eye growth caused by local blur (Smith et al., 2010). Therefore, following studies shifted the focus to non-accommodation pathways. Animal studies suggested that visual input was received by the retina and regulatory signals transferred to the sclera to facilitate gene expression and scleral remodeling, and atropine affected biological mechanisms in the retina and scleral (Upadhyay & Beuerman, 2020). Atropine appears to act as a nonselective antagonist for muscarinic ACh receptors. The muscarinic ACh receptors have five subtypes and are widely distributed in ocular tissues. It was found that intravitreal injection of muscarinic M1 or M4 receptor antagonists could inhibit myopia (Arumugam & McBrien, 2012; McBrien et al., 2011). Production of Nitric oxide (NO) has also been shown to be involved in the process of atropine application (Carr & Stell, 2016).

There is no consistency in published studies as to whether atropine affects retinal function. One study indicated that topical application of atropine for two years did not change the mfERG in children (Luu et al., 2005). Myopic children have a longitudinal decrease of cone function, which was also not affected by atropine (Chia et al., 2013). A further study demonstrated the effect of atropine on the ERG of the peripheral retina to defocus stimuli in humans (Khanal et al., 2019). Other animal studies have reported decreased GABA receptors after topical atropine

application (Barathi et al., 2014), and increased dopamine and its receptors after intravitreal injection of atropine indicated the potential for retinal functional changes (Schwahn et al., 2000).

4. Retinitis Pigmentosa

Retinitis Pigmentosa (RP) is a group of heterogeneous inherited eye disorders leading to retinal degeneration. It has a prevalence of approximately 1:5000 worldwide (Ferrari et al., 2011). The disease usually begins in young adults, with symptoms including night blindness. It progresses with peripheral vision loss and often ends in total loss of vision. The timeframe between the commencement of the disease and final vision loss varies among patients, but progressive vision loss, beginning at a young age, and the severe consequences bring tremendous physical and psychological burdens to RP patients.

The various mutations at gene level first affect the rods leading to the loss of rod photoreceptors (Ferrari et al., 2011). Cones degenerate later and at a slower rate, but eventually leading to a severe loss of visual function (Campochiaro & Mir, 2018). Rods and cones are the main cell types affected in RP. However, studies have indicated that the remaining retinal structures were also affected after photoreceptor degeneration (Jones et al., 2016; Marc & Jones, 2003).

Treatment of RP includes gene therapy, neurotrophic factors, stem cell therapy, and visual prosthesis. The inherited manner of RP is varied, as more than 40 genes are associated with RP. The complicated genetics of RP makes it difficult to target the causative gene. To date, only Luxturna gene therapy, which targets gene RPE68, is available for humans (Ameri, 2018). Neurotrophic factor has been reported to be able to slow the progression of retinal degeneration in animals, but its delivery and efficacy still need further studies in humans (Birch et al., 2016). Retinal implants and prostheses are used for late-stage patients with severe vision loss.

The mouse retinal degeneration (Rd) model is a well-characterized animal model to study retinal degenerative disease (Chang et al., 2002). This mouse model has mutations on the beta-subunit of the cGMP phosphodiesterase (PDE) gene, leading to rod photoreceptor degeneration. The Rd10 mouse is a suitable model to study human RP because of the similar degenerative progress observed. The rods of the rd10 mouse start to degenerate at postnatal day18 (P18),

reaching a peak wave at P25. Most rods are eliminated around P35 and cones by P50 (Gargini et al., 2007). There is a timeframe at which most rods are eliminated while functional cones are still retained (Toychiev et al., 2013). However, RGCs tend to keep normal structure and survival through the disease (Mazzoni et al., 2008a). Spontaneous activity of RGCs was reported to be increased (Stasheff et al., 2011b), while quiescent RGCs also existed (Toychiev et al., 2013). Light-evoked responses of RGCs were decreased with age (Telias et al., 2019).

Photoreceptor degeneration leads to an imbalance of excitation and inhibition. Higher inhibition may exist in retinal degenerated conditions. Enhanced level of GABA and $GABA_A$ receptor was reported (Yazulla et al., 1997), and rod bipolar cells had a higher sensitivity to GABA in the Rd mouse (Varela et al., 2003). Blocking $GABA_C$ receptor increased the light response of RGCs in P23H rat retinal degeneration model (Jensen, 2012). Decreased intrinsic excitability was reported in retinal degenerated rat (Ren et al., 2018). Ribbon synapses which represent activity of glutamate receptors were decreased in rd1 mice (Chen et al., 2012; Saha et al., 2016). However, contrary studies suggested increased glutamate leaded to excitotoxity in Rd mice (Liu et al., 2013).

5. Glaucoma

Glaucoma, the second leading cause of vision loss worldwide, is characterized by progressive neuron death. High Intra Ocular Pressure (IOP) is an important risk factor, so lowing IOP is currently the main therapy for glaucoma patients (Jonas et al., 2017; Weinreb et al., 2014). However, the damage of the retina leads to the consequence of vision loss.

Retinal function in glaucoma is changed both before and after vision loss (Porciatti, 2015). The changes include reduction of all types of electroretinogram (ERG) and photopic negative response (PhNR) (Bach & Poloschek, 2013; Bach et al., 2006; Chan & Brown, 1999; Drasdo et al., 2001; Falsini et al., 2008; Fortune et al., 2002; Horn et al., 2011; North et al., 2010). Animal studies have confirmed that the trend of ERG change was descending (Bayer et al., 2001a; Bayer et al., 2001b; Bui et al., 2005; Holcombe et al., 2008; Lakshmanan et al., 2019), and two studies reporting an increased b wave (Frankfort et al., 2013; Khan et al., 2015).

RGCs are the neuron type most vulnerable to high IOP damage, which is responsible for visual field loss in glaucoma. The functional changes, including decreased spontaneous spikes, sensitivity, and inter-spike interval (ISI) variance, are apparent before RGC death (Della Santina et al., 2013; Ou et al., 2016; Pang et al., 2015). However, increased spontaneous spikes were reported by (Ward et al., 2014) and receptive field temporal properties by (Tao et al., 2019).

Gap junction blockers were found to have a neuroprotective effect in the presence of IOP elevation, indicating that secondary cell death conveyed by gap junctions may accelerate the glaucoma progress (Akopian et al., 2017). Gap junctions underlie the concerted electrical activities, which can provide extra information of connectivity. However, how the gap junction blockers provide neuroprotection remains unclear.

6. Research questions

6.1 What is the morphology and circuitry of αRGCs in the mouse retina?

ON and OFF αRGCs were previously classified as G2 and G3 subtypes. They have different morphologies and coupling patterns with ACs; ON αRGCs only couple to the ACs located in the GCL, OFF αRGCs couple to homozygous RGCs and ACs in the INL. However, the specific subtypes and detailed morphology of the ACs coupled with ON and OFF αRGCs are not clear.

6.2 Does defocus affect RGC signaling?

Defocus is recognized as an important trigger factor of myopia and the retina is postulated to sense defocus before transferring the signal to the sclera, facilitating the remodeling of the eye. Previous studies have demonstrated that defocus changed the RGC firing pattern, and light-evoked spike frequency of ON and OFF αRGCs was changed under defocus projection by microscope. However, ON and OFF RGCs' responses to defocus at the single-cell level have not been clarified.

6.3 Does atropine affect RGC signaling in myopia control?

Low-dose atropine is the only medication widely used to control myopia, but the results of studies are inconsistent concerning the effects of atropine on retinal function. Atropine is thought to target the muscarinic ACh receptors in the retina and the sclera. An anti-cholinergic effect on RGC firing was demonstrated. Atropine has been detected in the retina after topical application of low-dose atropine. However, whether this low concentration of atropine could affect RGCs' electrical activity is not certain.

6.4 What is the status of RGC electrical signaling in the rd10 mouse? Is it possible to unmask the signal and recover RGC signaling?

The rd10 mouse model mimics human RP disease, which begins with the loss of rods, followed by cones degeneration, leading to a severe decrease in visual acuity. The light responses of

RGCs are also affected. Even with the substantial loss of photoreceptors, the circuitry downstream seems to remain intact structure during a window period when most rods have died, but some cones are still retained. RGCs, as the output neurons, are responsible for the final signals transferred to the brain. Is there a method that could recover the light response of RGCs, so that extends the timeframe of effective visual acuity?

Photoreceptor degeneration leads to loss of input signals. Unmasking signals via removing inhibition has been well documented in the neuronal system. In addition, light sensitivity of RGCs could be elevated by removing GABAergic inhibition. Thus, we would like to investigate whether eliminating inhibition could also unmask the light response signals of RGCs in rd10 mice.

6.5 What is the status of RGC electrical signaling in mice with elevated IOP?

IOP elevation is the major risk factor for glaucoma. Loss of RGCs is the main characteristic of glaucomatous progression, leading to vision loss. A dysfunctional state occurs in RGCs before their death. Studies have reported that RGCs show increased or decreased spontaneous activity and light response under high IOP. The electrical signaling of RGCs in the early stages of IOP elevation is unknown.

7. Objectives and hypothesis

Aim 1: To characterize the morphology of the ACs coupled with αRGCs.

Hypothesis: The ON and OFF αRGCs labeled in the KCNG-YFP mice might have different coupling patterns, in that ON αRGCs couple to ACs in the GCL and OFF αRGCs couple to ACs in the INL and homogeneous OFF RGCs. The coupled ACs should be wide-field ACs.

Aim 2: To investigate the effect of focused/defocused image projection on αRGCs.

Hypothesis: As the spikes of RGCs have been demonstrated to decrease in defocused conditions, it is postulated that the postsynaptic currents of RGCs would change under defocused conditions.

Aim 3: To investigate the effect of various concentrations of atropine on αRGCs.

Hypothesis: Low-dose atropine may not affect RGCs signaling after short-term application. Higher concentrations of atropine could affect the muscarinic receptors in the retina subsequently affecting RGCs activity.

Aim 4: To investigate the effect of eliminating GABAergic inhibition by PTX on αRGCs in P38-P46 rd10 mice

Hypothesis: Most rods are degenerated, while cones are still functioning in P38-P46 rd10 mice. The loss of the photoreceptors is accompanied by damaged input signals, while the retinal downstream structure related to the inhibitory mechanism is still intact. Previous studies have indicated that removing inhibition could unmask excitatory input signals, and sensitivity of RGCs could also be elevated by blocking GABAergic inhibition. Thus, it is postulated that the application of PTX could unmask the excitatory signals of RGCs in the rd10 mice, allowing recovery of partial visual function.

Aim 5: To characterize the effect of elevated IOP on the signals of αRGCs

Hypothesis: Microbeads injected into the anterior chamber could increase the IOP of the mouse. Changes in RGC electrical activity may be observed in RGCs under IOP elevated conditions before the onset of neuron death. It is hypothesized that a hyper-excited status of RGCs exists in this early stage, including elevated spontaneous activity, light sensitivity, and synchronizing firing of RGCs. Blocking the gap junction may reverse this hyper-excitability, thereby providing neural protection effects under IOP elevation.

Chapter 2 Morphology of αRGCs and coupled ACs

1. Introduction

There are approximately 40 types of RGCs in the mouse retina. Alpha RGCs are the group with the largest soma body and distinct properties of light response, ON, OFF, or ON-OFF, representing the main characteristics of the RGCs. It has been reported that RGCs make electrical synapses with multiple types of ACs, but the specific types of ACs are unknown. Electrical synapses (gap junctions) play an important role in RGC signaling functions. Clarifying the morphology of RGCs and their coupled ACs are essential to the understanding of the function of the RGC circuitry. Therefore, dye injection was used to characterize the morphology of αRGCs, as well as their coupled ACs.

2. Methods

2.1 Animals

Mice were used in all the studies described here. The mouse is currently the most studied mammalian model for human disease and retinal circuitry. Although mice are nocturnal animals and lack the fovea structure of humans, the basic neuron types and functions are very similar to humans. Mice have small bodies that are easy-handled and their use in experimental studies raises fewer ethical problems. More importantly, strains of mouse models with numerous of genetic manipulations are readily available.

The KCNG-YFP mice (Duan et al., 2015) (6-8 weeks) of either sex were used. The KCNG-YFP mice were generated from the Ai32 mice (B6;129S-Gt(ROSA)$^{26Sortm32(CAG-COP4*H134R/EYFP)Hze}$/J, RRID:IMSR_JAX: 012569) and KCNG4^{cre} mice (B6.129(SJL)-KCNG4$^{tm1.1(cre)Jrs}$/J, RRID:IMSR_JAX:029414). KCNG4^{cre} mice have Cre recombinase

inserted to locus encoding potassium channel modulator, and Ai32 mice express a channelrhodopsin-2/EYFP fusion protein following exposure to Cre recombinase. The offspring of Ai32 and KCNG4^{cre} mice have YFP labeled αRGCs (Duan et al., 2015), including ON and OFF αRGCs (Krieger et al., 2017).

Homozygous KCNG mice were selected in genotyping and used for breeding. The genotyping process was performed as described below. A small portion of the tail was removed and added to a lysis solution (88µl dH2O, 10µl KAPA Express Extract Buffer, and 2µl KAPA Express Extract Enzyme). DNA was extracted using the DNA-EX program (75°C for 10 min, 95 °C for 5min, kept at 12°C) of the thermal cycler machine for 15mins. The tubes were centrifuged at Relative Centrifugal Force 9503 xG (10000 Revolutions per minutes, Mikro 200R) for 2 min, and the supernatant, which contained the DNA, was retained. A 25 µl reaction mixture was prepared by adding 12.5µl Taq (Taq DNA polymerase, hot start, Talara Cat#R028A), 8.5µl dH2O, 0.5µl of each primer, and 2µl DNA sample. The reaction solution was added in the Eppendorf tubes placed in the thermocycler (MJ Research PTC-200 Peltier Thermal Cycler) to 95°C for 5 min, and subjected to 35 cycles of 95°C for 30s, 60°C for 30s, 72 for 1 min, then 72°C for 5 min and hold at 4°C. The final PCR products were mixed with loading buffer and run on a 1.8% agarose gel with TAE (Tris Base, Acetic acid, EDTA, dH2O) electrolyte solution for 1 h at 90V. The gel was exposed under UV for visualization. Homozygous KCNG mice were used in breeding with AI32 to obtain the KCNG-YFP mice.

All animals were maintained in a 12-hour light/dark cycle. The mice were deeply anesthetized with an intraperitoneal injection of ketamine and xylazine (Alfassan International, B.V. Holland) [100 mg/kg and 20 mg/kg, respectively] and lidocaine hydrochloride (20mg/ml) was applied to eyelids before enucleation. The anesthetized animals were killed by cervical dislocation immediately after enucleation. All animal procedures were approved by the Animal Subjects Ethics Sub-Committee of the Hong Kong Polytechnic University.

2.2 Retina preparation

Eyes were removed under dim red illumination and hemisected anterior to the ora-serrata. Anterior optics and the vitreous humor were removed, and the resultant retina-eyecup was placed in a chamber with bicarbonate buffered solution (125mM NaCl, 2.5mM KCl, 26mM $NaHCO_3$, 1.25mM NaH_2PO_4, 20mM D-Glucose, 1mM $MgCl_2$, 1mM $CaCl_2$). Radial incisions were made peripherally, and the retinas were removed from the eyecup using a homemade glass rod. For patch-clamp recordings, the retinas were dissected into pieces and attached to a modified translucent Millicell filter ring (Millipore, Bedford, MA). The retinas were superfused with oxygenated mammalian Ringer's solution (120mM NaCl, 5mM KCl, 25mM $NaHCO_3$, 0.8mM Na_2HPO_4, 0.1mM NaH_2PO_4,10mM D-Glucose, 1mM $MgSO_2$ $7H_2O$, 2mM $CaCl_2$, 0.01mM L-Ascorbic acid)(Bloomfield & Miller, 1982). The bath solution was continuously bubbled with 95% O_2-5% CO_2 and maintained at approximately 32 °C.

For sections, retinas were fixed and embedded in 4% agarose gel and cut into 50-80um thick sections with a Vibratome (model VT1200S; Leica Microsystems, Bannockburn, IL, USA).

2.3 Dye injection

The YFP-labeled cells were visualized at 40x magnification under mercury epifluorescence with a BV-2A filter. The sharp microelectrodes, fashioned from borosilicate glass tubing (Sutter Instrument Co., Novato, CA), were tip filled with 4% N-(2-amino-ethyl)-biotinamide hydrochloride (Neurobiotin; Vector Laboratories, Burlingame, CA, US, Cat# SP-1120) and 0.5% Lucifer Yellow-CH (Molecular Probes, United States, Cat# L12926) in distilled water and then backfilled with KCl. The impaled cells were then injected with a biphasic current (seal test, 1.0 nA, 5 Hz).

In a further experiment, Popro1 (PO-PRO-1 iodide, Thermo Fisher Scientific, Cat#P3581) was used, as it can pass through gap junctions and be visualized under a BV-2A filter. Popro1

(10mM) and 594 (Alexa Fluor 594 hydrazide, Molecular Probes, Cat#A10442) in distilled water backfilled with KCl were iontophoresed (5Hz, for 5mins) into the YFP labeled cell. After approximately 10 min, which is usually sufficient for diffusion to visualize the coupled ACs and ganglion cells, 4% Neurobiotin and 0.5% Lucifer Yellow-CH were iontophoresed (seal test, 5Hz, for 3 mins) into the Popro1 targeted cell.

2.4 Immunohistochemistry

The eyecups were fixed in 4% paraformaldehyde for 20 min then washed several times in washing solution (0.1M PBS, 5mM Triton, 0.015mM NaN3). The retinas were blocked in 3% donkey serum (Sigma-Aldrich Cat# D9663, RRID: AB_2810235) for 2 h at room temperature. The tissues were then incubated with primary antibodies diluted in 0.1M PBS containing 1% donkey serum for 3-5 days at 4°C. After washing, tissues were incubated in secondary antibodies at 4°C overnight. Tissues were then mounted in Vectashield mounting medium (Vector Laboratories Cat# H-1000). The primary antibodies used are listed below. The secondary antibodies used were 488 donkey anti-rabbit IgG (Thermo Fisher Scientific Cat# A-21206, RRID:AB_2535792), 488 donkey anti-mouse IgG (Molecular Probes Cat# A-21202, RRID:AB_141607) , Alexa Fluor 633 Donkey anti-Goat IgG (Thermo Fisher Scientific Cat# A-21082, RRID:AB_2535739), Cy3 Donkey anti-Mouse IgG (Jackson ImmunoResearch Cat# 715-166-150), Cy3-Donkey anti-Rabbit IgG (Jackson ImmunoResearch Cat# 711-166-152). Neurobiotin was visualized by 1:200 streptavidin-488 (Molecular Probes Cat# S32354, RRID: AB_2315383) or Streptavindin-Cy3 from Streptomyces avidin (Merck Cat# S6402-1ML) at 4°C overnight.

Mouse anti-Cx35/36 (mCx36, 1:1,000, EMD Millipore Cat# MAB3045, RRID: AB94632) was used for the mouse retina. Goat anti- Choline Acetyltransferase Antibody (ChAT)(1:500; Millipore; Cat# AB144P, RRID: AB_2079751) was used to label the ON and OFF layers in the IPL. Anti-Neurofilament H Non-Phosphorylated Mouse Ab (SMI-32; 1:500; Biolegend;

Cat#201702) was used to stain αRGCs, anti-GFP conjugated with 488 antibody (1:1000; Invitrogen; Cat#A21311) was used to stain the GFP labeled cells. Monoclonal mCx35/36 and polyclonal anti-Cx36 were verified by Western blot in mouse retinas (Kothmann et al., 2007).

The primary antibodies used in all five studies are listed in **Table 2.1**.

Table 2.1 Antibodies used in following studies

Antibody	Host	Company; Cat#	Concentration
Anti-Cx35/36 antibody	mouse	Millipore; Cat# MAB3045	1:1000
Anti-Choline Acetyltransferase antibody	goat	Millipore; Cat# AB144P	1:500
Anti-Neurofilament H Non-Phosphorylated antibody	mouse	Biolegend; Cat#201702	1:500
Anti-GFP conjugated with 488 antibody	rabbit	Invitrogen; Cat#A21311	1:1000
Anti-red/green opsin antibody	rabbit	Chemicon; Cat# AB5405	1:500
Anti-Brn-3a antibody	mouse	Santa Cruz; Cat#SC8426	1:500

2.5 Image acquisition and analysis

Images of immune-labeled tissues were taken by a ZEISS LSM 800 with Airyscan (Zeiss, Thornwood, NY) confocal microscope with 20x or 40x or 63x objectives.

To show the dendritic stratification of RGCs in the IPL, the dendrites of RGCs were acquired in confocal image stacks. A z-stack of the images was acquired at 0.35μm-0.45μm steps at a resolution of 1024×1024 pixels. The ChAT bands were used as references. Dendritic fluorescence intensity was calculated relative to the location of the ON band of ChAT-positive ACs.

Diameters of soma and dendritic field were acquired by Image J (National Institutes of Health, Bethesda, MD, RRID: nif-0000-30467). To measure the dendritic field area, a polygon was drawn by connecting the ends of the dendrites using Zen 2.6 software (ZEISS Microscopy).

2.6 Data analysis

Statistical significance was determined using the student's t-test or one-way ANOVA. The results shown are mean ± standard error of the mean (SEM).

3. Results

3.1 Morphology of αRGCs

RGCs morphologies visualized by Neurobiotin injection (ON αRGCs n=34, OFF αRGCs n=54, ON-OFF RGCs n=7). **Fig 2.1** shows representative morphologies of ON α, OFF α, and ON-OFF RGCs and their dendrites stratifications. The soma and dendrites of ON and OFF starburst ACs were stained by ChAT antibody to differentiate ON and OFF sublamina in the IPL. The proximal dendrite band of ON starburst ACs is located in the ON sublamina, whilst the distal dendritic band of OFF starburst ACs is in the OFF sublamina of the IPL. The distinct dendritic stratifications in the IPL of ON α, OFF α, and ON-OFF RGCs are shown in **Fig 2.1 A B C**. The quantitative distribution also shows that ON αRGCs stratify in sublamina ON (depth=0), OFF αRGCs stratify in sublamina OFF (depth=1), while ON-OFF RGCs stratify in both sublaminas (depth=0/1) (**Fig 2.1 D, E, F**). With respect to the dendritic field, ON αRGCs was 49783 ± 3412 μm^2 (n=34), OFF αRGCs 49272 ± 3550 μm^2(n=54), ON-OFF RGCs 67296 ±7962 μm^2 (n=7). There was no significant difference among the three types (F=1.835, p=0.1655) **(Fig 2.2 A-D**). Soma diameter of the cell types varied significantly (F=6.419, p=0.0025): ON αRGCs 20.82±0.548 μm (n=34); OFF αRGCs 19.57±0.3882 μm (n=54); ON-OFF RGCs 16.57±0.8411 μm (n=7). Post hoc test revealed ON-OFF RGCs have smaller soma than both ON αRGCs (p=0.0018) and OFF αRGCs (p=0.0097) (**Fig 2.2 E-H**).

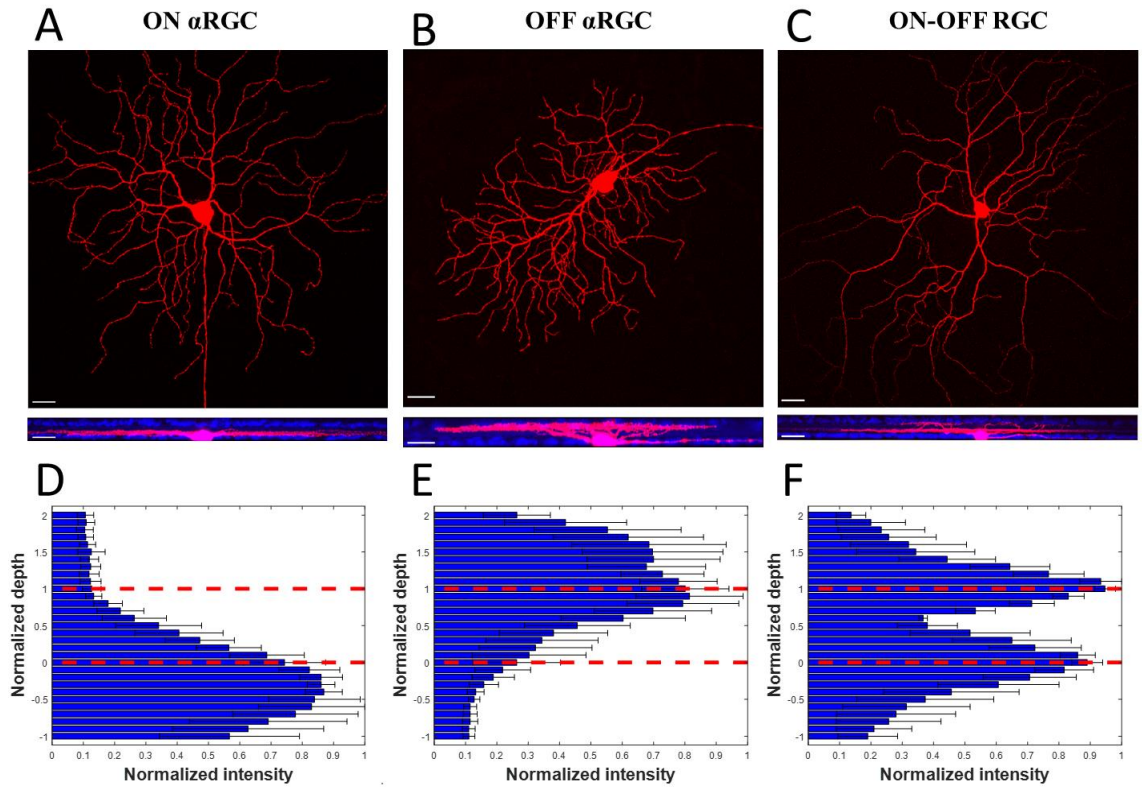

Figure 2.1 Morphology of αRGCs in WT mice.

[A, B, C] Morphologies of ON αRGC, OFF αRGC, ON-OFF RGC, respectively. The square and rectangle panels are aerial and lateral views of the maximum projection of z-stack images, respectively. The bars in the pictures are 20 μm. Neurobiotin (red) was used to label RGCs. ChAT antibody (blue) was used to label soma and dendrites of starburst ACs, to differentiate ON and OFF layers of IPL.

[D, E, F] Quantitative distribution of mean dendritic stratification of ON αRGCs (n=3), OFF αRGCs (n=3), ON-OFF RGCs (n=3), respectively. The x-axis is normalized fluorescence intensity of Neurobiotin (red). Y-axis is the normalized depth of IPL. Zero and one position are specified by red dashed lines, indicating the ON and OFF sublayers of IPL, respectively.

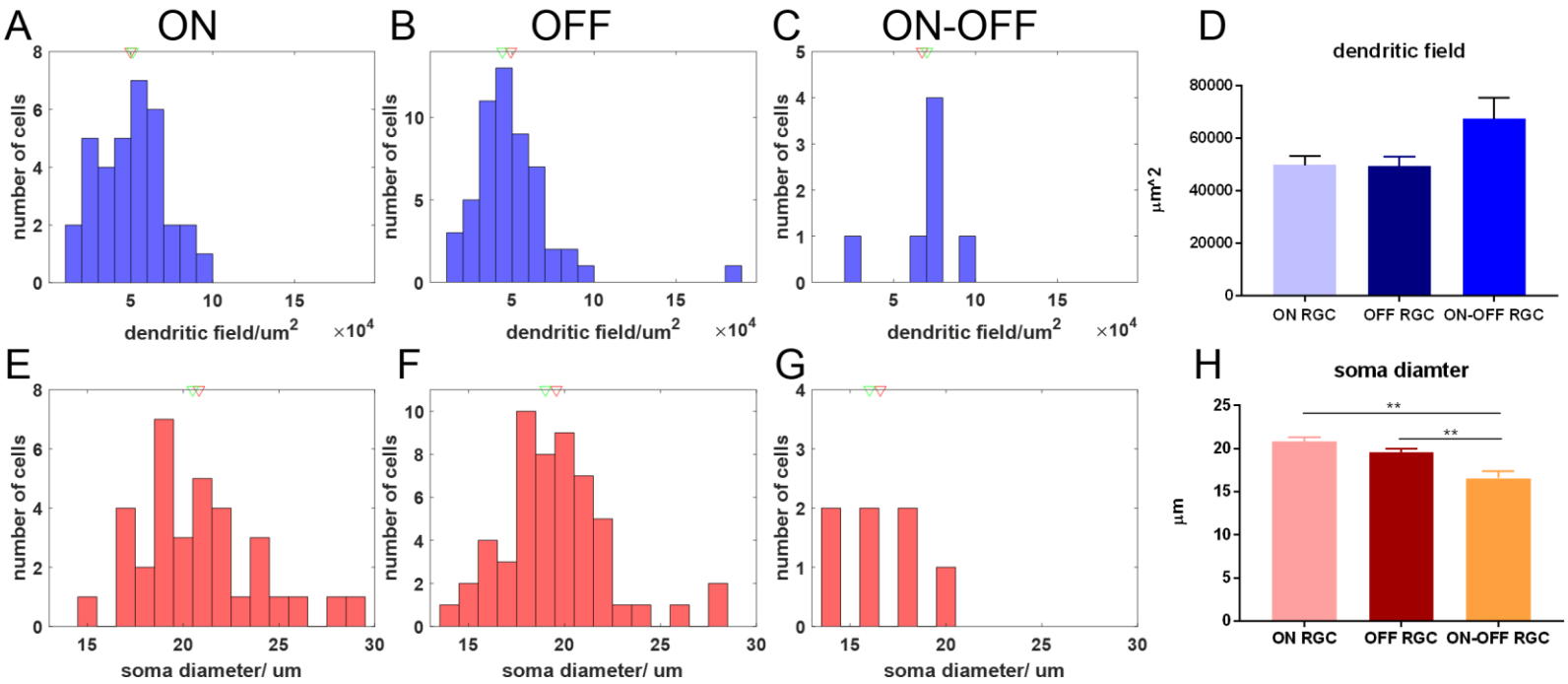

Figure 2.2 Dendritic field and somatic size of αRGCs and ON-OFF RGCs.

[A, B, C] Distribution of dendritic field of αRGCs and ON-OFF RGCs. The x-axis is the dendritic field, y-axis is the number of cells. **[D]** Quantitative summary of the dendritic field of αRGCs. **[E, F, G]** Distribution of soma diameter of α RGCs. The x-axis is soma diameter, y-axis is the number of cells. The red triangle indicates the mean, green triangle indicates the median of soma diameter. **[H]** Quantitative summary of soma diameter of αRGCs. ** indicated significant differences ($p<0.01$).

3.2 Morphology of coupled ACs

Mixtures of Alexa 594 and Popro1 were injected into αRGCs. Popro1 can pass through gap junctions and is visible under the microscope, allowing coupled ACs to be shown in real time and targeted by Neurobiotin. Popro1 also went to other RGCs in some cases. However, they could be differentiated from ACs by the larger soma size. Totally 24 pairs of ON αRGC-AC couplings, 30 pairs of OFF αRGC-AC couplings, and 2 pairs of ON-OFF RGC-AC couplings were observed. Representative morphologies of coupled ACs, their dendritic fields, and soma diameters are shown in **Fig 2.3-2.5**.

The plain and lateral views of the confocal images show close contact of dendrites of RGCs and ACs in sublamina b and a (**Fig 2.3 A, 2.4A, and 2.5A**). The corresponding soma diameter and dendritic field types are shown in **Table 2.2** and **Fig 2.3 B-C**, **2.4 B-C**, **2.5 B-C**.

Comparison of ACs coupled to ON α, OFF α, and ON-OFF RGCs revealed distinct dendritic stratification and contact with corresponding RGCs. Most coupled ACs were widefield with dendritic fields diameter of >500 μm. OFF ACs had a much smaller soma diameter than ON ACs ($p<0.0001$) **(Fig 2.6 A)**. Cx36 was present at the crossover of dendrites of RGCs and coupled ACs (**Fig 2.6 B**).

Table 2.2 Parameters of ACs coupled to RGCs

Coupled cells	Dendritic location	Soma diameter	% wide-field ACs
ACs to ON αRGCs	sublamina b of IPL (location of ON RGCs)	10.99±0.48 μm	90%
ACs to OFF αRGC	sublamina a of IPL (location of OFF RGCs)	8.57±0.19 μm	93%
AC to ON-OFF RGC	both sublamina a and b of IPL	8.8±0.6 μm	Only 2 observed, both wide field

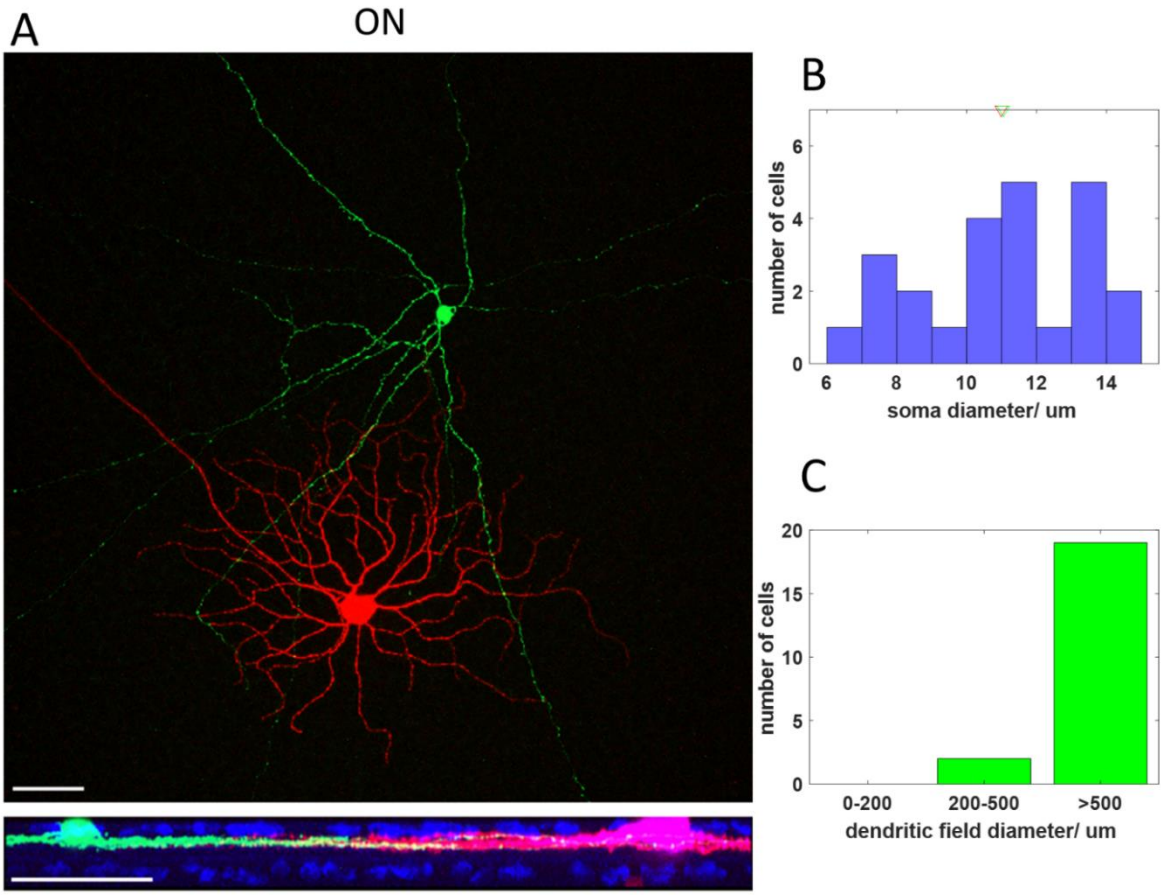

Figure 2.3 Morphology of ACs coupled to ON αRGCs

[A] Representative aerial view and lateral view of an ON αRGC and a coupled AC. RGCs are labeled with Alexa 594 (red), coupled ACs with Neurobiotin (green). The image is a maximum projection of z-stack images by confocal microscopy.

The bars are 50 µm.

[B] Distribution of soma diameters of coupled ACs. Red and green triangles indicate the mean and median of soma diameter, respectively.

[C] Distribution of dendritic field diameter of coupled ACs.

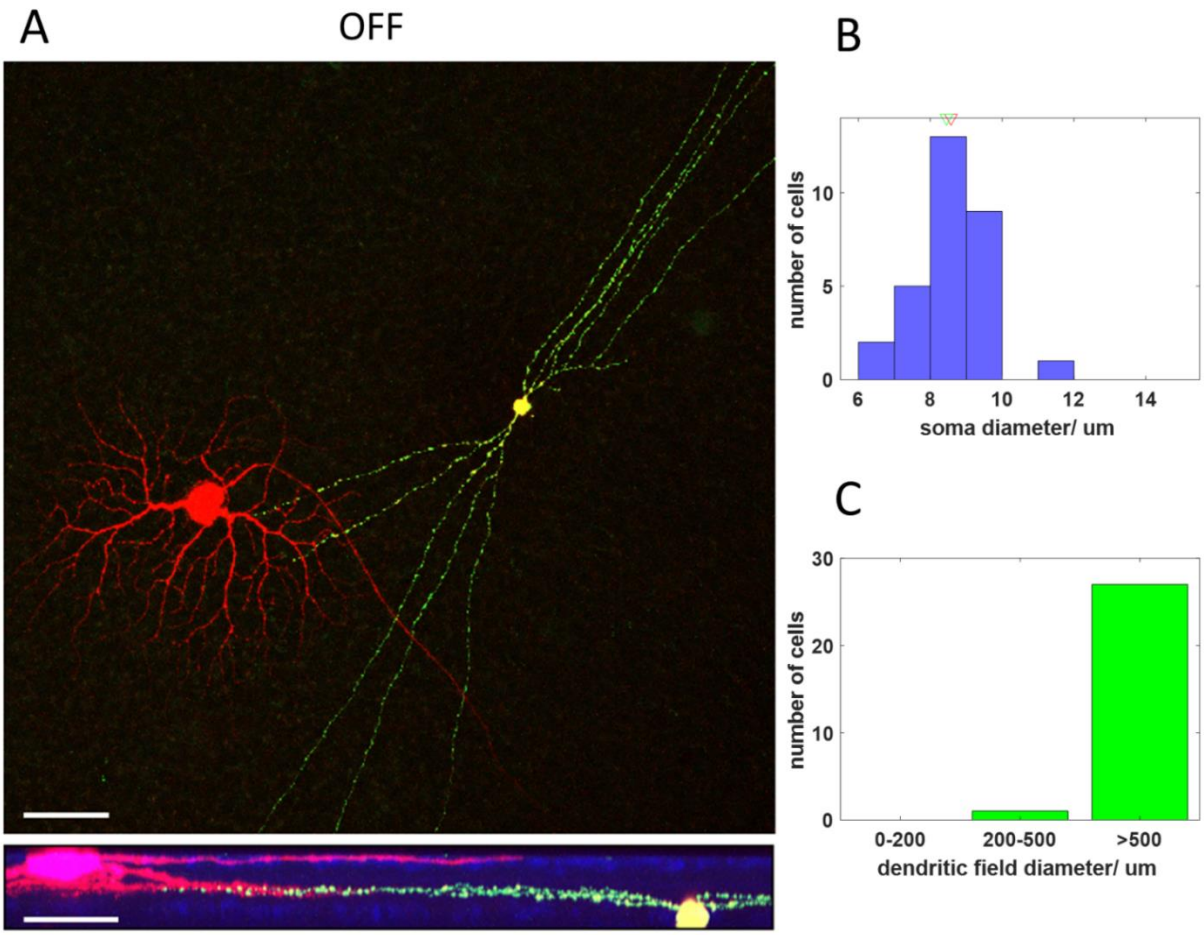

Figure 2.4 Morphology of ACs coupled to OFF αRGCs

[A] Representative aerial view and lateral view of an OFF αRGC (red) and a coupled AC (green). The image is a maximum projection of z-stack images by confocal microscopy. The bars are 50 μm.

[B] Distribution of soma diameter of coupled ACs. Red and green triangles indicate the mean and median of soma diameter, respectively.

[C] Distribution of dendritic field diameter of coupled ACs.

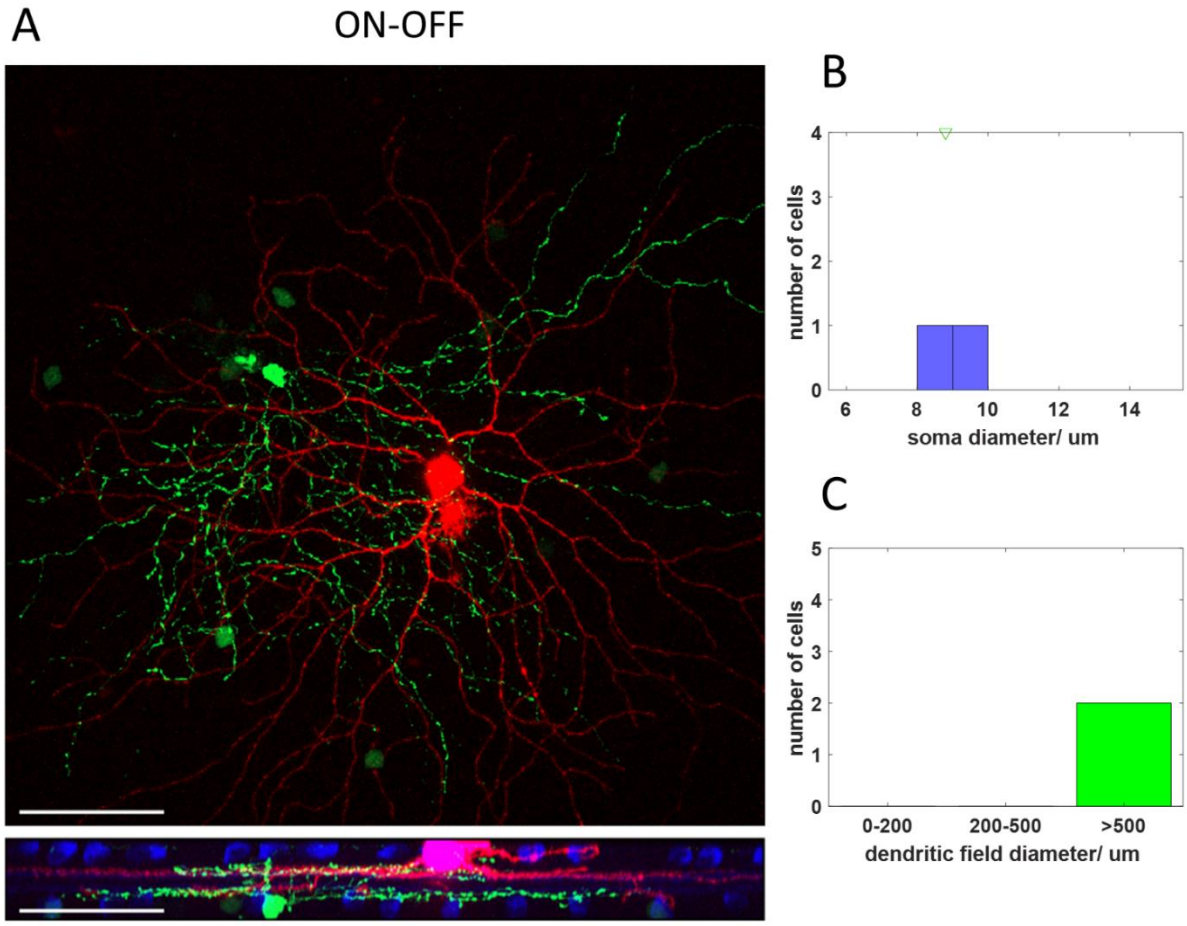

Figure 2.5 Morphology of ACs coupled to ON-OFF RGCs

[A] Representative aerial views and lateral views of ON-OFF RGC (red) and coupled AC (green). The image is a maximum projection of z-stack images by confocal microscopy. The bars are 50 μm.

[B] Distribution of soma diameter of coupled ACs. The green triangle indicates the mean or median of soma diameter.

[C] Distribution of dendritic field diameter of coupled ACs.

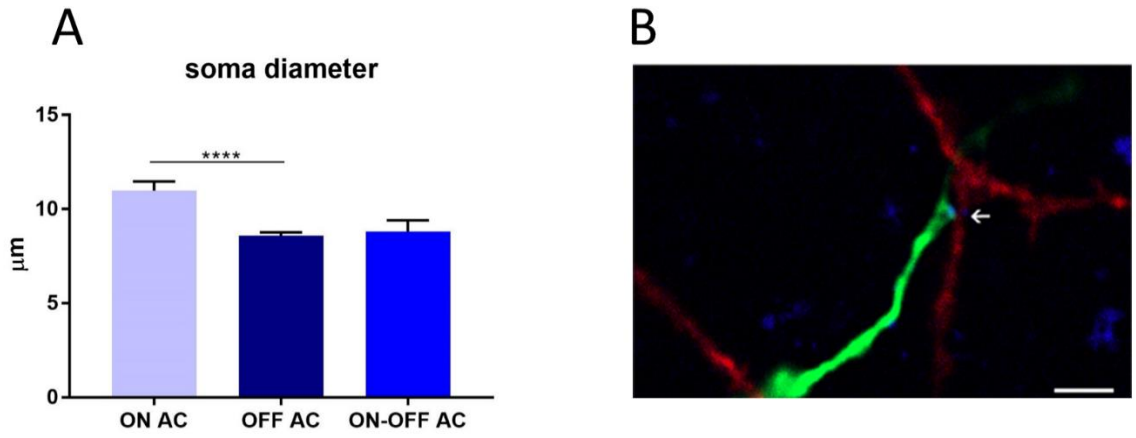

Figure 2.6 Somatic diameter and cross of ACs

[A] Quantitative summary of soma diameter of coupled ACs. **** $p<0.0001$.

[B] Dendritic cross of RGCs (red) and coupled ACs (green). Cx36 is stained as blue dots. The co-localization of the dendritic cross and Cx36 is indicated by the arrowhead.

Scale bar: 2µm.

4. Discussion

4.1 αRGCs are the special type of RGCs

In this study, the KCNG4^{cre} mice crossed with the Ai32 reporter line were used to characterize the morphology of ON α, OFF α, and ON-OFF RGCs. A prior study had demonstrated labeled murine RGCs of the KCNG^{cre} line crossed with other similar reporter lines, in which the labeled cells were primarily αRGCs, including ON-transient/sustained and OFF-transient/sustained subtypes (Krieger et al., 2017). Except for the different properties with respect to ON or OFF response to light with transient or sustained responses, they were similar in other morphological parameters such as soma size and dendritic length, and light response parameters including receptive field, peak spike rate, and spike shape, as well as the molecular signature (Krieger et al., 2017). The current study produced similar results for ON and OFF αRGC, which had similar large soma diameters and dendritic fields. The ON-OFF type had a smaller soma diameter. It was previously reported that αRGCs preferentially resist degeneration (Duan et al., 2015). RGCs are the last surviving neurons in the retina and display pathological changes in many eye diseases, but different types have different morphological and functional properties so they are not comparable. Although there are around 40 types of RGCs, αRGC could be used as a unique type to distinguish the changes in pathological conditions.

4.2 Wide-field ACs are coupled to αRGCs

The morphologies of coupled ACs were also characterized. In addition to the different stratifications in IPL, the ACs coupled to ON αRGCs had larger soma sizes compared with the other two types. Cx36 was found in the connection between αRGCs and ACs.

Most of coupled ACs had dendritic field diameter over 500 μm, which were defined as wide-field ACs. However, various sizes of AC bodies might represent different subtypes. There was a large variety of ACs morphologies in mouse retina (Lin & Masland, 2006). It is known that

wide-field ACs use GABA as the neurotransmitter, giving inhibitory synapses on RGCs. In contrast, wide-field ACs make gap junctions with αRGCs, which is a sign-conserved, excitatory synapse. Therefore, the effect of ACs on RGCs may underlie two sign-reverse mechanisms.

Revealing the morphologies of ACs coupled to RGCs provided the basic knowledge to study the function of the gap junction between RGCs and ACs. The electrical synapses between RGCs and ACs contributed to the synchronous electrical activity of RGCs (Volgyi et al., 2013), which was suggested to be responsible for global object perception (Roy et al., 2017). The concerted activities among RGCs play important functional roles in detection and transfer of visual information (Bloomfield & Volgyi, 2009; Usrey & Reid, 1999). In addition, blocking gap junctions to diminish the “bystander” effect provided neuroprotection in glaucoma and other neurodegenerative disease (O'Brien & Bloomfield, 2018; Ripps, 2002).

Chapter 3 RGCs activities in defocused conditions

1. Introduction

The prevalence of myopia, an eye disorder that affects millions worldwide, has increased rapidly in children and young adults, especially in east Asia (Morgan et al., 2012). Although myopia can be corrected by various methods, the pathological condition cannot be reversed or cured. High myopia leads to increased risks of potentially blinding eye diseases.

Defocus as an environmental factor, is suggested to have a strong relationship with myopia. Animal studies have suggested that optical defocus may regulate eye growth in a sign-dependent manner (Smith Iii & Hung, 1999). Similar conclusions were drawn from animal studies that compensated changes in axial length and choroidal thickness with short-term defocus stimuli (Chiang et al., 2018; Ho et al., 2012; Hoseini-Yazdi et al., 2019; Read et al., 2010). Defocus could also affect human refractive development, although published findings are not consistent about which type of defocus is the causal trigger. Several methods including progressive lenses, which incorporate areas producing myopic defocus, have shown effective results in retarding myopia (Berntsen et al., 2013; Phillips, 2005). In contrast, studies have reported that myopic defocus due to under-correction with spectacles accelerates myopic progression in children (Chung et al., 2002). Overall, the evidence has suggested that defocus plays an important role in myopia, acting as a trigger factor.

As the sensing tissue of the eye, the retina is postulated to sense defocus. ERG scans of human subjects showed sign-dependent results to myopic and hyperopic defocus (Chin et al., 2015; Ho et al., 2012). RGCs are the final neurons of the retina, and they are classified into ON, OFF, and ON-OFF types, which participate in ON and OFF retinal signaling pathways. Studies have reported that ablation of the ON pathway increased susceptibility to myopia (Chakraborty et

al., 2015). Pharmacological inhibition of the ON or OFF response was shown to prevent myopic and hyperopic transference (Crewther & Crewther, 2003). It can be hypothesized that the retina can sense the defocus of an image, via the circuitry of RGC signaling. Previous experiments have demonstrated that defocus could change the light-evoked spike response frequency of single RGCs (Pan, 2019) and RGC population firing patterns (Banerjee et al., 2020). This study was aimed to explore the change of light-evoked excitatory and inhibitory postsynaptic currents, in order to determine the particular mechanism of changing the activity of RGCs.

2. Methods

2.1 Animals

Adult mice (6-8 weeks) C57BL/6J (RRID: IMSR_JAX:000664) of either sex were used in the study. All animal procedures were approved by the Animal Subjects Ethics Sub-Committee of the Hong Kong Polytechnic University.

2.2 Light stimulation and defocus projection

For full-field light stimulation, a green (λ = 525 nm) light-emitting diode (HLMP-CM3A-Z10DD, Broadcom Limited, San Jose, CA) was used to deliver full-field light to the retina. Recordings were performed in dark-adapted conditions. Light intensity was calibrated with a radiometer (S370, UDT Instruments, San Diego, CA, USA) and converted to the estimated time-averaged rate of photoisomerizations per rod per second (Rh*/rod/s), based on an average rod density of 437,000 rods/mm^2 (Jeon et al., 1998b), a quantum efficiency of 0.67 (Penn & Williams, 1984), and the fraction of incident light absorbed by the pigment of 0.2 (DeVries & Baylor, 1995).

For pattern light stimulation, a green light-emitting display (OLEDXL, Olightek, China; 800 × 600-pixel resolution, 85 Hz refresh rate) was used, controlled by an Intel Core Duo computer with a Windows 7 operating system. With the use of a Nikon 40× water-immersion objective (CFI Apo 40× W NIR, NA = 0.8), the area of the retina that received light stimuli was 250 μm in diameter. Pattern stimulus (spatial frequency: 0.002, reversal rate: 10 reversals /min, sinusoidal edge) were generated onto the photoreceptor layer by PsychoPy (PsychoPy, RRID: SCR_006571)(Peirce, 2007). The background light intensity was 700 isomerizations Rh*/rod/s, in which the rod pathway is saturated and only the cone pathway mediated the light response (Borghuis et al., 2013). The details of the light-projected pathway have been published previously (Pan, 2019) and shown in **Fig 3.1**. The 40x immersion lens of the microscope was

moved upwards or downwards to allow the system to project defocused images above or below the outer segments of photoreceptors. It has been reported that 5 μm axial length elongation could induce 1 diopter myopia (Schmucker & Schaeffel, 2004). Therefore, the objective lens was moved 100 μm upwards and downwards to mimic -20D myopic defocus and +20D hyperopic defocus, respectively. The projected images and view of recording were shown in **Fig 3.2**.

2.3 Electrical recording

Recordings were obtained from single RGCs of the mid-peripheral retina. Recordings were performed using an Axopatch 700B amplifier connected to a Digidata 1550B interface and pCLAMP 10 software (Molecular Devices, San Jose, CA). Cells were visualized with near-infrared light (>775nm) at 40x magnification with a Nuvicon tube camera (Dage-MTI, Michigan City, IN) and differential interference optics with a fixed-stage microscope (Eclipse FN 1; Nikon, Tokyo, Japan). The retinas were superfused in a chamber at a rate of 1-1.5 ml/min with Ringer's solution. Electrodes were pulled to 5-7 MΩ resistance and backfilled with the internal solution. Spike trains were recorded digitally at a sampling rate of 10 kHz using Axoscope software. Internal solution: 120mM potassium gluconate, 12 mM KCl, 1 mM MgCl2, 5 mM EGTA, 0.5 mM CaCl2, and 10 mM HEPES (adjusted to pH 7.4). This internal solution was used in experiments to avoid blockage of spiking. Ringer's solution: 120mM NaCl, 5mM KCl, 25mM $NaHCO_3$, 0.8mM Na_2HPO_4, 0.1mM NaH_2PO_4,10mM D-Glucose, 1mM $MgSO_2$ $7H_2O$, 2mM $CaCl_2$, 0.01mM L-Ascorbi (adjusted to pH 7.4)(Bloomfield & Miller, 1982).

The loose patch was used for extracellular recordings, which recorded the spikes of RGCs. The whole-cell recording was used to record the postsynaptic currents of RGCs. In whole-cell recordings, to improve the space clamp, the internal solution contained cesium methanesulfonate (Sigma-Aldrich Cat#C1426) rather than potassium gluconate to block the potassium channel and increase cell impedance. Absolute voltage values were corrected for

11 mV liquid junction potential in the cesium-based intracellular solution. The excitatory and inhibitory current responses were recorded approximately at the chloride or cation equilibrium potentials. The cation currents were recorded when holding the membrane potential at the chloride equilibrium potential, which is -68 mV. This reflects the cation conductance, which is affected by glutamate released via BCs. Thus, the recorded EPSCs reflected the input of BCs to RGCs. Similarly, holding the membrane potential at the cation equilibrium potential, which is 0 mV, to record the chloride currents. The chloride conductance is gated by GABA or glycine released via ACs. The recorded IPSCs reflected the input from ACs.

Data sorting and analysis

Spikes recorded were sorted by an Offline Sorter (Plexon, Dallas, TX) and NeuroExplorer (Nex Technologies, Littleton, MA, USA) software. Rate histograms, PeriEent Histograms, Joint ISI Distribution, Crosscorrelograms functions in NeuroeExplorer were used to obtain spontaneous frequency, response polarity, inter-spike interval distribution, and synchrony patterns. The currents were measured and exported from Calmpfit 10.7 (pClamp, Molecular Device, USA).

2.4 Data analysis

Statistical significance ($P < 0.05$) was determined using the t-test. The results shown are mean ± SEM.

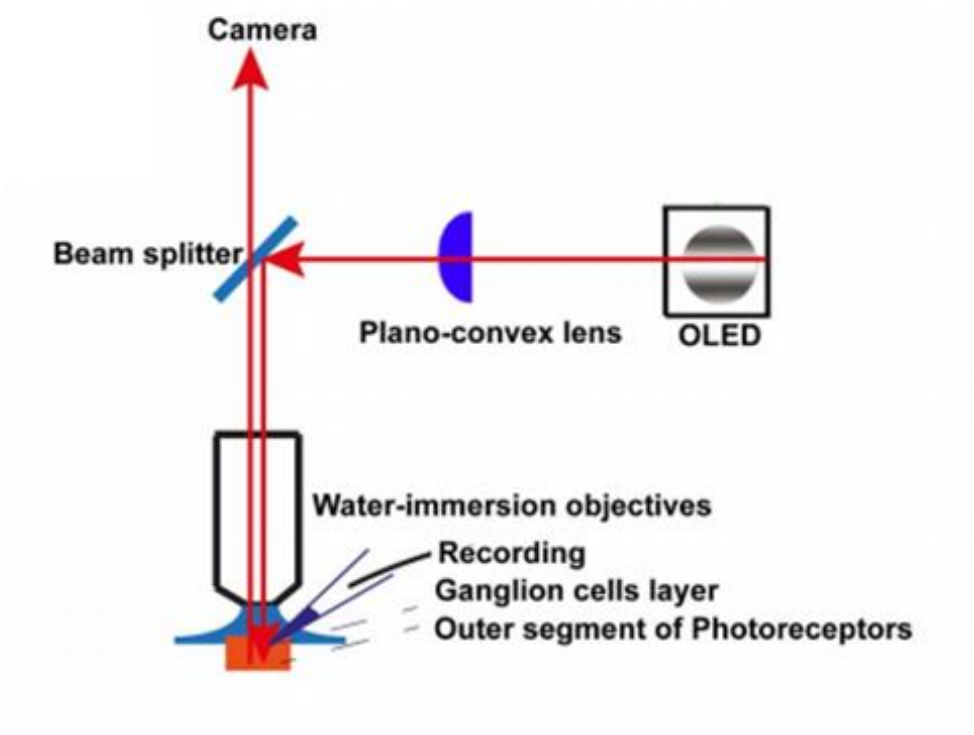

Figure 3.1 Schematic diagram of experimented setup for patterned light stimulation recording.

Patterned visual stimuli emitted from an OLED, projected onto the retina through a plano-convex lens, a beam splitter, and a 40x water immersion objective. The OLED was connected to the screen of a computer, which generated light patterns to show the same images simultaneously. At the same time, the computer generated TTL (transistor-transistor logic) pulses at the onset of the stimulus, which was sent to an Analog-to-Digital converter to synchronize the signals from the light stimulus with the recording computer. It was previously described in (Pan, 2019).

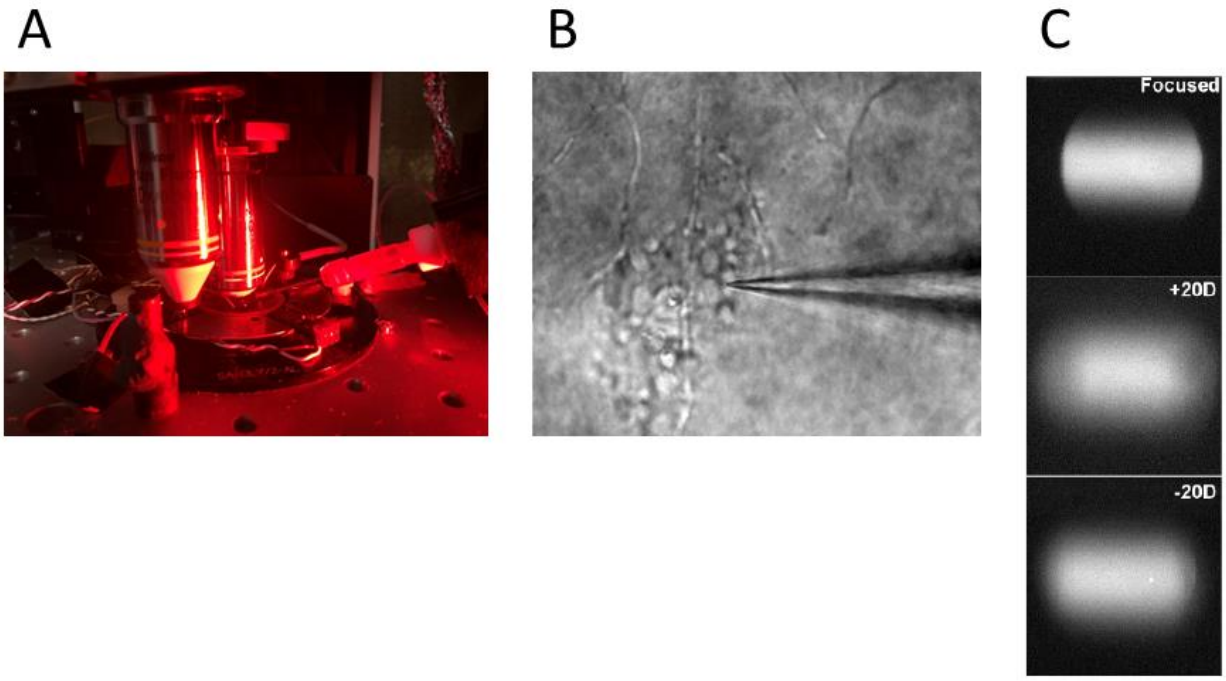

Figure 3.2 Images of patch clamp recording.

[A] 40x water-immersed objective and the recording electrode.

[B] The retina visualized by infrared light.

[C] The focused and defocused pattern stimuli projected on the retina. The image is size is 250 μm in diameter, spatial frequency is 0.002 cycles/degree, light intensity is 5×10^4 Rh*/rod/s.

3. Results

As this study was part of the collaborative work published by my teammate Seema Banerjee in 2020 (Banerjee et al., 2020), only the data about current responses of RGCs were shown here.

3.1 Defocus decreased the amplitude of light-evoked postsynaptic currents in the αRGCs

The representative EPSCs and IPSCs of the three types of RGCs are shown in **Fig3.3 A-C**. The results showed that defocused image projection changed the kinetics of EPSCs and IPSCs of RGCs. **Table 3.1** and **Fig 3.3 D-E** show the quantitative results of ON αRGCs (6 of 11), OFF αRGCs (7 of 9) and ON-OFF RGCs (10 of 13). Defocus stimuli decreased the EPSCs and IPSCs of ON αRGCs and IPSCs of OFF αRGCs. For ON-OFF RGCs, plus defocus decreased EPSCs and minus defocus decreased IPSCs of ON response, both the defocus image decreased EPSCs of OFF response. Defocus affected the ON and OFF response of ON-OFF RGCs in different manners.

Table 3.1 Effect of defocus on current response of RGCs

Cell type	n	Light	Response type	Response (pA)		
				Focus	-20D	+20D
ON αRGC	6	ON	EPSC	142.6 ± 8.9	73.4 ± 1.9**	49.9 ± 5**
			IPSC	375.2 ± 14.5	327.3 ± 3.53**	120.1 ± 3.2**
OFF αRGC	7	OFF	EPSC	235 ± 3.8	197 ± 15	184.5 ± 16.5
			IPSC	346.7 ± 6.8	269.3 ± 8.3*	308.2 ± 8.5**
ON-OFF RGC	10	ON	EPSC	43.7 ± 3	37.6 ± 4	11.7 ± 8.9*
			IPSC	61.3 ± 6.4	25 ± 3*	49.7 ± 0.9
		OFF	EPSC	64.3 ± 2.3	37.9 ± 1.1**	30 ± 4.5**
			IPSC	97.1 ± 1.6	90 ± 5.2	99.3 ± 4.3

**$p<0.01$, * $0.01<p<0.05$

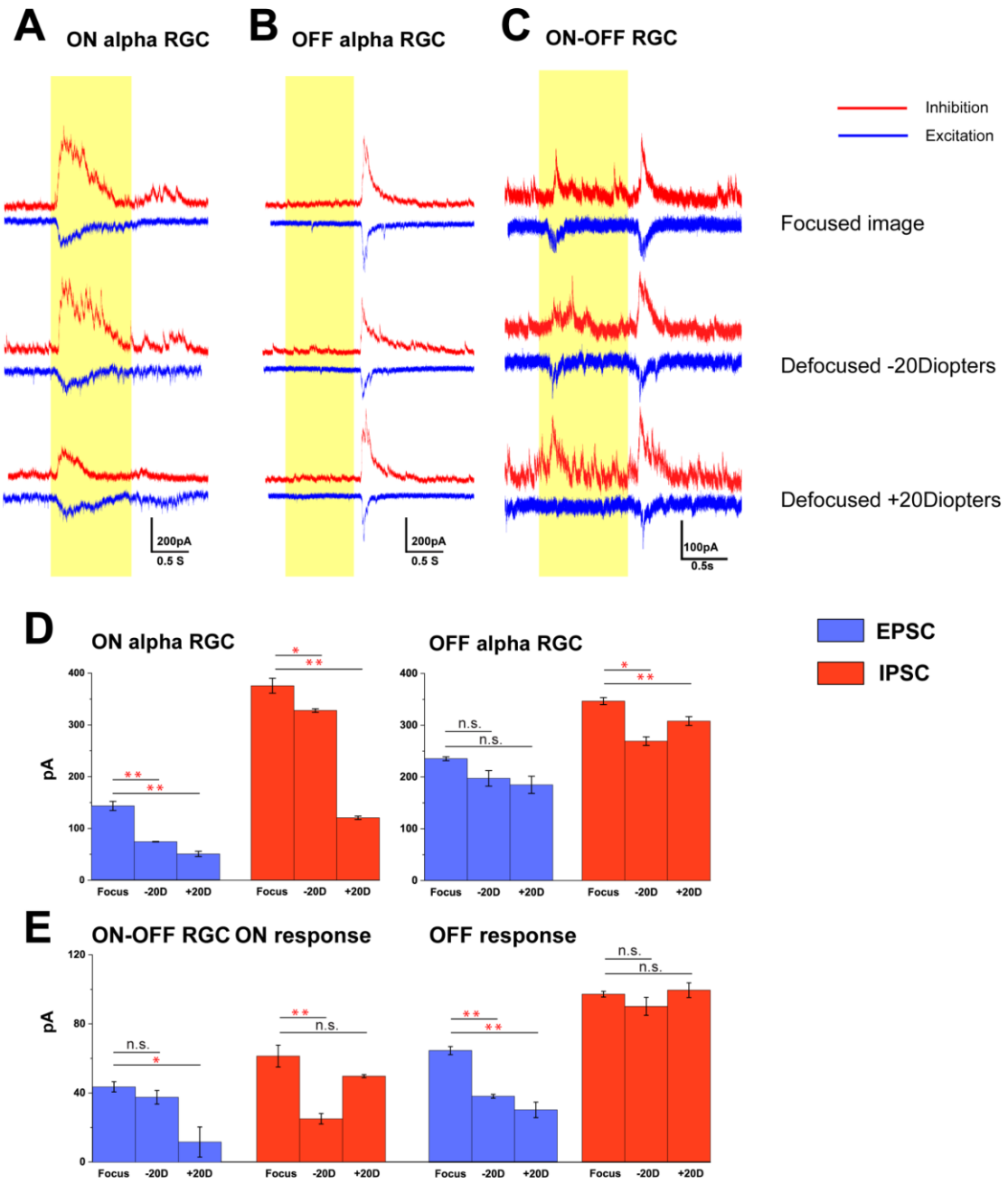

Figure 3.3 Varied responses of αRGCs to focused and defocused images.

[A-C] Inhibitory(red) and excitatory (blue) currents measured in voltage-clamped ON αRGC, OFF αRGC and ON-OFF RGCs, with holding potentials -68mV and 0 mV, in response to focused and defocused images. Light stimuli of 1s, 0.002 cycles/degree light stimuli (light intensity=$5.09*10^4$ Rh*/rod/sec) were projected onto the outer segment of the photoreceptor layer. **[D, E]** Defocused images had significantly different effects on EPSCs and IPSCs responses in these cells. **p<0.01, * 0.01<p<0.05, n.s. p>0.05.

4. Discussion

Defocus is an important factor that breaks the emmetropia progress and induces myopia. After characterization of the morphometry of RGCs, electrical activity changes under defocus conditions were observed. Previous studies had shown that both light-evoked spiking and the populations firing patterns of RGCs changed when defocused images were presented (Banerjee et al., 2020; Pan, 2019). This study aimed to further explore how excitation and inhibition changed in this process.

4.1 RGCs could sense the defocused light stimulus

The results showed that defocus decreased the excitatory input in the current response, except for the OFF αRGCs and ON response of ON-OFF RGCs. Defocus also decreased the inhibitory inputs in both ON and OFF αRGCs, and the ON response of ON-OFF RGCs. Therefore, the overall effect of defocus is to decrease either excitatory or inhibitory input.

In an earlier study, the αRGC spike response to the defocus light stimuli was measured. Although some RGCs responded to minus and plus defocus differently, the overall tendency of change suggested that defocused images decreased the light-evoked spike response (Pan, 2019). This indicated that the decreased spike response may be attributable to the decrease of excitatory and inhibitory synaptic currents.

It should be noted that the defocus in this study could change the light intensity. A prior study demonstrated that for 0.002 cycles/degree image, -20 D to +20 D defocus led to an increase of light intensity from 4.95×10^4 to 5.15×10^4 Rh*/rod/sec (Pan, 2019). Alpha RGCs were shown to be low-intermediate sensitivity RGCs whose light response was saturated by more than 10^3 Rh*/rod/sec (Pan et al., 2016). Therefore, the change of light intensity by defocus should not interfere with the light response in αRGCs.

Studies have been conducted to reveal the connection between myopia and the retina, including

retinal neurotransmitters and circuitry. Presence of dopamine (Stone et al., 1989), retinal vasoactive intestinal polypeptide (Stone et al., 1988), and retinoic acid (Mertz & Wallman, 2000) in the retina have all been revealed to affect eye growth. It was indicated that ON and OFF retinal pathways were implicated with emmetropization in a sign-dependent manner (Crewther & Crewther, 2003), and ablation of the ON pathway leads to susceptibility of myopia (Chakraborty et al., 2015). These findings suggested the important effect of retinal signaling on myopia. In addition, RGCs were suggested to be useful to study the relationship between defocus and the etiology of myopia. ON-delayed RGCs were implicated as defocus detectors in the mouse retina (Baden et al., 2017; Mani & Schwartz, 2017). The current study has demonstrated that spikes and currents activity of both ON and OFF cells were changed under plus or minus defocus, with ON cells having a more obvious change in EPSCs. However, an obvious sign-dependent change was not observed. The ON response of ON-OFF RGCs showed diverse responses to plus and minus defocus. Previous MEA study found that ON-OFF RGCs showed diverse number of responded cells to plus and minus defocus, suggesting the potential role to differentiate focused and defocused image (Banerjee et al., 2020).

In respect of the mechanism of how the RGCs decode the defocus stimulus, previous research has indicated that the retina senses the defocus by RGCs changing their polarities to light (Banerjee et al., 2020). Another intriguing study showed ON-delay RGC could decode the stimulus size and was shown to be the most sensitive type in elevating their response with increasing blur (Mani & Schwartz, 2017). The response changes were different from this study. Noticeably, half of the tested cells including OFF αRGC could not differentiate the blur in Mani et al's study, and the method used to produce defocus was texture blur. It is well known that defocus results in blur images, affecting spatial frequency and edge sharpness. Projecting texture blur could study the effect from reduced spatial frequency with invariant light intensity. However, the retina not only encodes the blur, but also the sign of defocus. How the defocus is

detected by the retina is complicated and elusive (Burge & Geisler, 2011). Thus, imposing defocus images by microscope in this study aimed to mimic the lens-induced plus and minus defocus, providing access to study the sign-dependent manner.

4.2 Defocus effect on RGCs in vivo and ex vivo study

The effect of defocus to eye growth has been widely investigated in vivo, among animals and humans (Read et al., 2010; Smith Iii & Hung, 1999). Previous studies strived to clarify which factors take the roles in this process. One of the important questions is if the brain is required in emmetropization. Studies indicated that myopia could still be induced with optic nerve section (Troilo et al., 1987), and regional elongation of the eyeball could be induced by local blur (Rada et al., 2006). However, other studies also suggested intact optic nerve was required for normal bidirectional emmetropization (Wildsoet, 2003), and retinal ZENK expression became unrelated to sign of defocus in isolated eyes (Bitzer & Schaeffel, 2006). The other question underlies the alert conditions of subjects. The eye growth and ZENK expression did not change under general anesthesia in chicks, suggesting some factors except optic nerve in alert conditions were involved in myopia progression (Bitzer & Schaeffel, 2006). However, considerations about the variations among species should be raised when reviewing myopic mechanisms. The conclusions draw from chicks might not be applied to human.

Retinal function under defocus were studied via ERG. In humans, sign-dependent changes of ERG were shown after short-term defocus (Ho et al., 2012), the inner retina seems to be less sensitive (Chin et al., 2015). In chicks, plus and minus defocus reduced the pattern ERG (Ostrin et al., 2016). A recent study reported unchanged ERG in form deprivation mouse model (Sridhar et al., 2020), but how ERG changes under defocus conditions is unclear in mice.

RGCs are the output neurons of the retina, should reflect the retinal functional changes. However, the studies about the role of RGCs in defocus were not enough. It is still not clear that if RGCs electrical activity ex vivo could reflect the changes under defocus in vivo. Our

study investigated RGCs' activities under defocus and found decreased electrical spiking activity. This matched part of the ERG results in human and chicks, and suggested that electrical activities of RGCs ex vivo might also reflect the changes under defocus in vivo. However, as there was no ERG recording under defocus in mice conducted before, more experiments should be performed to verify the validation between the defocus effect to RGCs ex vivo and in vivo.

5. Conclusion and Further Study

This study found that defocused stimuli decreased input currents of some ON α, OFF α, and ON-OFF RGCs. It partially explained the reason for decreased spiking activity of RGCs by defocus observed before (Pan, 2019), indicating retinal functional changes under defocus in ex vivo preparation.

In the future, we would like to investigate the effect of defocus on specific type of RGCs, and the molecular changes involved in this process. ON-OFF RGCs may be the target cells. ON-OFF RGCs have double stratified dendrites in IPL. They have advantages in anatomy to detect different defocus planes in the retina. EPSCs of ON responses in ON-OFF RGCs showed diverse changes to different powers of defocus in this study. ON-OFF RGCs also showed diverse cell numbers responded to plus and minus defocused images (Banerjee et al., 2020). In addition, ON-OFF RGCs have the property of direction selectivity (Weng et al., 2005). We hypothesized ON-OFF RGCs might have different responses in vertical directions, and they might relate to eye movement, which was suggested to be an important role in myopia formation (Bitzer & Schaeffel, 2006). Therefore, we would like to focus on the electrical activity of ON-OFF RGCs under focused and defocused conditions.

Chapter 4 The effect of low-dose atropine on αRGC signaling

1. Introduction

Myopia affects a large proportion of the population worldwide, and high myopia increases the risk of severe eye diseases. Atropine has been demonstrated to reduce myopia progression (Chua et al., 2006). Low-dose (0.01% - 1%) atropine has been used for myopia control in clinical trials.

However, the mechanism of myopia control by topical atropine is not clear. Atropine is an antagonist for muscarinic acetylcholine (ACh) receptors. It was firstly used as a cycloplegic drug, which can block ciliary muscles contraction and reduce accommodation of the eye. However, the effect through accommodation to control myopia by atropine had been excluded by numerous animal studies. For example, myopia could still be developed in chicks with damaged accommodative pathway (Schaeffel et al., 1990; Wildsoet, 2003). Atropine could control myopia in chicks which accommodation is mediated by nicotinic ACh receptors rather than muscarinic receptors, and could be achieved via intravitreal injection (McBrien et al., 1993). It was postulated that retinal and scleral muscarinic receptors were related to myopia prevention effect of atropine. Muscarinic and nicotinic receptors have been demonstrated to affect light-evoked responses of RGCs (Reed et al., 2002; Strang et al., 2010).

However, it is not clear whether topical application of atropine would affect retinal function. A study reported topical application of atropine for two years did not change the mfERG in children (Luu et al., 2005). Myopic children have a longitudinal decrease of cone function, which was not affected by atropine (Chia et al., 2013). Another study demonstrated the effect of atropine on ERG of the peripheral retinal to defocus stimuli in humans (Khanal et al., 2019). A proteomics study in mice indicated that GABA receptors decreased after atropine application

(Barathi et al., 2014).

As the previous study revealed that defocused images changed multineuronal firing patterns and signaling of RGCs in mice, suggesting that RGC-involved retinal circuitry has a close relationship with defocus. Therefore, it would be interesting to investigate whether atropine affects RGCs signaling, and if these changes have a relationship with myopia progress.

It has been demonstrated that the concentration in the vitreous humor of rabbits 24h after application of 1% topical atropine is 0.4 μM (Wang et al., 2019). In the current study, 0.05-500 μM atropine sulfate was applied to αRGCs, and light-evoked response, spontaneous spike, and concerted activity were tested. The results indicated that concentrations lower than 50 μM atropine did not have much effect on the electrical activity of RGCs. However, ON responses were induced from more than 25% of OFF αRGCs after application of atropine. This unmasked ON signals may be attributed to decrease of GABA via gap junctions by using exogenous GABA and Cx36-knockout mice.

2. Methods

2.1 Animals

Adult (4-8weeks) C57BL/6J (RRID: IMSR_JAX:000664) mice of either sex (n=56) and homozygous Cx36-knockout mice (RRID: MGI:3810172) (6-8weeks) were used. Cx36-knockout mice first generated in Prof David Paul's laboratory, Harvard Medical School, were a kind gift from Samuel M. Wu, Baylor College of Medicine. Cx36-knockout mice were tested by genotyping to select homozygous animals.

2.2 Immunohistochemistry

Primary antibodies used were choline acetyltransferase antibody (ChAT, goat anti-ChAT, 1:500; Millipore; Cat# AB144P, RRID: AB_2079751). Image acquisition and analysis were the same as mentioned above.

2.3 Electrical recording

Extracellular recordings and whole-cell recordings were obtained from single RGCs from the mid-peripheral retina. In wide-type C57BL retina, αRGCs were recognized as the cells with largest soma size (around 20 μm in diameter) in GCL.

Spikes analysis

Spikes recorded were sorted by an Offline Sorter (Plexon, Dallas, TX) software and transfer to NeuroExplorer software (Nex Technologies, Littleton, MA, USA). Peristimulus time histograms (PSTHs) were plotted through "PeriEvent Histogram" function of NeuroExplorer, which showed spike frequency (spike/second) of one single RGC to the time (second). Light was on at 0 second and lasted for 1 second (indicated by yellow bar in figures). Quantity of "Light-evoked spike response" was determined by the maximum spike frequency at 0 or 1 second (onset or offset of light). "Joint inter-spike interval (ISI) distribution" was plotted via "Joint ISI Distribution" function of NeuroExplorer which showed the duration of preceding ISI

to the subsequent ISI. The ISI distribution threshold was determined by the edge of most clustering dots manually. “Synchrony patterns” between two neurons were plotted via “Cross-correlograms” function which showed probability or frequency over the time. “Shift predictor” was applied to exclude effect from light stimuli. The probability of correlograms more than confidence line (95%) indicated the firing activities between two cells were significantly synchronized. “Mean spike frequency” was calculated in “Rate histogram” function.

2.4 Pharmacological application of Atropine and GABA

Atropine sulfate salt monohydrate (Sigma-Aldrich, St. Louis, MO; Cat# A-0257, molecular weight 694.83) was used for immersion and recording. Enucleated eyes were immersed with the cornea side down to the level of the ciliary body in atropine sulfate diluted in Ringer’s solution to 800uM (equal to 0.05% atropine) for 30 min. Control eyes were immersed in Ringer’s solution. Subsequently, the retinas of both groups were isolated for targeted mass spectrometry. For electrical recording, atropine sulfate was diluted in Ringer’s solution at concentrations ranging from 0.05 μM to 500 μM.

1mM γ-Aminobutyric acid (GABA, Sigma-Aldrich Cat# A2129) was puffed using a Picospritzer III intracellular microinjection dispenser system connected to a patch pipette (resistance, 6–18 MΩ). Puff application of Ringer's solution did not evoke detectable responses in RGCs.

3. Results

3.1 Atropine had no noticeable effects on the morphology of ON and OFF αRGCs

Approximately 2μM atropine was detected in the mouse retina after applying 800μM (0.05%) atropine to the external ocular surface for 30 min. Considering that clinical application of 0.05% atropine eye drops would be diluted over time due to tear flow, retinas were immersed in 1μM atropine for 30 minutes, and morphologies of ON and OFF αRGCs were revealed by Neurobiotin.

The morphometry of ON and OFF αRGCs with and without atropine treatment is shown in **Table 4.1**; **Fig 4.1**. Application of atropine did not affect the stratification, soma diameter, or the dendritic field diameters of either ON or OFF αRGCs (**Table 1.4; Fig 4.1 B-C**). There was no statistically significant difference in the classes (**Fig 4.1E**) or numbers of dendrite branching (**Fig 4.1 F**) of ON or OFF αRGCs. In summary, the application of 1 μM atropine for 30 minutes had no noticeable effect on the morphologies of the ON and OFF αRGCs.

Table 4.1. Effects of 1 µM atropine on morphometry of ON and OFF αRGCs

Cell type	Dendritic field diameter (µm)			Soma diameter (µm)			Classes of dendrite branching			Number of dendrite branching		
	Atropine	**Control**	**p**	**Atropine**	**Control**	**p**	**Atropine**	**Control**	**p**	**Atropine**	**Control**	**p**
ON αRGCs	205.6 ± 10.6 n=4	203 ± 13.9 n=6	0.73	18.08 ± 0.62 n = 4	18.12 ± 0.49 n = 6	0.97	8.5 ± 1.2 n = 4	8.3 ± 0.7 n = 6	0.89	73.6 ± 5 n = 4	63.9 ± 5.2 n = 6	0.72
OFF αRGCs	172.6 ± 16.6 n = 4	173.7 ± 8.8 n = 4	0.91	17.22 ± 0.3 n =4	17.1 ± 0.33 n = 4	0.79	10 ± 0.4 n = 4	9.8± 0.8 n = 6	0.88	73.6 ± 5 n = 4	85.6 ± 5.9 n = 6	0.15

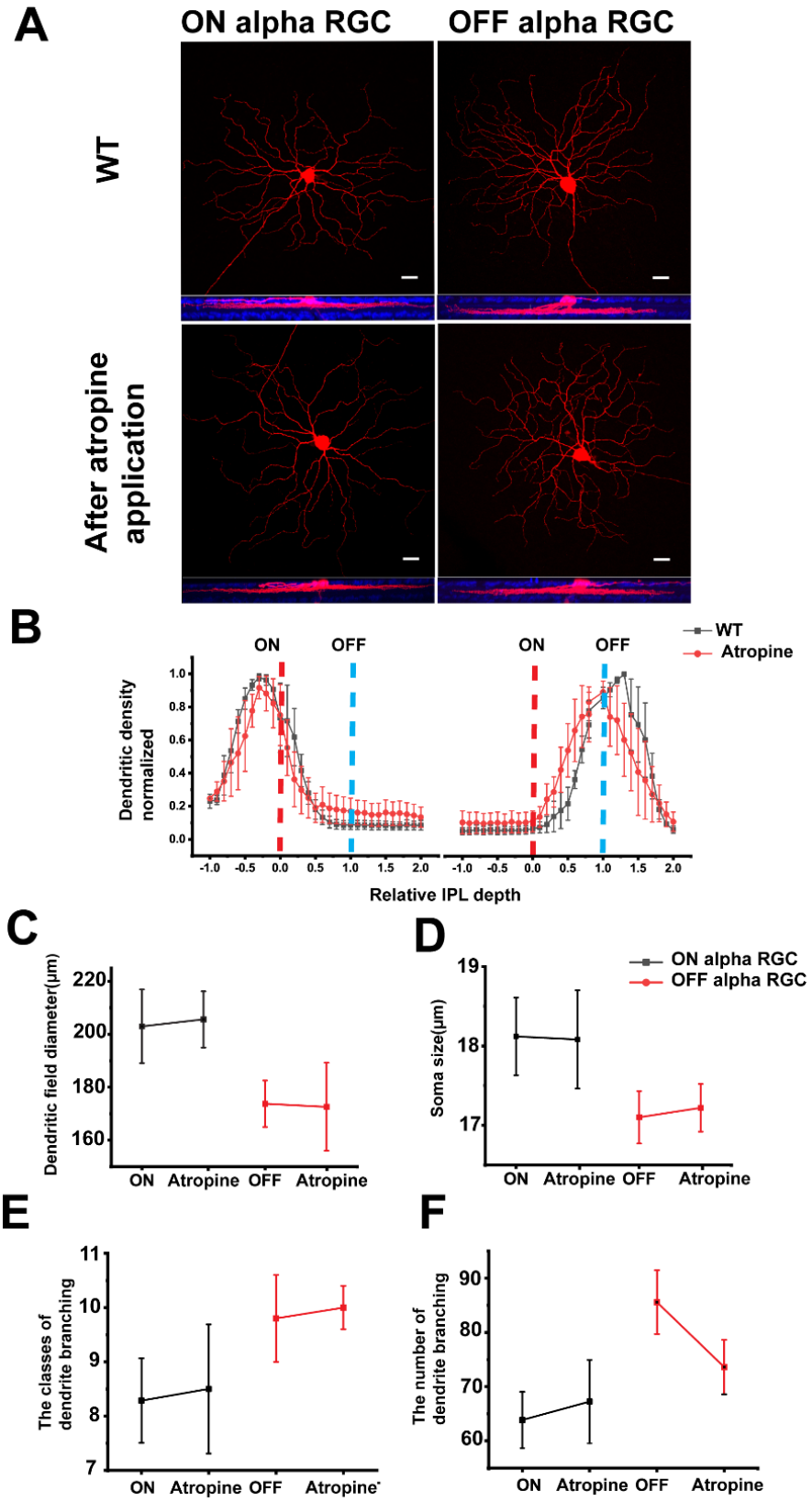

Figure 4.1 Morphology of αRGCs with and without atropine

[A] Aerial views and lateral views of the ON and OFF αRGCs filled by Neurobiotin (red).

ChAT (blue) was used to differentiate the ON and OFF layers of IPL.

[B] Dendritic stratification of ON and OFF αRGCs with and without 1 μM atropine application.

[C-F] Comparisons of dendritic field diameter, soma size, the classes of dendrite branching, and the number of terminal branches between atropine or control applications. Comparison between control and atropine groups, $p > 0.05$, Mann-Whitney U test, ON αRGCs: n=4, OFF αRGCs: n=6.

3.2 Dose-dependent inhibition of atropine on the light-evoked responses of ON and OFF αRGCs

To investigate the effects of relatively high concentrations of atropine to mimic extreme clinical situations like broken corneal barrier, 100, 300, and 500 μM atropine were applied. The light-evoked spike responses of ON or OFF αRGCs were measured as maximum spike frequency at "ON" or "OFF" of the light stimuli, respectively. The light-evoked spike responses did not significantly change after application of 100 μM atropine. However, 300 μM atropine significantly decreased light-evoked spike responses in ON cells. When the concentration was increased to 500 μM, the light-evoked spike responses almost disappeared in both ON and OFF cells. Washing for 5 min recovered the light-evoked spike responses of OFF cells but not ON cells (**Table 4.1**; **Fig 4.2 A-K**).

Table 4.1 Dose-dependent Effect of Atropine on Light-evoked Spike Frequency

	Spike Frequency after Normalization (mean ± SEM)				
	Atropine Concentration				
Cell Type	Vehicle Control	100 μM	300 μM	500 μM	After washing (5 min)
ON αRGCs n=5	1	0.94± 0.18 p = 0.76	0.57 ± 0.1 p = 0.048	0.22 ± 0.08 p = 0.001	0.37 ± 0.02 p = 0.001
OFF αRGCs n=7	1	1.01± 0.12 p = 0.93	0.81± 0.17 p = 0.33	0.34 ± 0.04 p = 0.004	1.05 ± 0.1 p = 0.69

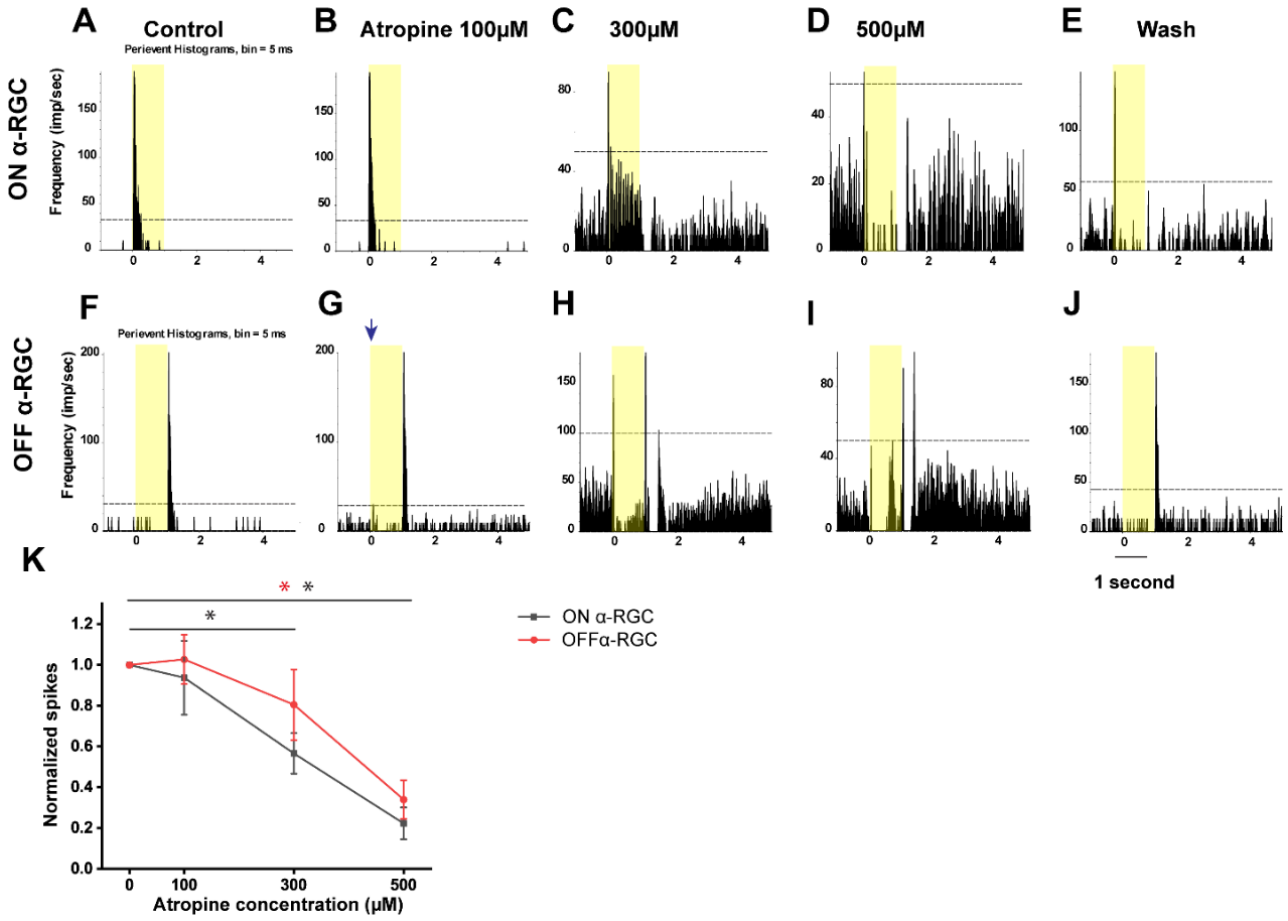

Figure 4.2 Dose-dependent effects of atropine on light responses of αRGCs

[A-E] Peristimulus time histograms (PSTHs) of light-evoked responses of ON αRGCs in control, 100µM, 300µM, 500µM atropine and washing for 5 minutes, respectively. The yellow bar indicated the presence of full-field light stimulation. The dotted line represents 99% confidence of which correlations are above chance.

[F-J] Light responses of OFF αRGCs in the same conditions as upper ON cell.

[K] Quantitative summary of normalized spike frequency of ON and OFF αRGCs to increasing concentration of atropine. Comparison to control condition (0 µM), * $p<0.05$, Wilcoxon signed-rank test; ON αRGC: n=5; OFF αRGC: n=7.

3.3 Time- and concentration-dependent effects of atropine on ON and OFF αRGCs

The concentration of atropine eye drops used in clinical trials has ranged from 0.01% to 1%. As the previous experiment indicated there may be a three-log unit drop from the external to the retinal concentration, the tested concentration was as low as 0.05 μM, and increased to 0.5 μM, 10 μM, and 100 μM, respectively.

The time-dependent light-evoked spike responses were recorded in ON and OFF αRGCs. For concentrations of 100 μM and 10 μM, the light-evoked spike responses of αRGCs showed no significant difference over time. Interestingly, an ON response was induced in 78% (7 of 9) and 62.5% (5 of 8) OFF αRGC after 5 min exposure to 100 μM and 10 μM atropine, respectively (**Fig. 4.3 and 4.4**). Application of 0.5 μM and 0.05 μM atropine had even less effect on the spike frequency of the ON and OFF αRGCs over time. Once again some OFF αRGCs, 33% (2 of 6) and 28.6% (2 of 7), showed an ON response after exposure to 0.5 and 0.05 μM atropine for 5 min, respectively (**Fig. 4.5, 4.6, 4.7**). The value of normalized light-evoked spike frequency was listed in **Table 4.2**.

Table 4.2 Effect of Low-dose Atropine on Light-evoked Spike Responses

Cell Type	n	Concentration (μM)	Normalized Spike Frequency (spikes/s)		
			1 min	3 min	5 min
ON αRGC	5	0.05	0.92 ± 0.05 p = 0.27	0.96 ± 0.05 p = 0.39	1.06 ± 0.1 p = 0.58
	7	0.5	1.05± 0.05 p = 0.27	0.94 ± 0.07 p = 0.42	0.81 ± 0.1 p = 0.11
	6	10	1.02 ± 0.15 p = 0.9	0.95 ± 0.06 p = 0.47	0.85 ± 0.06 p = 0.06
	5	100	0.89 ± 0.12 p = 0.42	0.79 ± 0.03 p = 0.10	0.77 ± 0.02 p = 0.09
OFF αRGC	7	0.05	1.07 ± 0.08 p = 0.41	0.98 ± 0.08 p = 0.81	0.9 ± 0.08 p = 0.29*
	6	0.5	1.1 ± 0.07 p = 0.19	0.95 ± 0.03 p = 0.1	0.89 ± 0.05 p = 0.28*
	8	10	0.95 ± 0.06 p = 0.44	0.88 ± 0.07 p = 0.14	0.88 ± 0.06 p = 0.13*
	9	100	0.86 ± 0.06 p = 0.06	0.88 ± 0.06 p = 0.06	0.86 ± 0.08 p = 0.06*

*A percentage of cells displayed an ON response (see text)

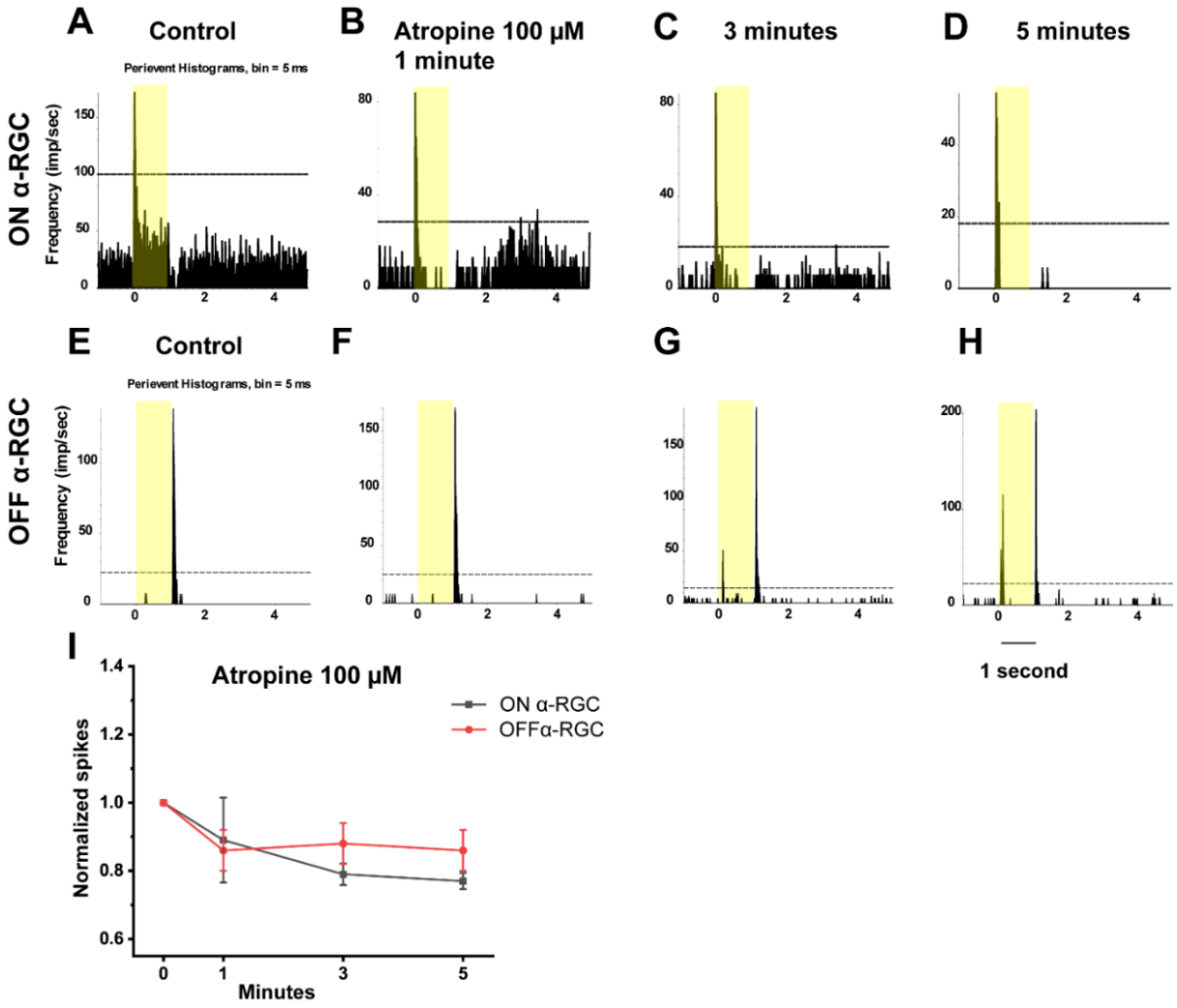

Figure 4.3 Effects of 100 µM atropine on light-evoked spike responses of αRGCs

[A-D] The light-evoked PSTHs of ON αRGCs in Ringer's solution, 100µM atropine for 1, 3, 5 minutes, respectively.

[E-H] The light-evoked PSTHs of OFF αRGCs in the same condition described above.

[I] A graph summarizing the normalized spikes of ON and OFF αRGCs to the time of 100µM atropine application.

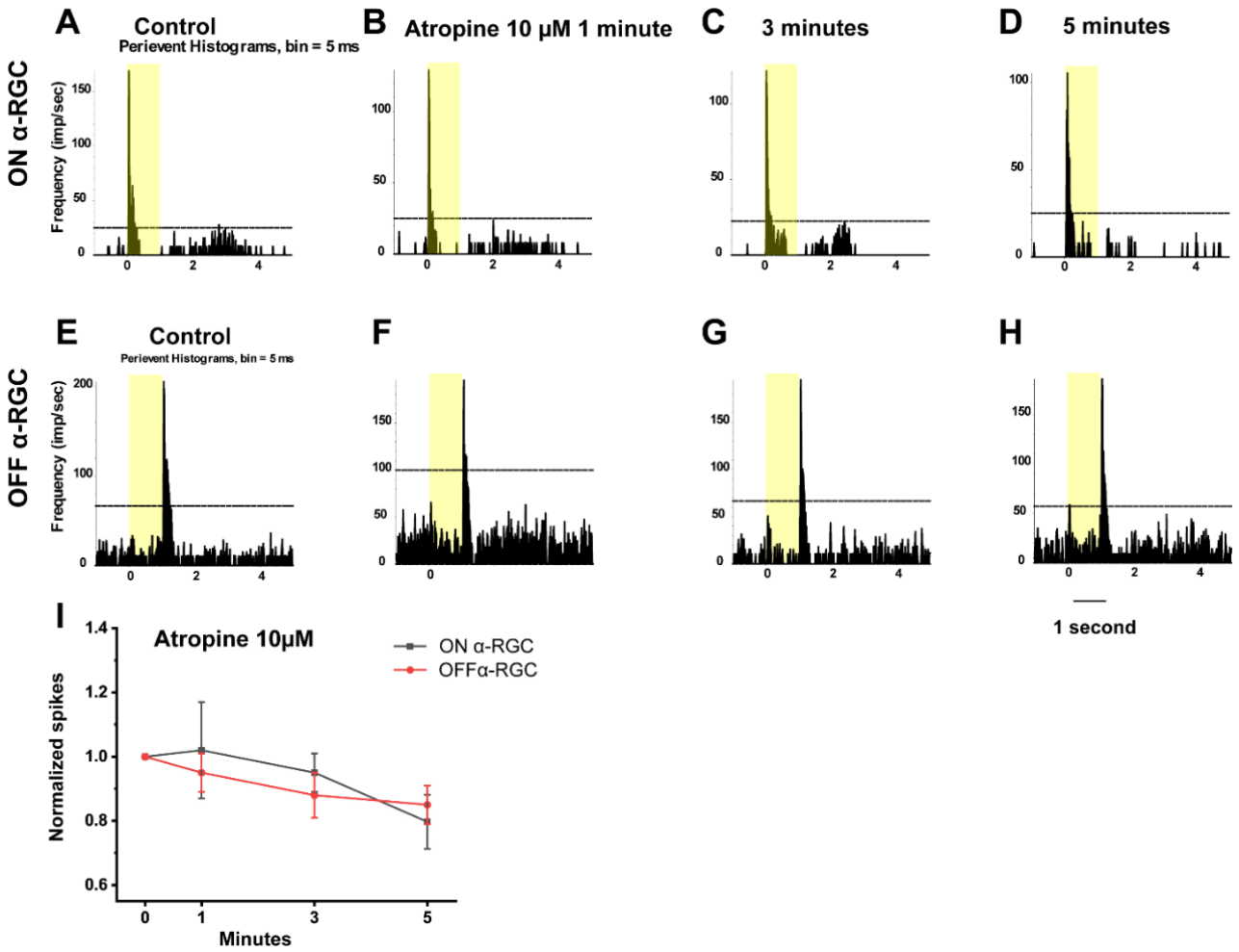

Figure 4.4 Effects of 10 µM atropine on light-evoked spike responses of αRGCs

[A-D] The light-evoked PSTHs of ON αRGCs in Ringer's solution, 10µM atropine for 1, 3, 5 minutes, respectively.

[E-H] PSTHs of OFF αRGCs in the same conditions described above.

[I] A graph summarizing the normalized spikes of ON and OFF αRGCs to the time of 10 µM atropine application.

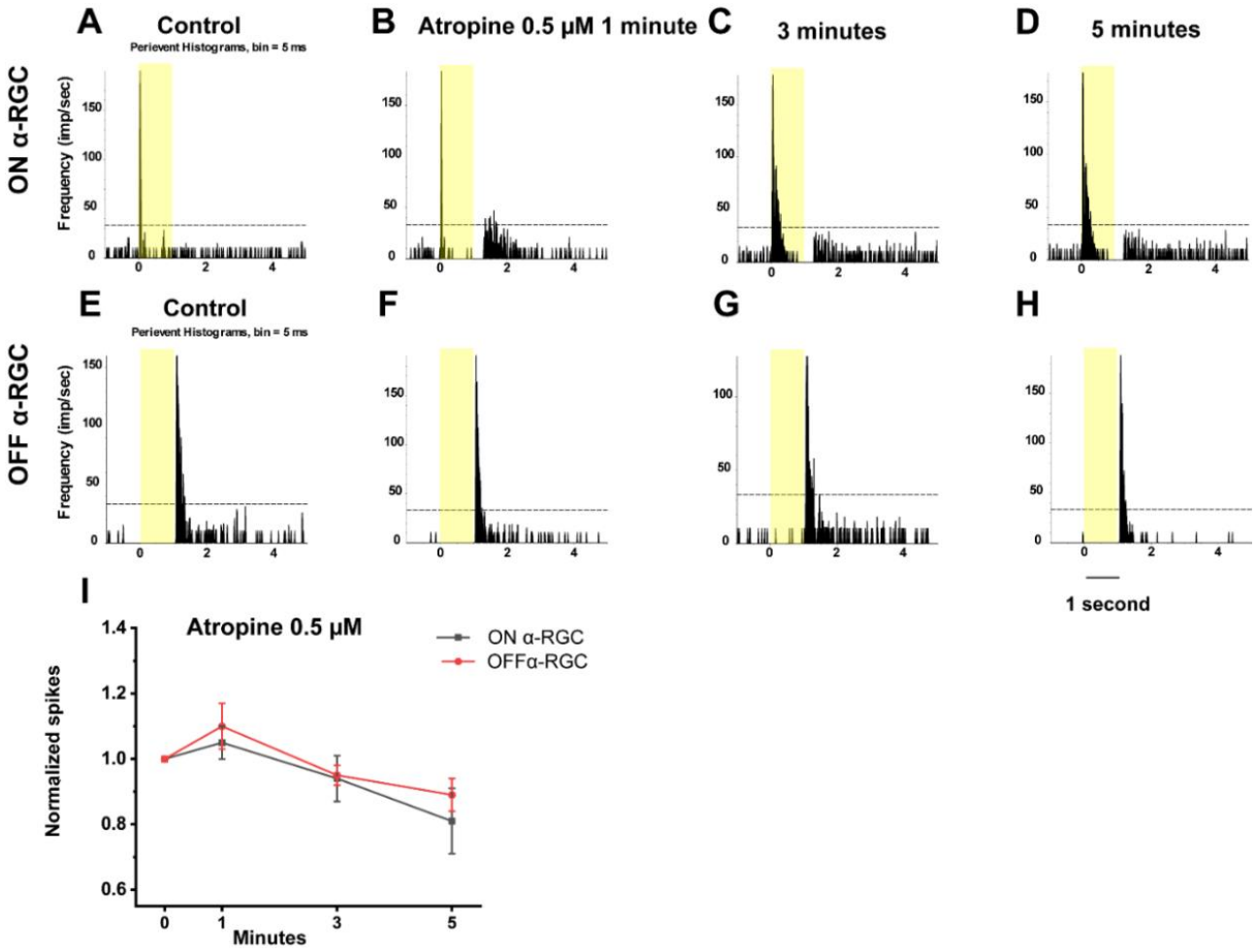

Figure 4.5 Effects of 0.5 µM atropine on light-evoked spike responses of αRGCs

[A-D] The light-evoked PSTHs of ON αRGCs in Ringer's solution, 0.5µM atropine for 1, 3, 5 minutes, respectively.

[E-H] PSTHs of OFF αRGCs in the same condition described above.

[I] A graph summarizing the normalized spikes of ON and OFF αRGCs to the time of 0.5 µM atropine application.

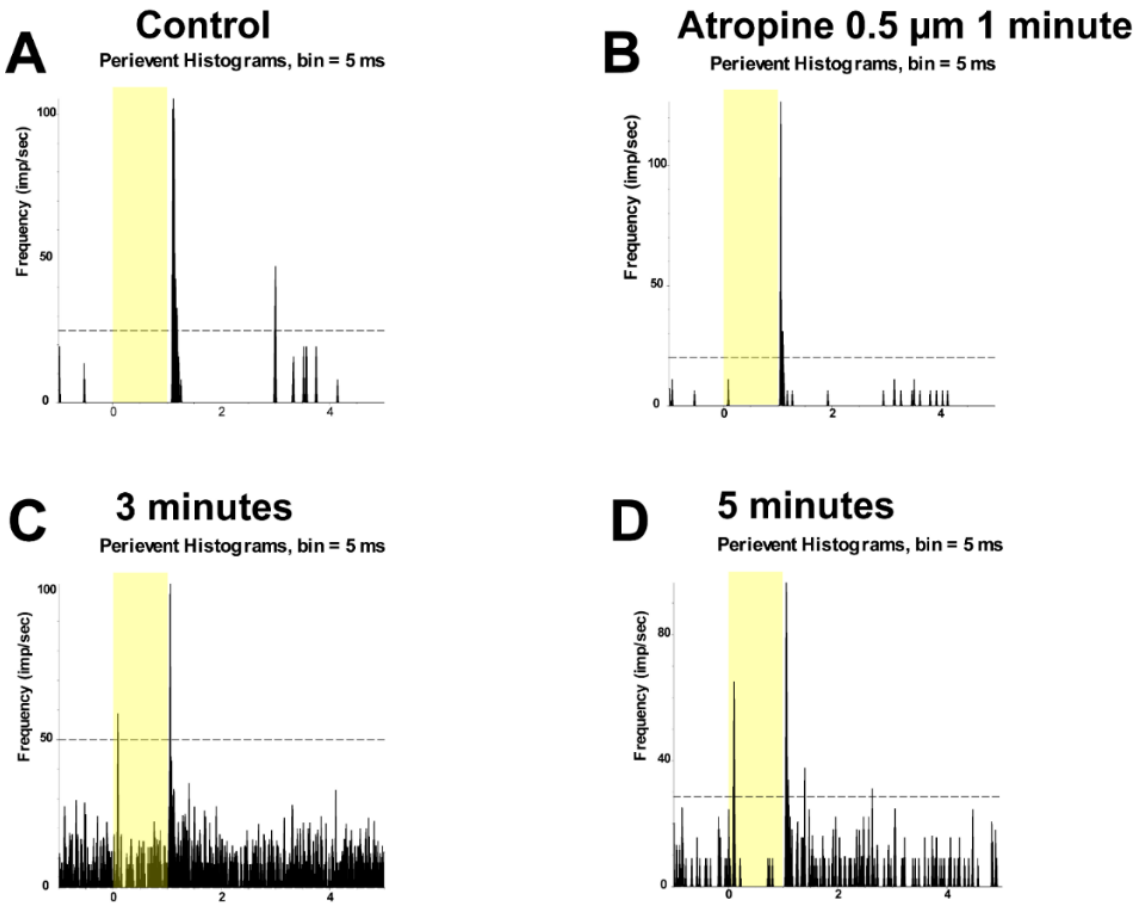

Figure 4.6 Application of 0.5 µM atropine induced ON responses in OFF αRGCs

[A-D] Light-evoked PSTHs of an OFF αRGC in Ringer's solution, 0.5 µM atropine for 1 minute, 3 minutes, and 5 minutes, respectively.

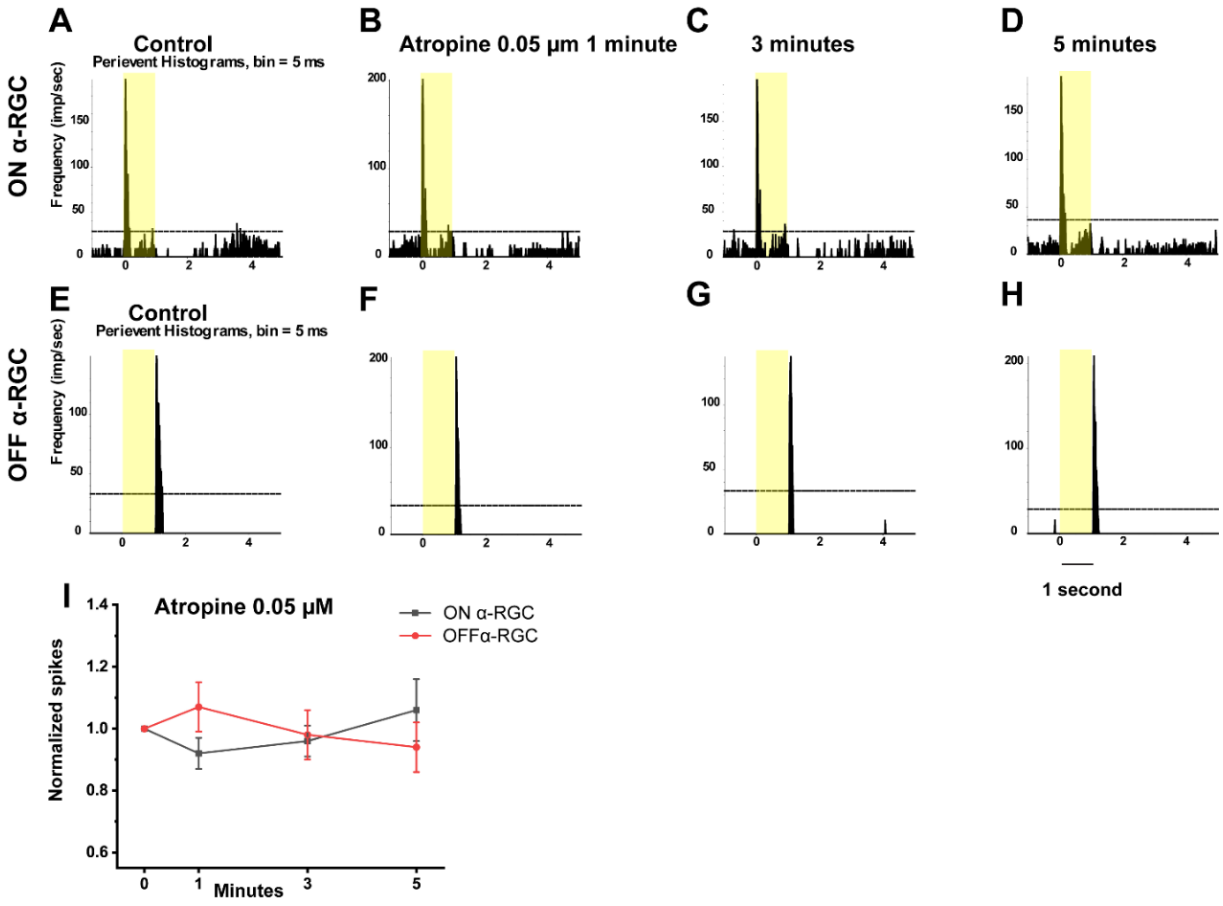

Figure 4.7 Effects of 0.05 µM atropine on light-evoked light responses of αRGCs

[A-D] The light-evoked PSTHs of ON αRGCs in Ringer's solution, 0.05 µM atropine for 1, 3, 5 minutes, respectively.

[E-H] PSTHs of OFF αRGCs in the same condition described above.

[I] A graph summarizing the normalized spikes of ON and OFF αRGCs to the time of 0.05 µM atropine application.

3.4 The effects of atropine on joint inter-spike interval (ISI) distribution and synchronized firing pattern

The spike train pattern of RGCs is defined by the average time of successive ISI. Joint ISI distribution based on the spike train patterns represent basic physiological properties of RGCs, can be used to distinguish unidentified RGC types (Zeck & Masland, 2007). Therefore, we tested the ISI distribution among different concentrations of atropine. The ISI distribution threshold was determined manually and indicated by the black arrow. There was no change of ISI distribution threshold with time in Ringer's solution (n=4) (**Fig 4.8 A-C, J**). After application of 0.5 μM atropine, there was no significant difference in ISI threshold (n=5) (**Fig 4.8 D-F**). After application of 50 μM atropine, the threshold of joint ISI distribution had a significant increase (**Fig 4.8 G-I**).

The synchronized firing was two cells fired synchronized more than chance. It is mediated through gap junctions and plays important role in encoding visual information in the retina. We examined the spontaneous spikes and light-evoked spike activity between two OFF αRGCs before and after atropine application (**Fig 4.9A**). Cross-correlogram profiles were generated to reveal activity-correlation exceeding chance at 99% confidence level. Data were time shuffled using a shift-predictor protocol, which was subtracted from the original cross-correlogram, to demonstrate spike correlations between two cells that were not time-locked to the light stimulus (**Fig 4.9 B**). A cross-correlation function (CCF) fit with a Gaussian function was used to analyze the spontaneous spikes. The unimodal CCFs showed the synchronized firing came from two RGCs. Application of 0.5 μM did not change the synchronized firing pattern (width=0.036ms before and after)(**Fig 4.9 C, D**).

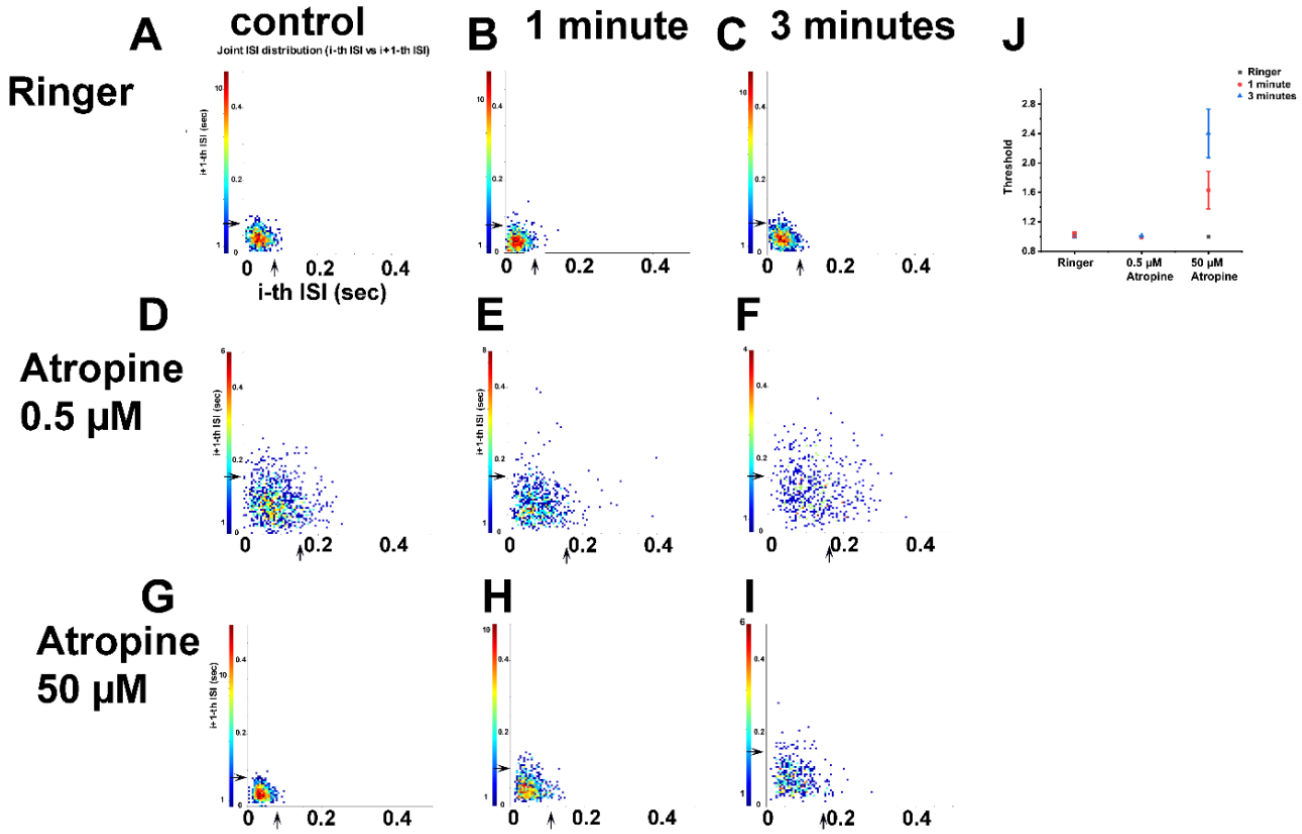

Figure 4.8 Effect of atropine on ISI distributions of αRGCs

For each spike, a point is plotted showing the duration of the preceding ISI and the duration of the subsequent ISI. The threshold is indicated by the arrowhead.

[A-C] ISI distribution of one αRGC in Ringer's solution for 0, 1, 3 minutes.

[D-F] ISI distribution of one αRGC in 0.5 μM atropine for 0, 1, 3 minutes.

[G-I] ISI distribution of one αRGC in 50 μM atropine for 0, 1, 3 minutes.

[J] A graph summarizing the effect of the Ringer's solution, 0.5 μM atropine, and 50 μM atropine on the threshold of ISI distribution.

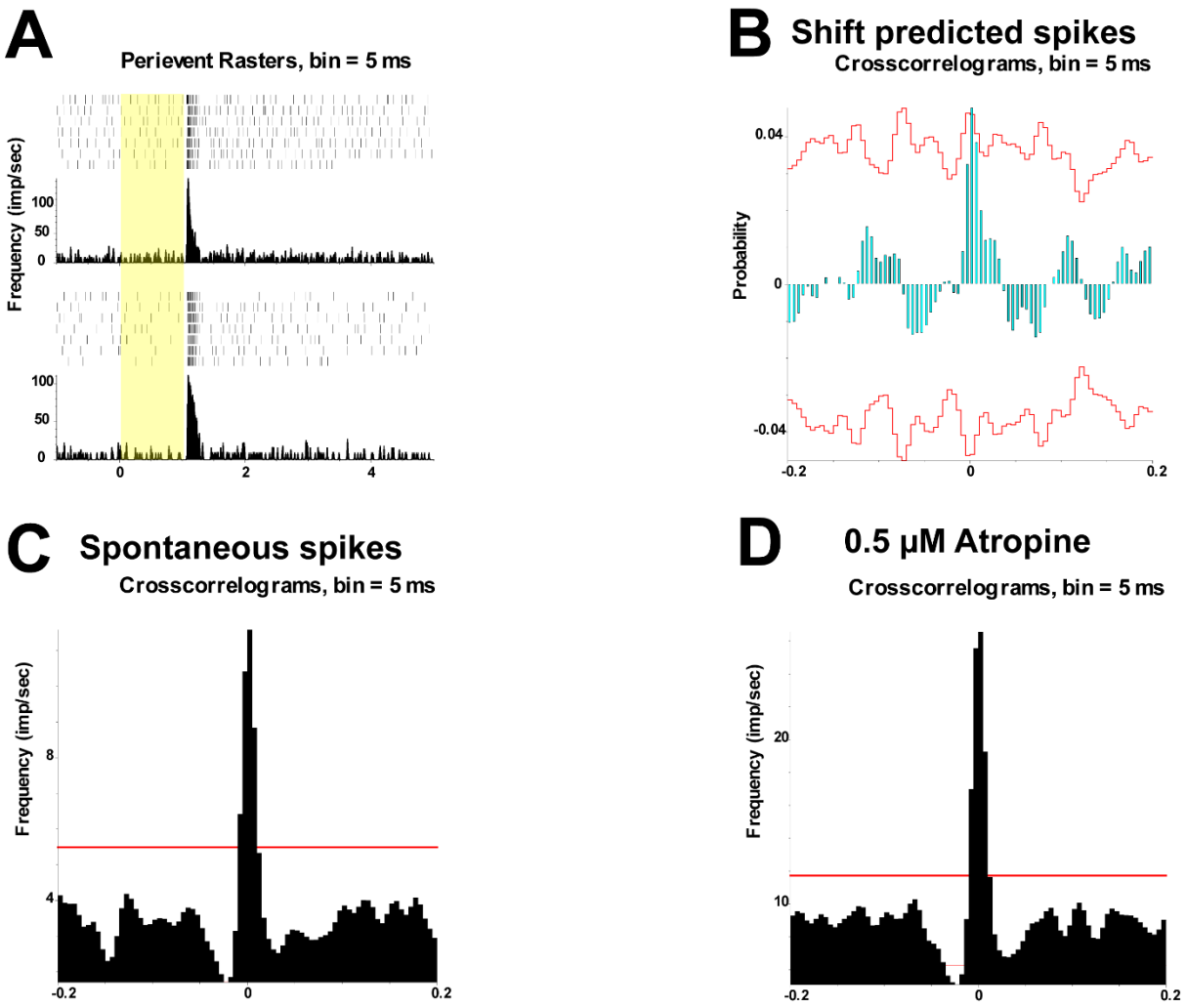

Figure 4.9 Effect of 0.5 µM atropine on the synchronized firing pattern of αRGCs

[A] PSTHs and perievent rasters showing light-evoked responses of 2 OFF αRGCs.

[B] Shift predicted synchronized firing pattern showing the synchronization between the 2 OFF αRGCs were not time-locked to the light stimulus.

[C, D] The synchronized firing between the spontaneous spikes of the 2 paired OFF αRGCs in Ringer's solution and 0.5 µM atropine, respectively. The red line represents the frequency above which the confidence is 99% that correlations are above chance.

3.5 Application of atropine did not induce ON responses in OFF αRGCs in the Cx36-knockout mice

Connexin36 is widely used by gap junctions in the inner retina. It was postulated the ON responses induced by atropine came from gap junction pathway. Thus, we tested the light responses of OFF αRGCs in Cx36-knockout mice, to investigate the mechanism behind the ON components inducement. Previous data showed atropine induced ON response in 78% OFF αRGCs. However, no ON response was induced after applying 100, 300, and 500 µM atropine in Cx36-knockout mice (**Fig 4.10**). It indicated that Cx36 was necessary for inducing the ON response.

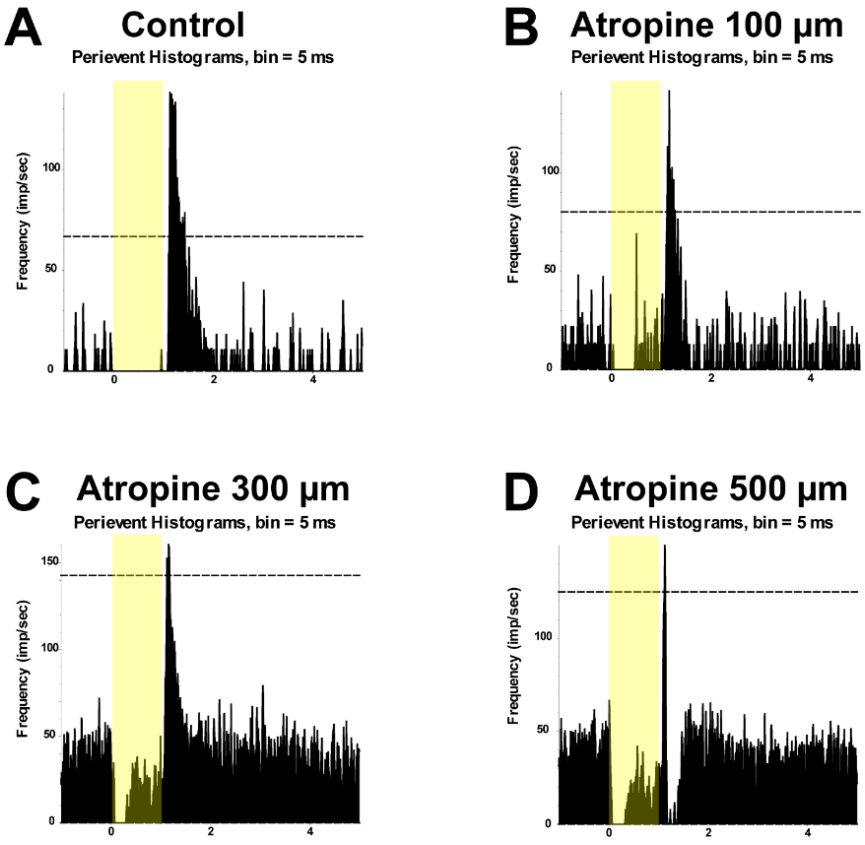

Figure 4.10 Application of atropine on αRGCs of the Cx36-knockout mice.

[A-D] Light-evoked PSTHs of an OFF αRGC in Ringer's (control), 100 µM, 300 µM, 500 µM atropine.

3.6 The role of GABA in inducing ON responses in OFF cells

It was known that ACh was released by starburst ACs that is also expressed GABA. Besides, decrease of GABA inhibition was reported to underlie the similar crosstalk of ON responses in OFF αRGCs before (Farajian et al., 2011). Thus, to test whether GABA was involved in the mechanism of inducing ON response in OFF αRGCs by atropine, we puffed external 1 mM GABA to OFF αRGCs with atropine induced ON responses. The results showed that GABA abolished the induced ON responses in OFF αRGCs (7 of 7), recovered the OFF responses (**Fig 4.11**). It indicated that a decrease of GABA may occur after atropine application, which contribute to unmasking the ON responses in OFF αRGCs.

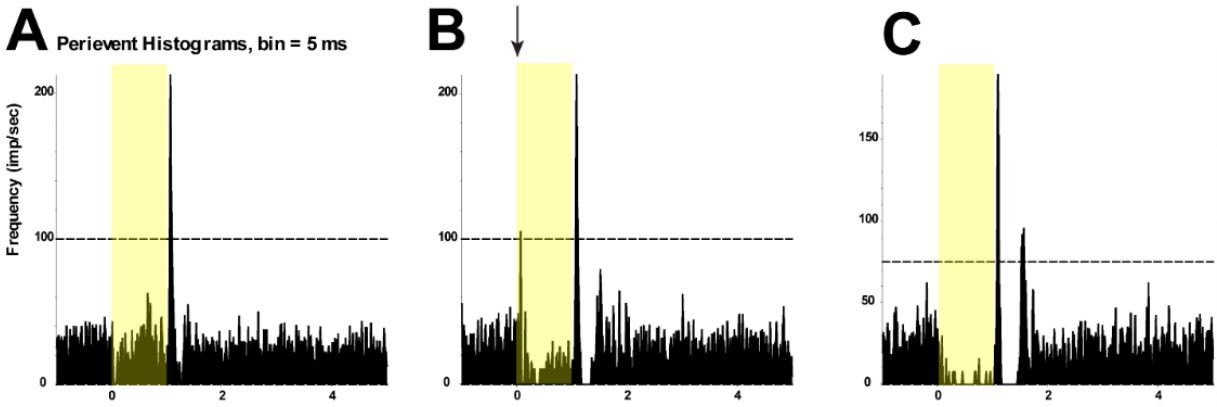

Figure 4.11 GABA inhibited the ON response induced by atropine in OFF αRGCs.

[A] The light-evoked PSTH of an OFF αRGC in Ringer's solution. **[B]** The light-evoked PSTH of the same RGC with 100μM atropine application. ON response was induced. **[C]** The light-evoked PSTH of the same RGC with 1mM GABA application, the induced ON response was abolished.

3.7 The firing frequency of αRGCs was affected by atropine

The mean spike frequency of RGCs with light stimulus involved the light-evoked spikes as well as the background spikes, which could also be seen as burst firing and tonic firing. Results above showed the changes of light-evoked spike responses. The changes of atropine on mean spike frequency were shown in **Fig 4.12 A**. The atropine less or equal to 100 μM did not show significant changes to mean spike frequency of αRGCs, only 200 μM atropine significantly elevated the firing rate. The representative αRGCs PSTHs were shown in **Fig 4.12 C**. However, an opposing phenomenon was observed when filtering the RGCs which have firing rates over 20 spikes/s before atropine application. In these original noise RGCs, application of atropine decreased the firing rate in most cases. 100 μM atropine significantly decreased the spike rates compared with Ringer's group. The representative PSTH was shown in **Fig 4.12 D**. It indicated that atropine application increased the firing frequency of originally quiet RGCs but decreased the initial noise RGCs. The compensation of the pulling mechanism and disproportionate sampling of noise and quiet RGCs may contribute to the insignificant changes under 100 μM atropine.

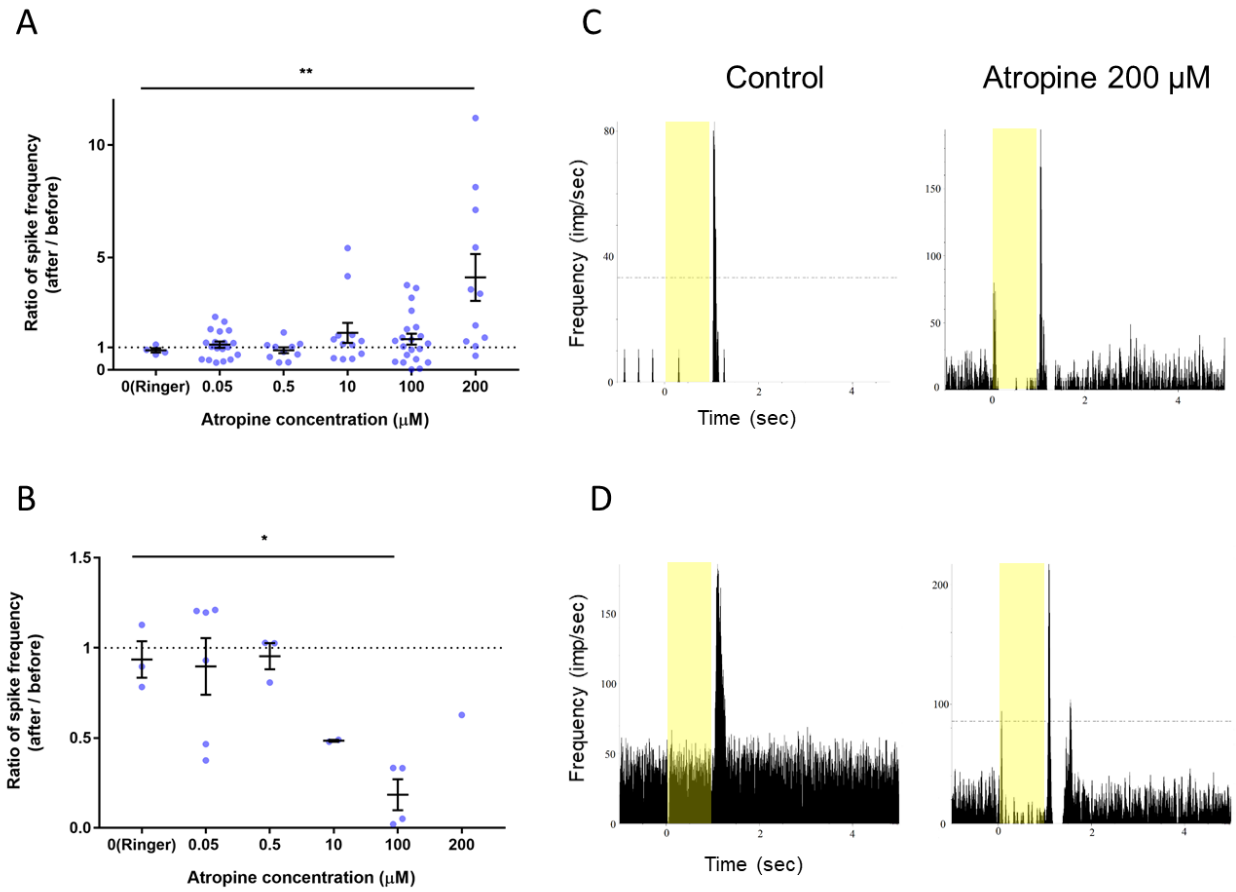

Figure 4.12 The effect of atropine on the average spike frequency of αRGCs.

[A] Spike frequency ratio of all the tested αRGCs after and before application of Ringer's (n=4), 0.05 (n=19), 0.5 (n=10), 10 (n=12), 100 (n=21), 200 μM (n=11) solution. Ringer's application was approximately equal to 1. Compared with Ringer's group, 200 μM atropine significantly increased the mean spike frequency of αRGCs (p=0.0038). The overall tendency is ascending. **[B]** Spike frequency ratio of αRGCs which have firing rate over 20 spikes/s mentioned in A, Ringer's (n=3), 0.05(n=6), 0.5(n=3), 10(n=2), 100(n=4), 200 μM (n=1). The overall tendency is descending. Compared with Ringer's group, 100 μM atropine significantly decreased the mean spike frequency of the noise αRGCs (p=0.0111). **[C]** Representative PSTH of the quiet OFF αRGC before and after 200 μM atropine. **[D]** PSTH of the noise OFF αRGC before and after 200 μM atropine.

4. Discussion

4.1 The low-dose atropine had a little effect on αRGCs

In the clinic, low-dose atropine, maximum 1% (i.e., 16mM) atropine eye drop, was used to prevent myopia progression. Atropine reaches the retina via transcorneal or transconjunctival-scleral pathway. However, the concentration reached the retina is much lower than topical administration because of the strong precorneal factors such as tear washing and resistance from layers of cornea, conjunctiva, and sclera (Gaudana et al., 2010). A previous study has demonstrated that 0.4 μM atropine was detected in vitreous humor after 24-hour topical exposure to 1% atropine in rabbits (Wang et al., 2019). In our study, after immersing the eyeball in 800 μM (i.e., 0.05%) atropine sulfate solution for 30 minutes, the tested concentration was 2μM. However, as the tear fluid and resistance in the pathways, the concentration and duration of atropine in real topical application could not reach the tested number. Therefore, it was estimated a three-log unit decrease of the atropine concentration from the topical application to the retina. The lowest tested concentration in this study was 0.05 μM. However, if the barrier in drug delivery is broken as inflammation or trauma, the retina exposure concentration would be elevated. Therefore, the concentration tested in this study was from 0.05 to 500 μM.

This study showed that low-dose atropine did not change the morphology of αRGCs. A previous study indicated AChR-mediated retina waves affect the dendritic morphology and synaptic connection of RGCs (Tian, 2011). However, chronic manipulation of AChR or genetic deletion was applied in these studies, which may underlie the different results from this study. In addition, a study also demonstrated that RGCs morphology did not change after blocking the synthetic enzyme for ACh (Stacy et al., 2005).

In this study, atropine of more than 100 μM decreased the spike frequency of light-evoked response. However, atropine of 100μM or below did not change the light-evoked spike

frequency and time latency of the original response of ON and OFF αRGCs. Also, 0.5μM atropine did not affect the aspect of joint ISI distribution and correlated firing activity. The synchronized firing was thought to contribute to carrying more visual information (Pillow et al., 2008; Shlens et al., 2009; Shlens et al., 2008). The joint ISI distribution reflects RGCs properties used for cell-type characterization (Zeck & Masland, 2007). It confirmed that the atropine of low concentration did not alter the electrical activity of RGCs, thus it is reasonable to say that application of eye drops of 1% (i.e., 16 mM, decreasing three-log units to less than 16 μM) atropine or below mainly are unlikely to affect the signaling of ON and OFF αRGCs.

4.2 Relatively high concentration atropine decreased the light-evoked response of αRGCs

Relatively high concentrations of atropine were tested on αRGCs to mimic the increase of barrier permeability in extreme conditions like trauma. Although the low-concentration atropine did not affect the αRGCs' electrical activity, concentration more or equal to 300 μM decreased the light-evoked spike frequency, 50 μM atropine increase the threshold of ISI distribution. An increase of spontaneous miniature release (tonic firing) was observed after atropine administration.

Atropine is known as a nonselective muscarinic acetylcholine receptor (mAChR) antagonist. ACh is released by starburst ACs in the retina. There are 5 types of mACh receptors, all of them were present on subsets of BCs, ACs, and RGCs in rabbits (Strang et al., 2010). An early study indicated muscarine increased influx of Ca^{2+} of RGCs and 1 μM atropine eliminated the increase (Baldridge, 1996). Effect of 3 μM atropine on light response and firing rate of RGCs was also tested, but results are cell-specific (Strang et al., 2010). ACh tends to play the role as neuromodulator rather than directly excitatory or inhibitory effect in the CNS (Picciotto et al., 2012). In this study, the high concentrations of atropine were postulated to block the mAChRs on GABAergic ACs, reducing tonic inhibition to αRGCs and resulting the increased tonic firing

(small spikes in Figure 4.2). This might also underline the decreased light-evoked response (burst firing).

4.3 The ON response induced by atropine was mediated by GABAergic inhibition and gap junctions

Another significant change after high concentration atropine is the widely observed induced ON response in OFF αRGCs. Percentage of 78%, 62.5%, 33.3%, and 28.6% OFF αRGCs had an ON response induced after concentration of 100, 10, 0.5, and 0.05uM atropine administration, respectively.

This phenomenon might be attributed to decrease of GABA inhibition. ACh induced A17 ACs to release GABA via nAChR (Elgueta et al., 2015). Most mAChR-expressing ACs are indicated to be GABAergic, which produce GABA (Strang et al., 2010). Atropine, as a mAChR antagonist, would also inhibit GABA release. GABA is an inhibitory neurotransmitter, the decrease of GABA can disinhibit the function of the inner retina in previous studies (Farajian et al., 2011; Pan et al., 2016; Wang et al., 2020). In this study, an ON response was induced in OFF αRGCs after atropine application. Inhibition of the GABAergic receptor could also induce this similar crossover excitation in another study (Farajian et al., 2011). To verify this hypothesis, exogenous GABA was applied after atropine while recording. Results showed application of GABA diminished the ON responses induced by 100uM atropine. It verified our hypothesis that inducing ON response in OFF αRGCs by atropine was attribute to inhibition of GABA release. Previous study suggested the involvement of nitric oxide (NO) in atropine process, which may be attributed to the decrease of inhibition (Carr & Stell, 2016). The results of this study also suggested the decrease of the GABA inhibition by ACs.

The OFF RGCs receive chemical synapses from OFF BCs in sublamina a of IPL anatomically. Gap junction was shown to mediate crossover excitation of RGCs (Farajian et al., 2011). Thus,

the ON signal induced in OFF RGCs was postulated to come from gap junction with ACs. We applied the relatively high concentration of atropine in the retina of Cx36-knockout mouse and did not observe the ON response. Therefore, it verified that gap junctions are required to induce the ON responses. It is known that RGCs are coupled with ACs with different coupling patterns, which may affect the unmasking ON response. The results also showed that not all OFF RGCs have the induced ON response in this study, which may attribute to different numbers of coupled ACs.

Many studies suggested the retinal code is not fixed. It was observed similar changes of ON response in OFF cells with varied ambient luminance (Tikidji-Hamburyan et al., 2015). However, the luminance was consistent in this study. The other possible mechanism of the changed light response might underlie the effect of ACs. Wide-field ACs were indicated to switch the polarity of RGCs by periphery stimulus (Geffen et al., 2007). In this study, the ON responses induced in OFF cells by atropine may also indicate the decreased sign-inversing signals from the chemical synapses, and increase sign-preserving signaling from electrical synapses between RGC-AC, suggesting the bidirectional mediation effect of ACs to RGCs.

It was suggested that ACh has the role to decrease tonic firing and promote burst firing (Picciotto et al., 2012). Our study also found that atropine could elevate the tonic firing with concentration increase, suggesting the effect may take through ACh receptors.

Overall, the decrease of GABAergic inhibition may induce the crosstalk of ON response to OFF cells via gap junction pathway. It is noteworthy that GABAergic inhibition was demonstrated to mediate the light sensitivity of RGCs (Pan et al., 2016). Decrease of GABA caused by atropine could decrease the light sensitivity threshold of RGCs, which increases the whole retinal sensitivity. Besides, atropine suppresses the ACh effect, which may lead to increase in tonic firing. Thus, these mechanisms may underlie the side effect observed in topical

administration, such as photophobia, climbing with higher concentrations of atropine.

5. Conclusion and Further Study

This study assessed the effects of 0.05-500 μM atropine on physiological properties of RGCs in the mouse. We found that the low concentrations of atropine (0.05 -10μM, corresponding to around 0.003-0.6% topical administration) has no effects on morphology and physiological responses on αRGCs, but did induce ON response in more than 25% OFF RGCs. The mechanism might involve the decrease of GABA inhibition. This may indicate the potentials of affecting the retinal signaling and underlie the side effect brought by topical atropine. It gives reminders to the clinic that application of atropine should still be cautious, especially in children.

There are several limitations in this study. Firstly, the mouse eye is tiny, it has a bigger lens and smaller vitreous space compared with humans. The concentration of topical atropine reaches to the retinas should be different between mice and humans. Therefore, the results got in mice may not be applied to humans directly. Secondly, although we tested the retinal concentration of atropine and mimic that concentration in retinal perfusion, the method of drug delivery was different from topical applications. Short-term application of low-dose atropine could hardly have effect on the morphology of RGCs especially. Longitudinal application should be more rational to reveal the clinic effect of atropine. Thirdly, the experiments only tested the spontaneous and light response in αRGC. We did not know the atropine effects on other RGC types and their different functions.

Further experiments are needed to confirm the involvement of GABAergic pathway in the atropine process. The close relationship and mutual effect between GABA and acetylcholine have been suggested in numerous studies, especially in direction information coding (Massey

et al., 1997; Sethuramanujam et al., 2016). Combined with previous defocus study, it's interesting to investigate what's role atropine play in RGCs sensing the defocused stimuli, especially DS RGCs, which are mainly affected by acetylcholine and GABA.

Chapter 5 The Picrotoxin-unmasked signals prolongs neuronal function in the retinal degenerative mouse model

1. Introduction

Retinitis Pigmentosa (RP) is a blinding eye disease, which has a prevalence of approximately 1:5000 among the world (Ferrari et al., 2011). The disease usually begins in young adults, with symptoms like night blindness. It progresses with periphery vision loss and ends in final vision loss. The length of the timeframe between the disease start and final vision loss varies among patients, but the progressive vision loss at a young age and the severe consequence bring tremendous burden to patients. However, except for Luxturna gene therapy for Leber congenital amaurosis (LCA), there is no approved and effective therapy for RP disease.

Loss of photoreceptors, especially rods, is the main characteristic of RP disease. Cones degenerate after rods with a lower rate but leading to a severe loss of visual function (Campochiaro & Mir, 2018). The Rd model is a well-characterized animal model to study retinal degenerative disease(Chang et al., 2002). This kind of model has mutations on the beta-subunit of cGMP phosphodiesterase (PDE), which leads to rod photoreceptors degeneration. Among the Rd model, the Rd10 mouse is the suitable model to study human RP because of the similar degenerative progress. Rd10 mouse has the rods which start to degenerate at postnatal day 18 (P18), reaching a peak wave at P25. Most of the rods were eliminated by around P35 and cones were eliminated by P50 (Gargini et al., 2007). Since the cones are secondly eliminated, and responsible for the most severe consequence in humans, this study would focus on investigating the method of restoring cone function in the P38-P46 rd10 mouse, in which most of the rods are eliminated while cones are still retained functionally (Toychiev et al., 2013).

The light-evoked responses of RGCs were decreased with age in rd10 mice (Telias et al., 2019),

with bursting or quiescent spontaneous activity aberrantly (Toychiev et al., 2013). Degeneration of photoreceptors damaged the input signals of RGCs. However, cones, which lost secondly, may provide remaining signals in early progress.

Unmasking input signals was well demonstrated in the brain. Signals which does not show in physiological conditions could be unmasked by deafferentation (Dostrovsky et al., 1976; Rajan, 2001) or decreasing inhibition (Barron et al., 2016; Jacobs & Donoghue, 1991). Retina, as part of the CNS, is also believed to have the same plasticity and unmasking phenomena. Blockage of GABA release unmasked the ON response in OFF RGCs (Farajian et al., 2011). In addition, the inhibitory mechanism manipulated light sensitivity (Pan et al., 2016), response latency (Tengölics et al., 2019), even the polarities of RGCs (Geffen et al., 2007). Removing inhibition increased light response sensitivity of RGCs (Pan et al., 2016).

Therefore, the preexisting unmasking effect by removing inhibition was used to elevate the visual function in RP disease. Picrotoxin (PTX) is known as a non-specific antagonist for GABA and glycine ionotropic receptors. It blocks $GABA_A$ and $GABA_C$ receptors, and also inhibits homomeric glycine receptor. We used PTX to unmask the light-evoked signal derived from retained cones in rd10 mice.

2. Methods

2.1 Animals

Rd10 mice (P38-46) (RRID: MGI:2581193; B6.CxB1-Pde6b ^{rd10}/J; Jackson laboratory stock No: 004297) and (P38-46) C57BL/6J (RRID: IMSR_JAX:000664) wide-type (WT) mice were used. Rd10 mice are the mouse model of RP with mutations in the beta-subunit of rod-specific phosphodiesterase gene 6(PDE6β) in exon 13, which causes the degeneration of rod photoreceptors followed by the gradual degeneration of cones. The presence of the homozygous Pde6b mutation was tested periodically with PCR. P38-46 rd10 mice are used because all rods die after P38 and cones begin to be affected (Wang et al., 2014). During this stage, the cone light response is damaged (Gargini et al., 2007; Toychiev et al., 2013). P41 rd10 mice were used in ERG, and behavioral measurements because the results of behavioral measurement were uncertain after P42. After P44-45, the effects of PTX on the ERG test were also inexplicit.

Retina sections were cut with a Vibratome (model VT1200S; Leica Microsystems, Bannockburn, IL, USA). Retinas were fixed and embedded in 4% agarose gel and cut into 50-80 μm thick sections.

2.2 Immunohistochemistry and image acquisition

Red/green opsins (rabbit anti-red/green opsin 1:500, Chemicon, Temecula, CA, Cat# AB5405) antibody was used to label the out segments of cones.

Quantification of surviving cones stained with red/green opsins was conducted in whole mounts. For comparison, all retinal samples were obtained from the dorsal section of the mid-peripheral retina in the naso-temporal plane.

2.3 Electrical recording

Full-field green light stimulus was delivered by a light-emitting diode (λ = 525 nm) (HLMP-CM3A-Z10DD, Broadcom Limited, San Jose, CA). The intensity of the square wave light stimuli was calibrated and expressed in terms of the time-averaged rate of photoisomerization per rod per second (Rh* per rod/sec).

Retina preparation and recordings were performed in dark-adapted conditions. Eyes were enucleated. Anterior optics and vitreous humor were removed. Retinas were separated from the resultant eyecup and kept in bicarbonate buffered solution. A piece of retina was dissected and put on a translucent Millicell filter with GCL layer upwards. Neurons were visualized by infrared light. αRGCs were differentiated by the large soma size.

The extracellular and whole-cell patch clamp was conducted to record light-evoked spikes and current responses, respectively. The amplitudes of excitatory postsynaptic currents (EPSCs) and inhibitory postsynaptic currents (IPSCs) were measured in Calmpfit 10.7 (pClamp, Molecular Device, USA).

2.4 Pharmacological application

For the electrical recording of rd10 mice retina (ex vivo), Picrotoxin (PTX, Sigma-Aldrich Cat# P1675-1G), strychnine (Cat# S8753-25G), SR95531 (Cat# S106-10MG), 1,2,5,6-tetrahydropyridin-4-yl-methylphosphinic acid (TPMPA, Cat# T200-10MG), SCH 23390 (Cat# D054-10MG), and eticlopride (Cat# E101-25MG) obtained from SigmaAldrich (St Louis, MO, USA) were used and applied in the bathing of Ringer's solution.

In ERG and Optokinetic measurement experiments (in vivo), PTX was delivered to mice via subcutaneous MINI osmotic pumps (Alzet model 2001D; DURECT, CA). To implant the minipumps, mice were anesthetized under intraperitoneal anesthesia and placed on a heating pad. The minipumps were filled with PTX solution (Phosphate-buffered saline was loaded as

vehicle control) and inserted subcutaneously on the dorsum by an incision 1.5 times the diameter of the pump, and the wounds were closed with sutures (nylon 6-0). The LD50 (lethal dose causing death of 50% animals) of PTX via subcutaneous administration is 4.1 mg/kg. It was found that PTX at doses of 1 mM (0.015 mg/kg/d) had effectively induced ERG and behavioral responses of rd10 mice compared to control groups.

2.5 Electroretinogram (ERG) recording

A full-filed Ganzfeld (Q450; RETI Animal, Roland Consult, Brandenburg a der Havel, Germany) was used to measure the electrical signals. Mice were dark-adapted overnight and anesthetized with an intraperitoneal injection of 100 mg/kg ketamine and 20 mg/kg xylazine. Proxymetacaine (Provain-POS, Ursapharm, Saarbrücken), topicamide 1% (Mydriacyl, Alcon) and Carbomer gel (Lacryvisc, Alcon) were applied topically for anesthesia, pupil dilation and corneal hydration. The animal was placed on a water-bath platform to maintain the body temperature at 37°C. A pair of gold wire corneal electrodes (inner ring diameter: 3 mm; wire diameter: 0.5 mm) (Roland Consult) was used as the active electrode. Two needle electrodes inserted into the lateral canthi of each eye to serve as references; one needle electrode inserted into the base of the tail as a ground electrode. The impedance of the electrodes was maintained below 10 kΩ. White light-emitting diode light was chosen as a source for flash stimuli. The signals were amplified and band-pass filtered from 1 to 30 Hz and 0.1 to 1000 Hz for scotopic threshold response (STR) and scotopic ERG respectively. Stimuli were presented in multiple levels with increasing energy ranged from log −4.32 cd*s/m^2 to log 1.30 cd*s/m^2. To enhance the signal-to-noise ratio, individual ERG waveform was averaged from multiple sweeps for STR and scotopic ERG.

2.6 Optokinetic measurements

The optomotor responses of mice were measured using the OptoMotry System

(CerebralMechanics). Visual acuity testing was performed at 100% contrast with varying spatial frequency thresholds, while contrast-sensitivity testing was performed at a fixed spatial frequency threshold (0.092 cycles per degree, c/d). The temporal frequency was set at 1.5 Hz for both tests. After a series of test episodes, the same computer program to determine the acuity or contrast sensitivity was applied to both eyes.

2.7 Data analysis

Statistical analyses were performed by using Origin (OriginLab, Northampton, MA, USA). Statistical significance ($P < 0.05$) was determined by using the t-test.

3. Results

3.1 The rd10 mice experiencing retinal degeneration still had surviving cones at P46

Retinal degeneration 10 (rd10) mice carry a spontaneous mutation of rod-phosphodiesterase (PDE) gene, which leads to rod degeneration starts around the second week. In this study, P38-P46 of rd10 mice were used, because all rods are lost and cones start to degenerate but still retain in this period (Gargini et al., 2007; Toychiev et al., 2013).

The retina section of WT and P46 rd10 mice were stained with DAPI and compared. Rd10 mouse retina had only 1-2 layers of photoreceptors (1.3±0.2, n=12), compared with 12-15 layers of photoreceptors in WT mouse (12.9±0.4, n=12) (**Fig 5.1 A-B**). Cone outer segments were stained with red/green opsin (**Fig 5.1 C D**). There were significantly fewer cones in rd10 mouse (6830±267, n=8) than in WT mouse (12969±307, n=8, $p < 0.01$), but more than half of cones were retained in the P46 rd10 mouse retina.

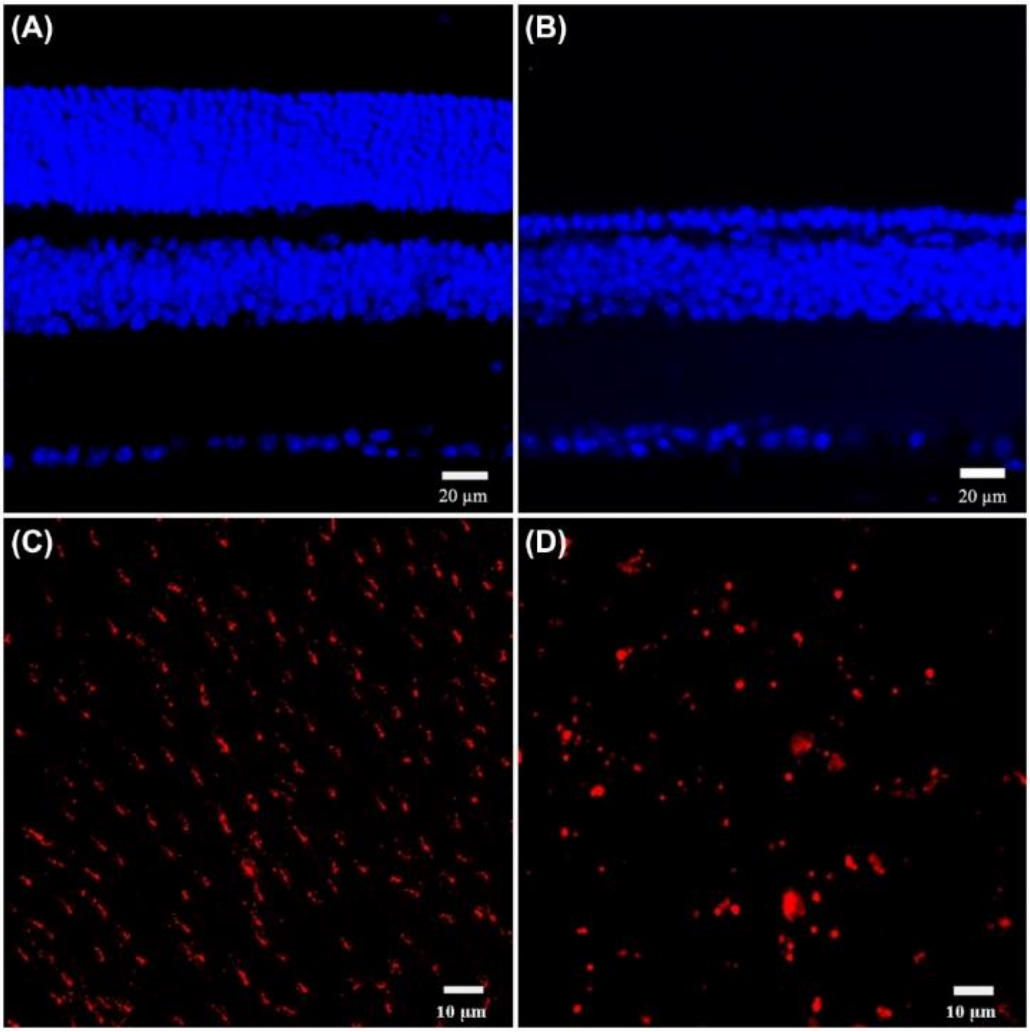

Figure 5.1 Morphology of photoreceptors in WT and the rd10 mouse retina

[A, B] DAPI nuclear staining of vertical section of P46 WT and rd10 mouse. There were 12-15 layers of photoreceptors nuclei in WT mouse, only 1-2 layers in rd10 mouse. Scale bar = 20µm.

[C, D] Cone outer segments labeled by red/green opsin in P46 WT and rd10 mouse. Opsin labeling showed that cones lost their morphology and indicated cell death. Scale bar=10µm. The picture was adapted from (Wang et al., 2020).

3.2 RGCs of P46 rd10 mouse maintained normal morphology as WT mouse

In this study, αRGCs were targeted, as they are representative and easily identified. Morphology of αRGCs of P46 rd10 mice and WT mice were determined by injecting Neurobiotin. **Fig 5.2 A** showed the representative morphologies of ON α, OFF α, ON-OFF RGCs in the rd10 and WT mouse retinas. They shared similar dendritic stratification depth in the inner plexiform layer (IPL) (**Fig 5.2 B**). αRGCs in the rd10 mice had similar dendritic field diameter and soma size as WT mice (**Table 5.1; Fig 5.2 C, D**). Therefore, the three types of RGCs in the P46 rd10 mouse had similar morphologies to the WT mouse. These results showed the morphology of RGCs remained stable, consistent with other studies (Lin & Peng, 2013; Mazzoni et al., 2008a), indicating the RGCs' potentials in functional restoring.

Table 5.1 Morphometry of RGCs in rd10 and WT mice

	Dendritic Field Diameter (μm)			**Soma Diameter (μm)**		
Cell Type	Rd10	WT	P value	Rd10	WT	P value
ON RGC	207 ± 23.4 n=5	211.1 ± 6.9 n = 18	>0 .05	17.9 ± 0.9 n = 5	17 ± 0.6 n = 18	>0 .05
OFF RGC	176.3 ± 7.1 n = 6	193.9 ± 7.2 n=19	>0 .05	17.3 ± 0.8 n = 6	17.4 ± 0.3 n = 19	>0 .05
ON-OFF RGC	179 ± 7.3 n = 4	180.2 ± 12.7 n = 6	>0 .05	15.5 ± 0.8 n=4	16.4 ± 0.6 n = 6	>0 .05

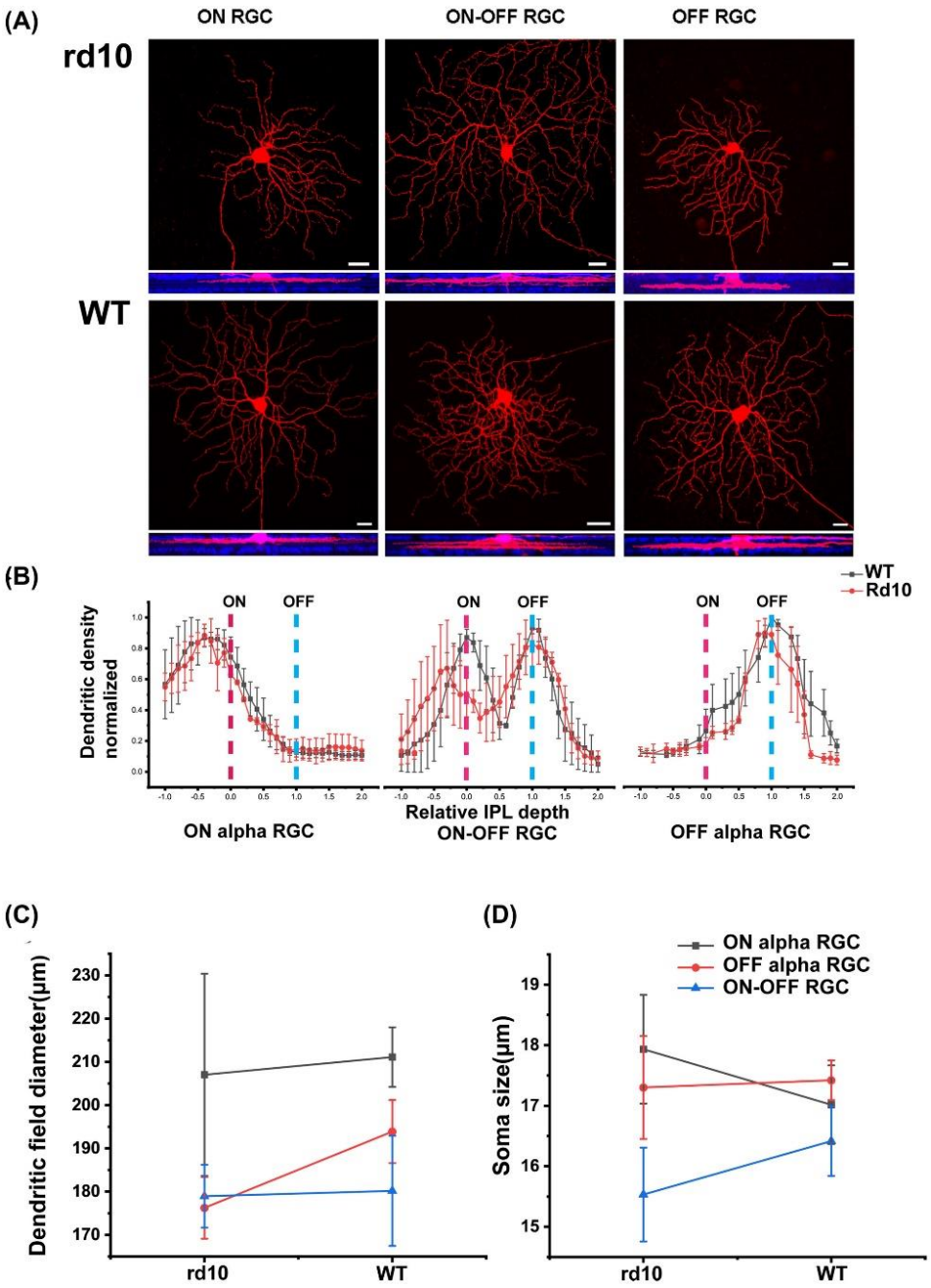

Figure 5.2 Morphology of αRGCs of the rd10 and WT mice.

[A] Morphology of ON α, OFF α, ON-OFF RGCs of rd10 and WT mice, respectively. **[B]** Dendritic stratification of ON α, OFF α, ON-OFF RGCs RGCs in WT and Rd10 mice. **[C]** Dendritic field diameter of three types of αRGCs in WT and rd10 mice. **[D]** Soma diameter of three types of αRGCs in WT and rd10 mice. There was no significant difference between comparisons.

3.3 The Effect of PTX on Excitatory/ Inhibitory Postsynaptic Currents (EPSCs/IPSCs) of RGCs in P46 rd10 mouse

There was no light-evoked spike response in P46 rd10 mice even when light stimulation was applied in the photopic range (525nm, 0-108.53 Rh*/rod/s). However, as shown above, more than half of the cones survived in P46 rd10 mouse, the downstream circuit appeared to be intact and αRGCs remained stable morphology. To measure the excitatory and inhibitory input of RGCs, light-evoked excitatory postsynaptic currents (EPSCs) and inhibitory postsynaptic currents (IPSCs) were recorded in P38-46 rd10 mice and WT mice.

For ON αRGCs in rd10 (4 of 20 cells) and WT mice (4 of 10 cells), EPSCs increased and IPSCs decreased after PTX application in both groups. Similar changes were observed in OFF αRGCs of both rd10 (4 of 18 cells) and WT mice (4 of 12 cells). The responses of ON-OFF RGCs in rd10 (6 of 9) and WT mice (4 of 16) were also measured. EPSCs of ON response did not show significant changes, but IPSCs decreased in both rd10 and WT mice. EPSCs and IPSCs of OFF response increased and decreased in WT mice, respectively, while no changes were observed in rd10 mice (**Table 5.2**; **Fig 5.3**).

As to the changes of PTX in EPSCs and IPSCs, there is no statistical difference between rd10 and WT mice after PTX application ($P > 0.05$) (**Fig 5.3 D**), which indicated the similar effect of PTX on the excitatory and inhibitory input of RGCs in both WT and rd10 mouse.

Table 5.2 Effect of PTX on EPSCs and IPSCs of RGCs in WT and Rd10 mice

Cell Type	Mouse Type	Response	EPSC (pA)		IPSC (pA)	
			Control	PTX	Control	PTX
ONαRGC	Rd10	ON	114 ± 7.1	221.7 ± 24.3*	180.3 ± 9.2	123 ± 4.7*
	WT		113. 7 ± 5.2	376.7 ± 16.5*	77.3 ± 6.4	39 ± 4*
OFFαRGC	Rd10	OFF	159 ± 3.5	438.7 ± 35.5*	71 ± 4.4	20 ± 5.5*
	WT		71 ± 1.5	123.7 ± 4.6 *	159 ± 3.5	109 ± 2.1*
ON-OFF	Rd10	ON	247.1 ± 5.5	265.3 ± 1.5	300 ± 4.9	280 ± 2.6*
		OFF	52.3 ± 7	48 ± 1.7	92.7 ± 3.0	92.3 ± 8.6
	WT	ON	74.8 ± 7	64.6 ± 4.4	252 ± 8	193.8 ± 5.9*
		OFF	614.5 ± 46.2	1234.3 ± 14.2*	266 ± 4.1	150.8 ± 5.3*

* Comparison between Control and PTX, $p<0.05$

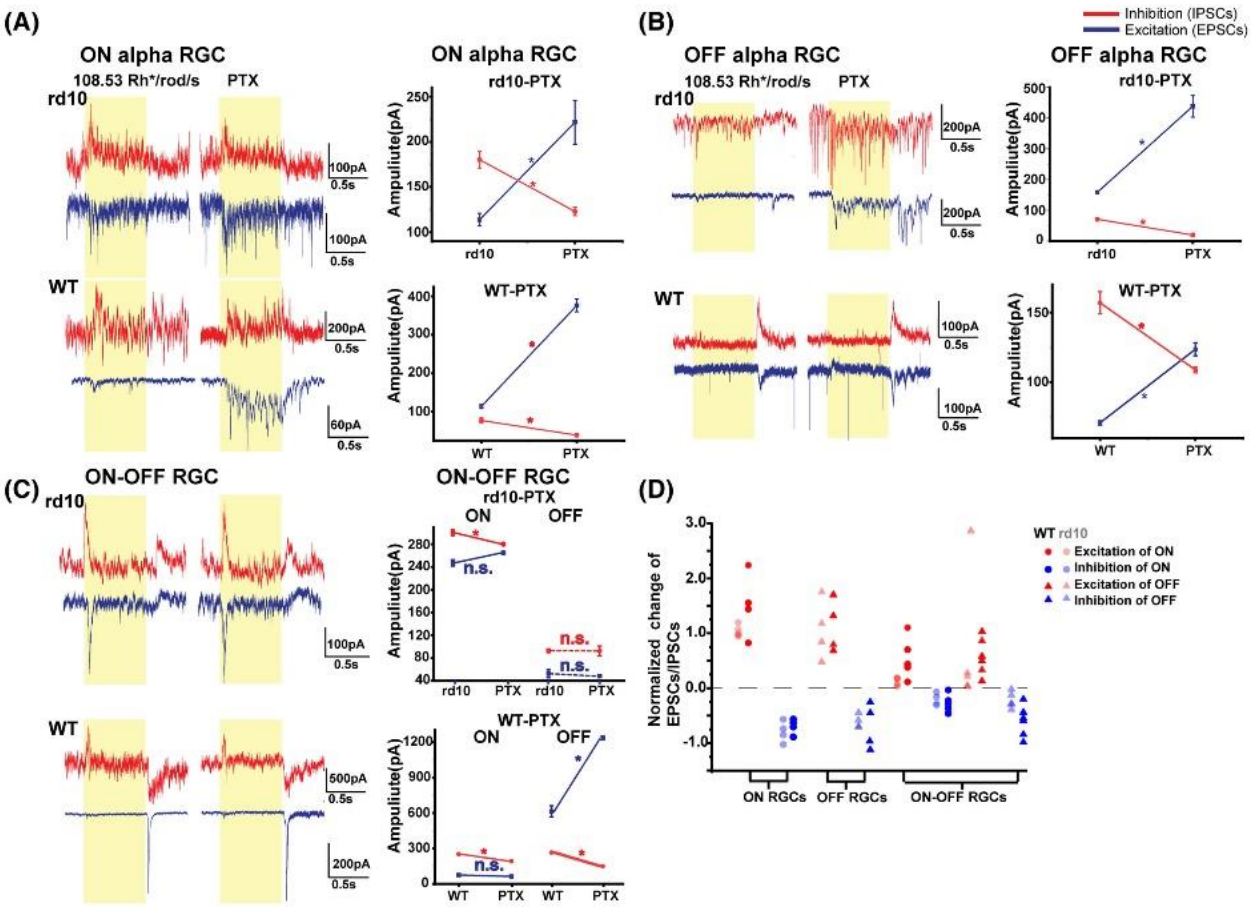

Figure 5.3 Effect of PTX on EPSCs and IPSCs of αRGCs in WT and rd10 mice

The EPSCs (blue) and IPSCs (red) of αRGCs had similar changing patterns before and after PTX (100μM) application in P46 WT and rd10 mice. The EPSCs and IPSCs were obtained by holding potential at -68 mV and 0 mV, respectively. **[A]** The EPSCs and IPSCs of ON αRGCs in WT and rd10 mice. Both ON αRGCs in WT and rd10 mice had a significant increase on EPSCs and decrease on IPSCs ($p<0.05$). **[B]** Both OFF αRGCs in WT and rd10 mice had a significant increase on EPSCs and decrease on IPSCs ($p<0.05$). **[C]** The ON responses of ON-OFF RGCs in both WT and rd10 mice had decreased IPSCs, with no significant difference on EPSCs. The OFF response of ON-OFF RGCs in WT mice had increased EPSCs and decreased IPSCs, while there was no difference in OFF response of ON-OFF RGCs in rd10 mice. **[D]** Normalized changes of EPSCs/IPSCs of αRGCs in WT and rd10 mice. The changes of EPSCs/IPSCs were similar between rd10 and WT mice.

3.4 PTX increased light-evoked response of RGCs in P46 rd10 mouse retina

The above results showed the excitatory and inhibitory input of RGCs still preserved in P38-P46 rd10 mouse. However, there was no light-evoked spike response observed. The reason may underlie that the relatively strong inhibition masked the excitation. We also found PTX increased the excitatory and decreased the inhibitory currents. Therefore, to explore whether PTX could unmask the spike signals, RGCs of P46 rd10 mice (n=40) were recorded before and after PTX application.

It has been observed that spontaneous hyperactivity of RGCs in rd10 mice (Stasheff et al., 2011a; Stasheff et al., 2011b; Toychiev et al., 2013) and the intrinsic bipolar cell oscillations were shown to be responsible (Borowska et al., 2011). In this study, silent RGCs, which are the quiescent RGCs defined by Dr. Sagdullaev (Toychiev et al., 2013), that produced spontaneous spikes occasionally were observed. These RGCs could be suspected of maintaining exacerbated masking inhibitory signals in the rd10 mouse.

The response of a representative αRGC was shown in Figure 5.4. It did not have light-evoked spikes from the least to highest light intensity (0- 108.53 Rh*/rod/s) (**Fig 5.4 A-C**). After 100μM PTX, light-evoked spike responses appeared from 13.69 Rh*/rod/s, and more obvious with the light intensity increase (**Fig 5.4 D-M**). The threshold sensitivity of the RGC was improved to 16 Rh*/rod/s (5% of the maximal response, **Fig 5.4 N**). Similar responses were also found in other RGCs. The application of PTX induced light-evoked responses in 47.5% (19/40) of the tested RGCs. The average results of these examinations showed that the threshold sensitivity was increased to 18.4 ±1.85 Rh*/rod/s (n=19 of 40) (**Fig 5.4 O**), which indicated that PTX application increase the light sensitivity. RGCs in P56 rd10 mouse were also recorded, but no light-evoked response was recorded before and after PTX application.

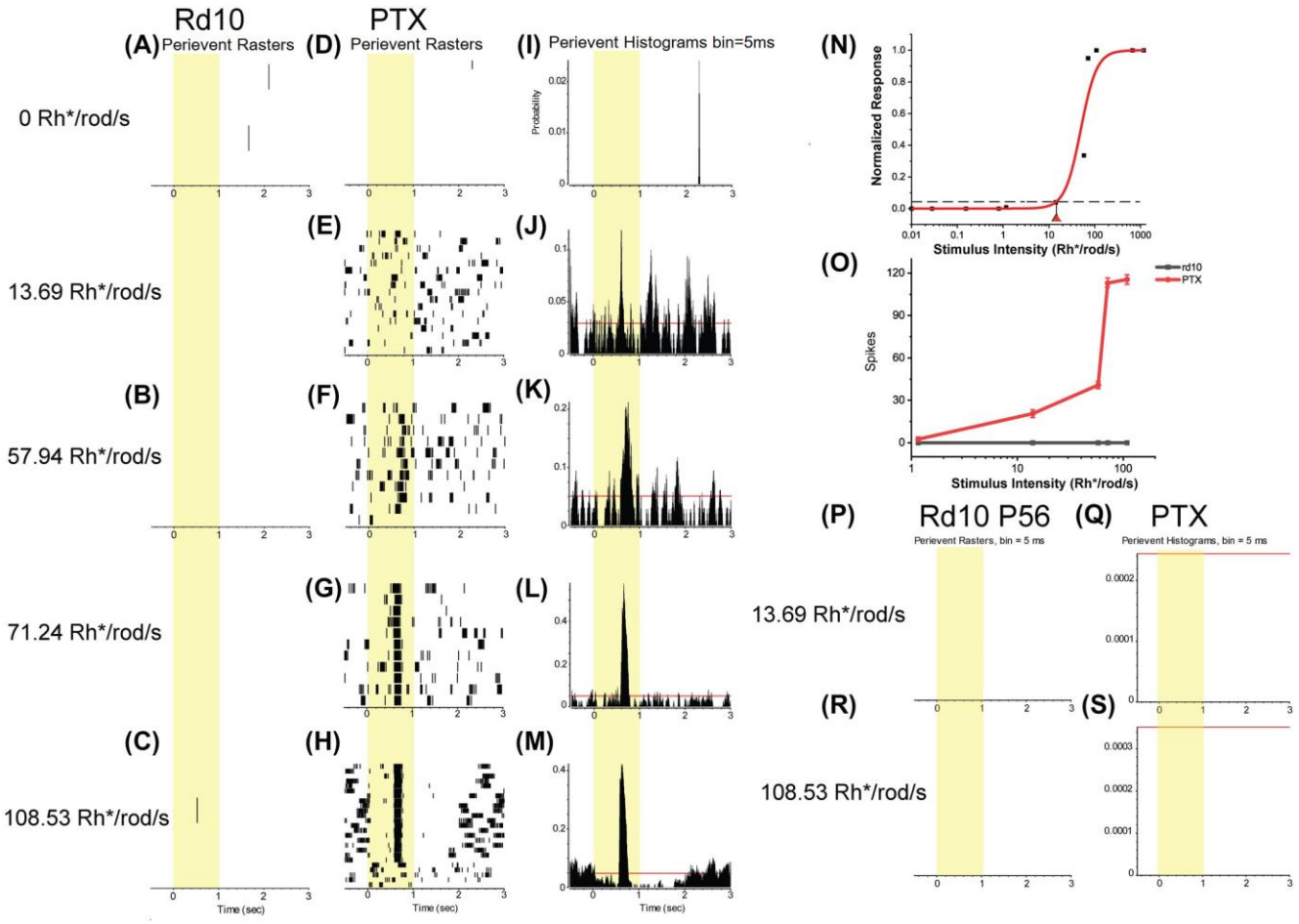

Figure 5.4 PTX induced light-evoked spike responses of αRGCs in P46 rd10 mice.

[A-C] Raster plot shows there was no light-evoked response with light intensity increase in αRGCs in P46 rd10 mice. **[D-H]** After PTX application, there were significant light-evoked responses with light intensity increase. **[I-M]** PSTHs showed the same effect, that PTX could increase the threshold sensitivity of this αRGC to approximately 33Rh*/rod/s of the stimulus. **[N]** Intensity-response plot of an αRGC with data points fitted by a Hill equation. The threshold sensitivity of this αRGC was calculated as 5% of the maximal response, 16Rh*/rod/s, indicated by the red arrowhead. **[O]** Spikes had a significant increase after PTX application. **[P-S]** Raster plot of αRGCs in P56 rd10 mouse retina.

3.5 The unmasked light-evoked response in RGCs is subserved mainly by $GABA_A$ receptors in the rd10 mouse retina

As a nonspecific GABA blocker, PTX blocked both $GABA_A$ and $GABA_C$ receptors, which locate differently at dendrites of RGC, ACs, and axons of BCs. To determine which receptor plays the main effect, $GABA_A$-selective blocker gabazine (SR-95531) and $GABA_C$-selective blocker TPMPA were applied by sequence.

The response was not induced when TPMPA was applied first. When SR-95531 was applied, the light-revoked response was induced immediately (**Fig 5.5 A-L**). Quantification results showed that application of SR-95531 had significant effects on the light-evoked response after TPMPA (TPMPA: 0.14 ± 0.05; SR-95531: 0.86 ± 0.05; $P < 0.01$; $n = 7$), while application of TPMPA had little effects after SR-95531 (SR-95531: 1.09 ± 0.09; TPMPA: 1.00 ± 0.09; $P > 0.05$; $n=8$) (**Fig 5.5 N**). Therefore, it indicated that the unmasked light-evoked response of αRGCs is mainly subserved by $GABA_A$ receptors.

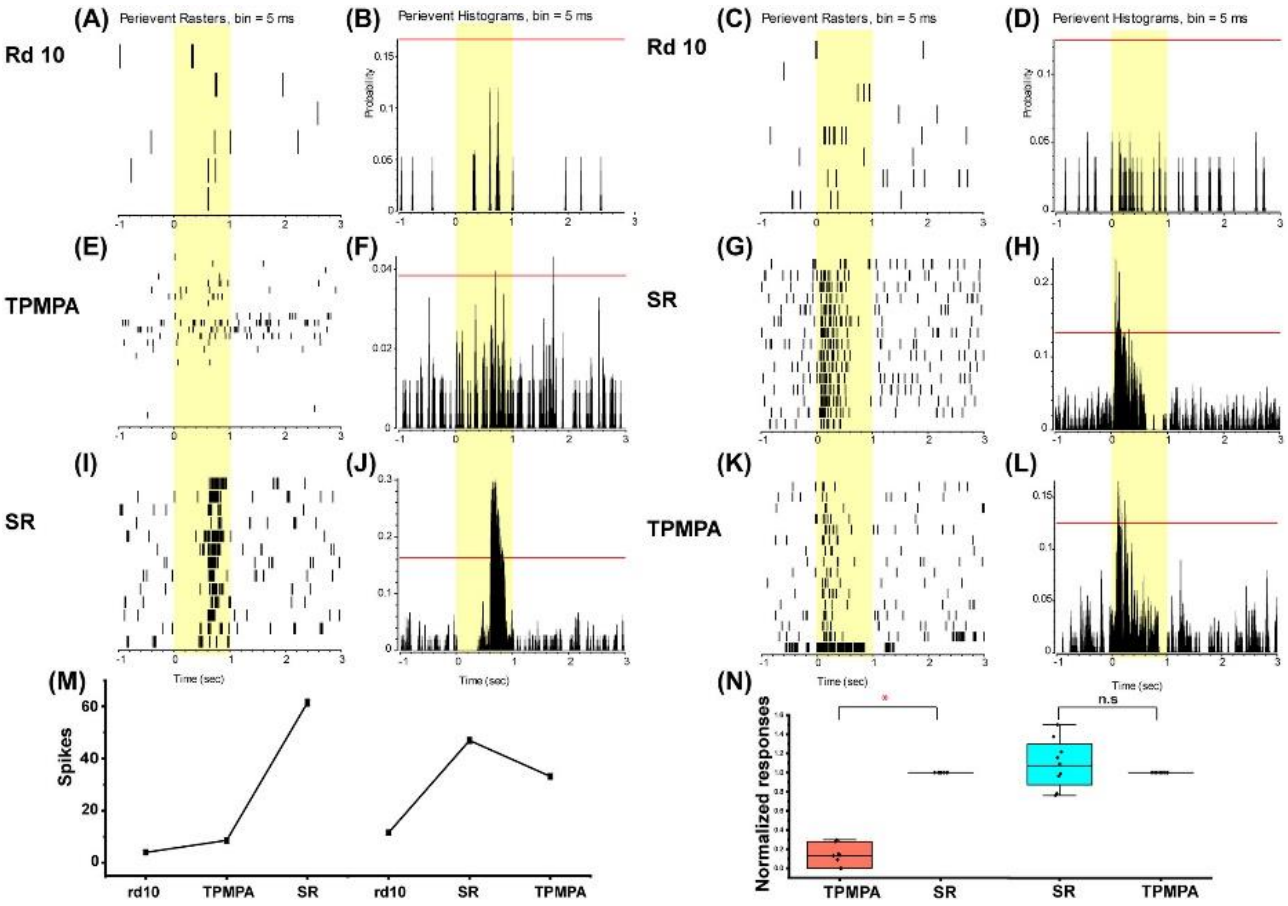

Figure 5.5 The effect of a selective GABA receptor blocker on αRGCs in P43 rd10 mice.

$GABA_A$ receptor blocker gabazine (SR-95531, 10μM) and $GABA_C$ receptor blocker 1,2,5,6-tetrahydropyridin-4-yl-methylphosphinic acid (TPMPA, 100 μM) were applied in a different sequence. **[A, E, I]** Raster plots of light-evoked spike response with TPMPA firstly and SR-95531 secondly applied. **[B, F, J]** PSTHs of the same responses showed that response appeared after SR-95531 application rather than TPMPA. **[C, G, K]** Raster plots of light-evoked spike with SR-95531 firstly and TPMPA secondly applied. PSTHs of the same response showed that response appeared once the SR-95531 was applied. **[M]** The spike plot of data in A-L shows SR-95531 is the effective component that induced light response in αRGCs. **[N]** Plots of normalized response after sequencing application of TPMPA and SR-95531. Application of SR-95531 had a significant effect on inducing the light response in the rd10 retina. *$P < 0.05$, (n.s.) not statistically $P > 0.05$.

3.6 Glycine does not contribute to unmasking of the light-evoked responses of αRGCs in the rd10 mouse

Glycine is another important inhibitory source in the retina. Besides blocking GABA receptors, PTX has also been shown to inhibit glycine receptors (Wang & Slaughter, 2005). In addition, glycine receptors were found on RGCs, as well as AII ACs and BCs in mouse retina to contribute to the threshold of RGCs (Arman & Sampath, 2012; Majumdar et al., 2007). Thus, the effect of PTX on RGCs mentioned above should also reflect the blockage of glycine inhibition. To explore if removing glycine inhibition could also contribute to the unmasking light-evoked light response, glycine receptor antagonist strychnine (1μM) was applied to P46 rd10 mouse RGCs (n=9). The application of strychnine increased the overall spike frequency, not the light-evoked spike response (**Fig 5.6 A-D**). Therefore, it suggested that removing glycine inhibition did not unmask the light-evoked signals.

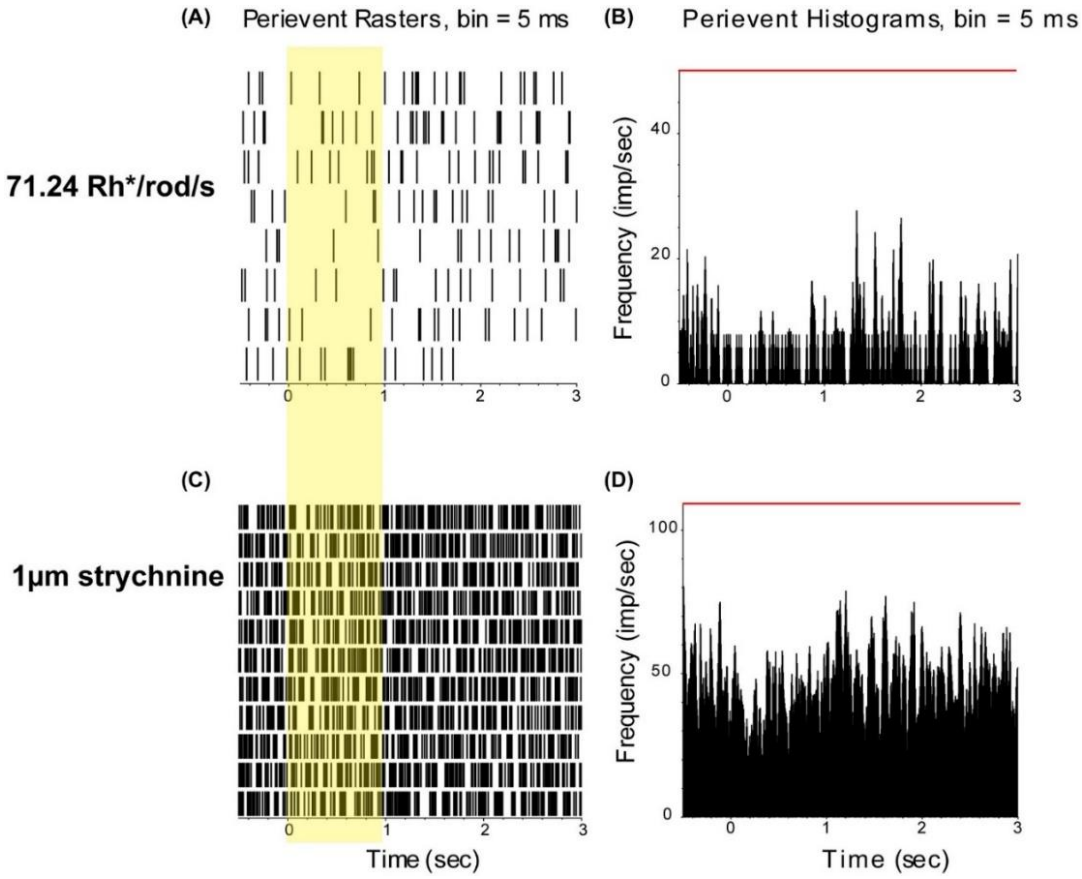

Figure 5.6 The effect of glycine receptor blocker strychnine on the rd10 mouse retina

[A, C] Raster plot with light stimuli of αRGCs before and after strychnine application.

[B, D] Corresponding PSTHs of the same response. Rasters and PSTHs show strychnine increased the overall spike frequency, but not the light-evoked spike response. The red line is the 95% confidence line.

3.7 The unmasked light-evoked response is independent to a dopaminergic circuitry

Application of PTX may cause a change of dopamine levels, perhaps through the activation of a dopaminergic circuitry, owing to removing the tonic inhibition. Dopamine affects the light sensitivity of retinal neurons, by suppressing rod-driven signals to a bright light and enhancing light sensitivity to a dim light (Herrmann et al., 2011; Li & Dowling, 2000). Besides, dopamine receptors were also found to regulate GABA release (Herrmann et al., 2011). Therefore, to test the hypothesis, it was examined whether blockage of dopamine receptors could also change the light response in RGCs or affect the process by PTX. Dopamine receptor 1(DR1) antagonist SCH23390 (5μM) or dopamine receptor 2 (DR2) antagonist Eticlopride (25μM) were applied to the rd10 retina.

After the application of DR1 antagonists SCH23390, there was no light response. However, the subsequent addition of PTX induced the light-evoked response of αRGCs (7 of 22) (**Fig 5.7 A-F**). After application of Eticlopride, no light response was induced. Similarly, the RGCs generated light-evoked spike responses after subsequent addition of PTX (5 of 19) (**Fig 5.7 G-L**). Therefore, it indicated that blockage of dopamine did not induce the light response, also, it did not interfere with the inhibition of $GABA_A$ receptors by PTX.

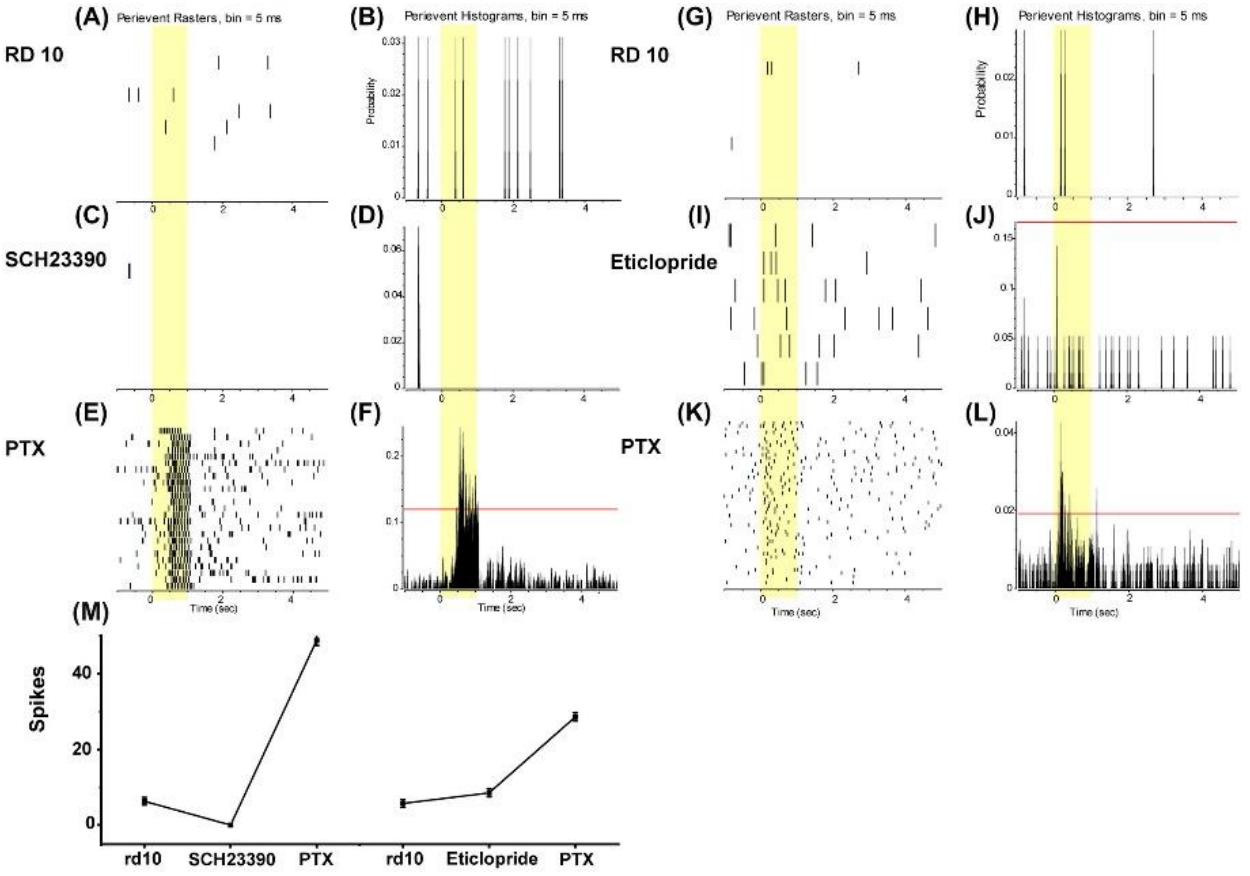

Figure 5.7 Blocking dopaminergic circuitry did not interfere with the light response of αRGCs in the rd10 mice.

[A-F] Raster plots and PTSHs of light-evoked spikes of an αRGC before, after SCH23390 (DR1 antagonist), and after PTX application.

[G-L] Raster plots and PTSHs of light-evoked spikes of an αRGC before, after Eticlopride (DR2 antagonist), and after PTX application.

[M] Summary plot of A-L. The application of dopamine receptor antagonists could not induce the light-evoked response of αRGCs in the rd10 retina.

3.8 The effect of PTX elevates the ERG b-wave and improves the spatial vision in the rd10 mouse

The effect of PTX could induce light-evoked spike response in the αRGCs in the rd10 mice. To determine whether the unmasking effect was predominantly from the outer or inner retinal origin, ERG was recorded in P41 rd10 mice with osmotic minipump delivered with PTX for 24h.

ERG results showed that no typical positive or negative scotopic threshold response (pSTR/nSTR) was observed in the control condition. STR originated from the inner retina, including the RGC layer. After PTX application, pSTR appeared at around 100ms (n=6), which reflected the function of RGCs (**Fig 5.8 A**). Compared with WT mice, P41 rd10 mice had smaller b wave amplitudes ($P< 0.05$, n=6). PTX significantly increased the amplitude of b wave ($P< 0.05$) in the rd10 mouse (**Fig B-D**). However, the amplitude of a-wave was not affected by PTX at almost all intensities (**Fig 5.8 E F**).

Decrease of contrast sensitivity is one of the clinical hallmarks of RP. To explore if the unmasking effect had transferred to the CNS and contribute to the vision improvement. Optokinetic measurements were conducted.

The visual acuity is determined as the highest spatial frequency to which the mouse regularly responded in 100% contrast. The contrast threshold was determined at the lowest contrast which elicited response with fixed spatial frequency. PTX at 0.015mg/kg/d was administrated via a minipump for 48h in P41 rd10 mice. Five rd10 mice loaded with PBS as vehicle control. The results showed that PTX significantly improved the spatial frequency (from 0.21 ± 0.02 to 0.29 ± 0.016, $n = 6$) and decreased the contrast threshold (from $62.3 \pm 6.6\%$ to $32.6 \pm 3.8\%$, $n = 6$) (**Fig 5.9**). Therefore, it suggested that the application of PTX could improve the visual acuity and contrast sensitivity, restoring part of the visual function in rd10 mice.

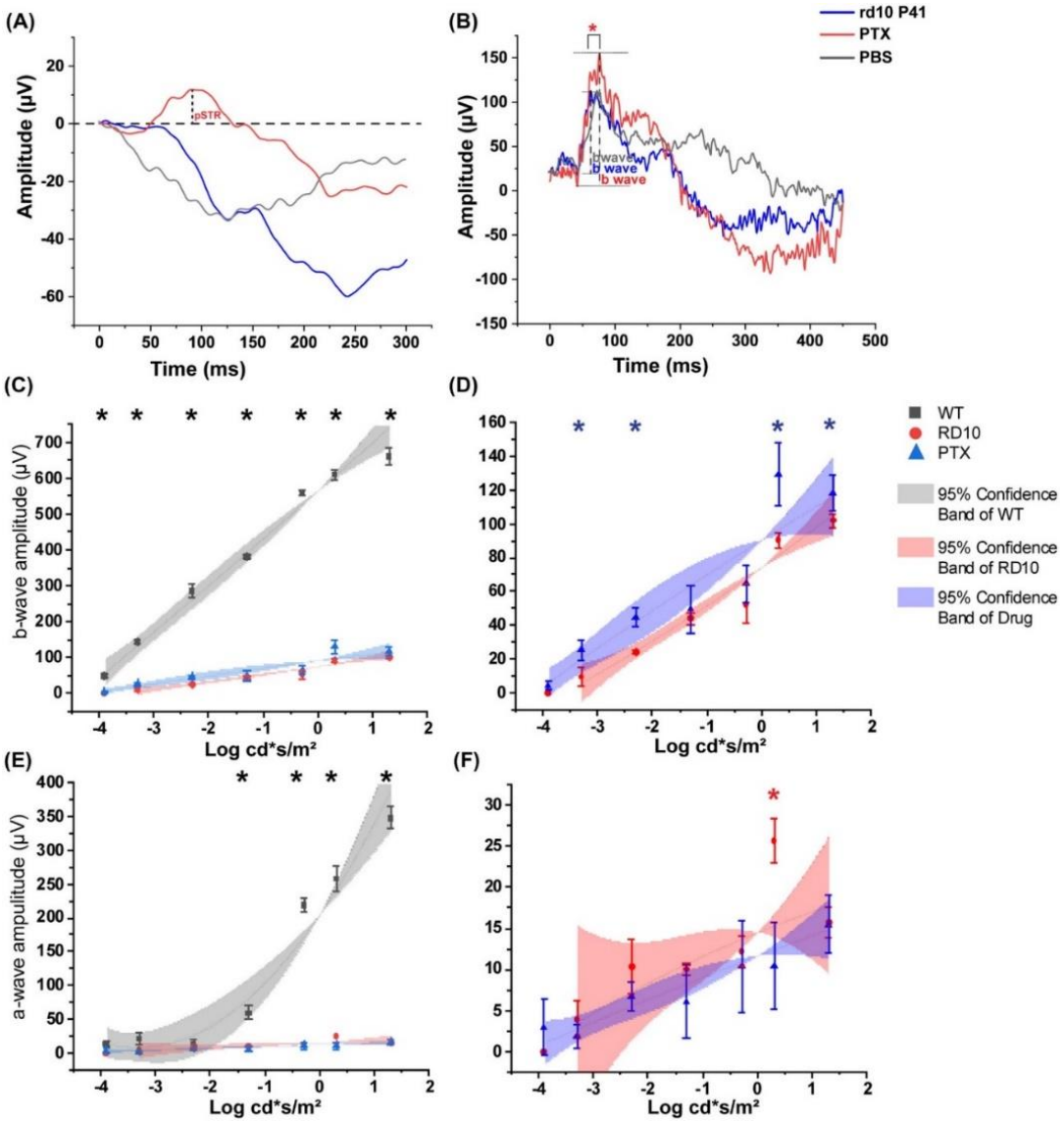

Figure 5.8 PTX induced pSTR and increased b wave in ERG from P41 rd10 mice.

[A] The representative STR waveform of rd10 mouse, rd10 mouse with PTX, and negative control. The PTX treatment induced pSTR at 100ms. **[B]** Representative waveform of scotopic ERG. **[C, D]** The b-wave of WT, rd10, and PTX treated rd10 mice. Rd10 mice had a significantly lower amplitude of b-wave, while PTX treated rd10 mice had increased b-wave than rd10 mice. **[E, F]** The a-wave of WT, rd10, and rd10 mice with PTX treated. There was no much difference between PTX treated and control groups. Polynomial fitting was applied from C-F. D and F are enlargements of C and E, respectively. Error bar indicates SEM. * P< 0.05.

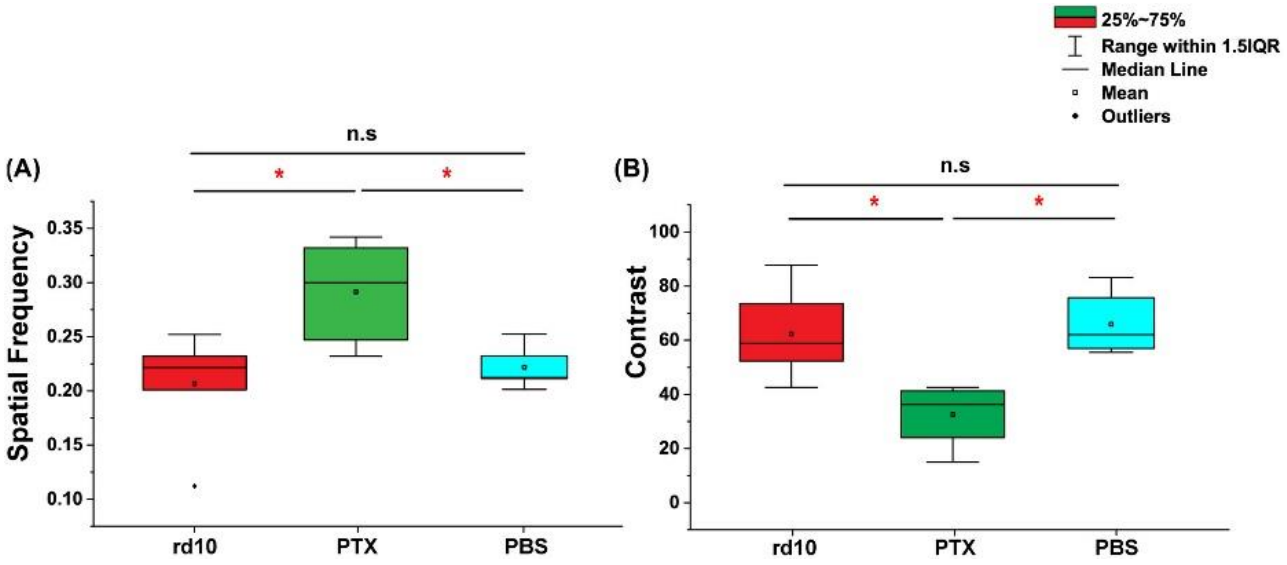

Figure 5.9 PTX increased spatial frequency and contrast sensitivity in P41 rd10 mice.

[A] Spatial frequency was tested at 100% contrast stimulation to the groups of rd10 mice, with and without PTX treatment (vehicle control). The PTX group had significantly higher visual acuity than the control and vehicle groups.

[B] Contrast sensitivity was tested at 0.092 cycle/degree (1.5 Hz temporal frequency). The PTX group had higher contrast sensitivity than the other groups. Error bars represent SEM. * P< 0.05.

4. Discussion

4.1 Unmasking input signals in neuronal system

Excitation and inhibition are two opposite forces, driving the neural system to work properly. The balance between them is crucial for physiological functions. There is a spatio-temporal equalization of the excitation/inhibition (E/I) ratio across cortical neurons in mice (Xue et al., 2014). In humans, a high E/I ratio leads to Autism, epilepsy; in contrast, a low E/I ratio leads to Schizophrenia.

Unmasking input signals has been well documented in the brain. It could be achieved by deafferentation and removing inhibition. One component for loss of afferent inhibition could unmask another afferent inhibition or excitatory response to keep the overall strength unchanged (Rajan, 2001). Deafferentation usually results in unmasking of normally ineffective connections (Dostrovsky et al., 1976). In addition, decreasing intracortical inhibition unmasked latency of intracortical connections and reshaped the cortical motor map (Jacobs & Donoghue, 1991). The dormant cortical memories are unmasked with reducing GABA in the human brain (Barron et al., 2016).

The retina, as a part of the CNS, is also believed to have the same plasticity and unmasking phenomena. Inhibition plays an important role in it. Blockage of GABA unmasked the ON response in OFF RGCs (Farajian et al., 2011). Inhibition controlled the light sensitivity of RGCs through the masking effect (Pan et al., 2016). Retinal circuits, particularly with the inhibitory mechanism, are tuning the response latency of RGCs (Tengölics et al., 2019). Inhibition also contributes to the modulation of the polarity of RGC response in the study (Geffen et al., 2007). It's noteworthy that removing inhibition could increase the light response sensitivity of RGCs (Pan et al., 2016).

In the rd10 mice, light input signals are lost due to photoreceptor degeneration, leading to the

damaged light responses in RGCs. In addition, a relatively strong inhibition may still exist in retinal degenerated retinas. Enhanced level of GABA was reported (Yazulla et al., 1997), and rod bipolar cells had a higher sensitivity to GABA in the Rd mouse (Varela et al., 2003). Therefore, this study applied the method to remove inhibition for unmasking the excitatory input signals to RGCs of the rd10 mice. It showed that application of PTX, a GABA antagonist, could unmask light responses of RGCs and restored a part of visual functions. Removing GABAergic inhibition might be one of the unmasking mechanisms in the rd10 retina.

4.2 GABAergic inhibition contributed to the PTX-induced unmasking effect

The rd10 mice carry a mutation of phosphodiesterase, which leads to rods lost, cones degenerate secondly. In this study, although a large number of photoreceptors were lost in section view, around half of cones were still retained in P46 rd10 mouse. We chose the date P38-P46, as it was supposed most of the rods died, but cones were still sustained in this timeframe. At the same time, the αRGCs in P46 rd10 mouse kept a relatively normal morphology as the WT mouse, which is consistent with the previous study indicating normal structure, survival and projections of RGCs in 3-9 months rd10 mouse (Mazzoni et al., 2008b). We recorded the light-evoked PSCs of αRGCs and found there are still excitatory and inhibitory current inputs. However, a large number of RGCs in the rd10 mouse did not have spike responses to light stimulus. It may be attributed to the excitatory postsynaptic potential did not reach the action potential threshold.

PTX is known as a non-specific GABA antagonist that could diminish GABA inhibition. PTX application increased the excitatory current amplitude and decreased the inhibitory current amplitude in single RGCs, and the effects of PTX were similar in rd10 and WT mice. Meantime, PTX induced the light-evoke spike response of RGCs. Removing GABAergic inhibition by PTX, reducing the direct inhibitory input from ACs to RGCs (feedforwards). At the same time,

inhibitory input from ACs to BCs (feedback) also reduced, leading to the increase of excitatory input of BCs to RGCs. The overall increased excitatory input may lead the cell potential to reach the action potential threshold, resulting in the light-evoked spike response.

The sustained cones suggested in results were hypothesized to provide the light signals for RGCs in rd10 mouse. However, the unmasked light-evoked spike responses might also come from melanopsin. Literature indicated that M4 intrinsically photosensitive RGC (ipRGC) is correspond to ON αRGC which have a larger soma than other types. PTX might induce the light-evoked spike responses on αRGCs by increasing sensitivity of melanopsin response.

As PTX could evoke the spike response, GABAergic circuitry was indicated to be responsible for masking the light-evoked response of RGCs in rd10 mice. Our results showed that $GABA_A$ receptor plays the main role than $GABA_C$ receptor. $GABA_A$ receptor located on AC and RGC dendrites and BC axon terminals, $GABA_C$ receptors located on the BC axon terminal. Feedback inhibition is ACs give dendrites on BCs or ACs, while feedforwards inhibition is ACs give dendrites on RGCs. Thus, $GABA_C$ only mediated the feedback inhibition, while $GABA_A$ mediated both feedback and feedforwards inhibition.

Feedback and feedforwards inhibition could also be reflected in synaptic currents recorded. The currents recorded when holding membrane potential at cation equilibrium potential (0mV) reflected the inhibitory input from ACs, which is the feedforwards inhibition. The currents recorded while holding at chloride equilibrium potential (-68mV) reflected the excitatory input from BCs. The current is the sum of bipolar cell excitation and AC inhibition, which is the feedback inhibition. As the study has shown the currents of 0 mv have decreased, reflecting the decrease of feedforwards inhibition. And the currents of -68 mv have increased, reflecting the decrease of feedback inhibition. Therefore, the involvement of $GABA_A$ receptor and the change of currents both indicated the role of feedback and feedforwards inhibition in masking signals.

Noticeably, not all tested cells showed the light response after PTX application. The reason may underlie the decrease of inhibition still could not reveal the signal from survived cones. In addition, the survived cones may not be distributed evenly in the retina. If all of the cones which one RGC received signals from have died, PTX could not induced the light responses on that RGC.

4.3 Glycine and dopamine had a little effect on masking the signal

Glycine was the inhibitory neurotransmitter released by small-field ACs. Glycine receptors are found on axons of BCs, dendrites of ACs, and RGCs. Blocking the glycinergic inhibition could not induce the light-evoked response in RGCs. It suggested that glycinergic inhibition which involves small-field ACs did not participate in the process of masking signal.

Dopamine is an important neurotransmitter underlying light adaptation and circadian rhythm. It affects the gap junction between AII-AII and AII-cone BCs. In this study, blocking dopaminergic circuitry also did not induce the light-evoked response, and did not interfere with PTX response-inducing process. It was reported dopamine receptors affect the GABA release from HCs in dim light (Herrmann et al., 2011). However, any modification of rod pathway is not likely to affect the signal in rd10 mice as it has been damaged already. Moreover, the retinal degenerative disease has dopamine deficiency (Djamgoz et al., 1997). The dopamine production in the rd10 retina may be rare, as the photoreceptors could not activate the dopaminergic ACs (Qiao et al., 2016). Therefore, blocking dopamine receptors in this process of rd mice has little effect on the signal manipulations.

4.4 PTX increased the results on ERG and behavior tests

Subcutaneous PTX administration increased the pSTR and b wave of ERG. The origin of pSTR is not fully clear, but part of it could reflect function of RGCs (Saszik et al., 2002). B-wave originated from the connection between photoreceptors and ON BCs. GABA receptors were

found in all of the five types of retinal neurons including BCs. Ionotropic GABA receptors were present at dendrites and terminals of BCs and could provide presynaptic and postsynaptic inhibition (Shields et al., 2000). Therefore, PTX might increase the b-wave through inhibiting the GABA receptors on BCs. Also, optic nerve transection which mainly affect RGCs could decrease b wave (Smith et al., 2014). Thus, the increased RGCs electrical activity may also contribute to the b-wave.

PTX increased visual acuity and contrast sensitivity of rd10 mice. These results showed that PTX could increase the function of the retina and elevate the vision in vivo. The application of PTX was through subcutaneous osmotic minipumps in ERG and behavior tests. It has pros that could take effect continuously without hurting the eye surrounding tissue. However, as a systematic administration, the pathways which took the effect may include multiple targets, which could not be directly attribute to the PTX effect on the retina. It only suggested the possibility that unmasking spikes code the effective information and transferred it to CNS.

5. Conclusion and Further Study

This study focused on P38-P46 rd10 mice, the early retinal degenerative model, in which most of the rods lost at age P38-P46 but some cones still retained. Applying PTX unmasked light response of RGCs, possibly by blocking GABA inhibition. PTX application also increased ERG and optokinetic responses to restore part of visual function.

However, there are limitations. The mechanism of PTX in increasing of visual function is not clear in this study. We only revealed the unmasking effect in a single RGCs level, but have not tested if the unmasking spikes could transfer to the CNS to increase the vision. Although the behavior test showed an increase of visual acuity, the targets were multiple and unclear. Therefore, further experiments should strive to reveal the activity in the visual cortex after topical or intravitreal injection of PTX.

This study also suggested the translational potential of PTX as RP therapy. However, toxicity and side effects of PTX should be considered. PTX is poisonous to humans and other mammals, it could lead to seizures and respiratory paralysis in a high concentration. It was used to counteract depressants poisoning as the effect on GABA inhibition, but using in medication has been abandoned due to the toxic effects of the agent. Only the plant it derived from, cocculus, is used in traditional medicine. The LDLo (lethal dose low) of PTX in humans is 0.357mg/kg. Whether the low concentration would have an effect on the eye is not clear. In addition, PTX as a non-specific GABA antagonist, might have similar side effects to other GABA receptor antagonists, which might cause anxiety, seizure, and other psychotic symptoms (Xu & Wong, 2018). Therefore, more experiments should be done with caution and discretion before clinical application of PTX in RP patients.

Chapter 6 RGCs changes by elevated IOP

1. Introduction

Glaucoma is the leading cause of vision loss, characterized by progressive neuron death. High IOP plays a major role in glaucoma, and lowing IOP becomes the key therapy for glaucoma patients nowadays (Jonas et al., 2017; Weinreb et al., 2014). RGCs cell death is responsible for vision loss during the glaucoma process. Exploring the method to protect the RGCs and decrease the RGCs' vulnerability is a feasible way to prevent and treat glaucoma.

Although inherited glaucoma was reported in DBA/2J mice, the variety in expression and the substantial pathological changes make it unsuitable to study the effect of high IOP (Turner et al., 2017). Increasing IOP experimentally is still the routine used to make glaucoma animal models. Episcleral vein injection or ablation could increase the IOP by reducing aqueous humor drainage, however, the extent and duration of IOP elevation varied. Translimbal laser photocoagulation could also reduce aqueous humor outflow to increase IOP. This technique requires multiple retreatments to maintain the IOP elevation and may cause corneal decompensation. Microbeads injection is recently used to increase IOP by obstructing the aqueous humor outflow. Simplicity and low cost of this technique make it widely used to study glaucoma (Johnson & Tomarev, 2016). In this study, microbeads injection method was adopted to elevate the IOP of the mouse.

In the previous study, the morphology, coupling patterns, and electrical signaling of ON and OFF RGCs were studied in normal conditions. The effects of high IOP on ON and OFF RGCs would be investigated in this study.

Retinal function was affected in glaucoma or ocular hypertension patients. Studies showed decreased amplitude of pattern ERG (Bach et al., 2006; Falsini et al., 2008) and multifocal

ERG (Chan & Brown, 1999), selective loss of oscillatory feature (Fortune et al., 2002), decreased PhNRs, d-wave and i-wave at offset (Horn et al., 2011), decreased amplitudes of cone ERG (North et al., 2010). Experimental glaucoma in animal models also brought reduction in amplitude in both positive and negative potentials in ERG (Bayer et al., 2001a; Bayer et al., 2001b; Bui et al., 2005; Holcombe et al., 2008; Lakshmanan et al., 2019; Viswanathan et al., 2000), with two studies reported increase b waves (Frankfort et al., 2013; Khan et al., 2015).

The RGCs' signaling was also changed in IOP elevation, including decreased spontaneous spikes, sensitivity, and ISI variance were showed before RGCs death (Della Santina et al., 2013; Ou et al., 2016; Pang et al., 2015). Gap junction blocker was shown to protect the RGCs in the high IOP. However, the detailed electrophysiological changes of ON and OFF RGCs including the synchronous firing were not clarified in the early stage of the IOP elevation.

This study aims to figure out signaling changes of RGCs in elevated IOP mouse models. Microbeads were injected into the anterior chamber to elevate the IOP of mice for 4 weeks. Retinal function was compared by ERG between normal and high IOP. RGC spontaneous activity and light response were tested by single-cell patch recording. Here we only showed the very preliminary data. Four-week elevation of IOP decreased the number of RGCs. Light sensitivity of OFF RGCs significantly increased in IOP elevation. Further experiments are needed to verify the changes. In addition, we also would like to test the possibility of recovering effects by blocking gap junction. We hypothesized that the IOP elevation could change the electrical signaling of RGCs, and the changing may favor increased excitable status, such as increased spontaneous activity, light sensitivity, ratio of excitation and inhibition currents, as well as concerted activity. Blocking gap junction might recover these responses.

2. Methods

2.1Animals

The KCNG-YFP (6-8 weeks) mice (Duan et al., 2015) of either sex were used in the experiments.

2.2 Induction of elevated IOP by microbeads injection

The elevated IOP was generated by injection of polystyrene microbeads into the anterior chamber. This method was used in other studies to successfully induce IOP elevation (Au - Ito et al., 2016; Sappington et al., 2010). In this study, a mixture of 6μm microbeads (Polybead dyed blue 6 micro microsphere, Polysciences, Cat# 15715) and 1μm microbeads (Polybead dyed yellow 1 micro microsphere, Polysciences, Cat#15713-15) were used. The solution of blue beads was concentrated 15-20 fold to reach the final concentration, which contains approximately $2.4*10^7$ yellow microbeads, and $4.7*10^6$ blue microbeads per 1.5-2 μl. Mice were anesthetized with an intraperitoneal injection of 100mg/kg ketamine and 20 mg/kg xylazine mixture. Pupils were dilated with 1% tropicamide ophthalmic solution (Mydriacyl, Alcon). Anesthetic drop lidocaine was applied to each eye. The sharp micropipettes were pulled from borosilicate glass capillaries (World Precision Instruments Cat#1B20F-4). The 1ml syringe connected to the micropipette by polyethylene tubing was used for injection. The cornea was punctured by a microsurgical stab knife (Sharpoint, Surgical Specialties REF 72-1501) 3mm central to the ora serrata. The micropipette was inserted into anterior chamber avoiding contact with the lens, inner cornea, and iris. A 1.5-2μl mixed microbeads solution was injected into the anterior chamber of right eye of the mouse. Left eye was left with no treatment as control. After injection, the animals were allowed to recover for 24 hours before resumption of IOP measurements.

Measurement of IOP was made using a tonometer (Tonolab). The mice were given a little

inhaled isoflurane to free constrain and tested IOP. As general anesthesia decreased IOP with time, IOP was tested immediately after the mouse losing moving ability to minimize differences from anesthesia. Subsequent measurements were performed at 9-10 am twice a week. The tonometer averages 6 tests as one reading. For each measurement, 3 readings were averaged. The measurement was conducted until 4 weeks after beads injection.

2.3 ERG recording

A full-filed Ganzfeld (Q450; RETI Animal, Roland Consult, Germany) was used to measure the electrical signals. A pair of gold wire corneal electrodes (Roland Consult) was used as the active electrode. Two needle electrodes inserted into the lateral canthi to serve as references; one needle electrode inserted into the base of the tail as a ground electrode. The impedance of the electrodes was maintained below 10 kΩ. Stimuli were presented in multiple levels with increasing energy ranged from log −4.32 cd*s/m^2 to log 1.30 cd*s/m^2. Subsequently, 10-min light adaptation was given and photopic responses were recorded. The Positive scotopic threshold response (pSTR) and negative scotopic threshold response (nSTR) reflected the function of RGCs. pSTR usually formed at 100-120ms, nSTR appears around 150-250ms. The wave reflected photoreceptor's function, and the b wave reflected the inner retina function. RGCs function could also be implicated in photopic negative response (PhNR).

2.4 Immunohistochemistry and cell counting

Anti-Brn-3a mouse antibody (1:500; Santa Cruz; Cat#sc8426), DAPI (Sigma-Aldrich Cat# D9542) were used.

To count the cell number, all the cells in GCL were labeled with DAPI (blue), RGCs were double stained with Brn3a (red). The images were analyzed by Image J (Bethesda, MD, 1.52i, RRID: nif-0000-30467). Briefly, use "color split" to split blue and red channel, which is DPAI and Brn3a-stained, respectively. Adjust the threshold to make the stained cells clearly show.

For DAPI channel, “Watershed” was used to split the connected clusters which should be two or more cells. “Analyze pixel” was used to count the numbers of clusters pixels and the results were the numbers of DAPI-stained cells. For the Brn3a channel, because it also stained the blood vessels in mouse retina, the automatic counting methods were not suitable. The Brn3a-stained cell numbers were counted manually.

2.5 Electrical recording

Green full-field light (λ = 525 nm) delivered by diode was used as light stimulus. Loose patch was used to record the spike activity of RGCs.

Intensity-response profiles for individual cells were generated by plotting spike frequency of the response with stimulus intensities ranged from 0.15 to 131 Rh*/rod/s. The frequency of light-evoked ON and OFF response of RGCs was calculated by subtraction of the background frequency from those evoked by the light stimulus onset and offset, respectively. Averaged response data were then normalized and plotted against the intensity of the light stimuli using Origin software (OriginLab, Northampton, MA, USA). Data points were fitted by the classic Hill equation(Thibos & Werblin, 1978) as follows:

$$\mathrm{R(I)} = \frac{\mathrm{Rmax}\ I^n}{(k^n + I^n)}$$

where R is the measured response, R_{max} is the maximal response, I is the stimulus intensity, n is the slope factor, k is the light intensity that produces a response of 0.5 Rmax. Response thresholds for individual cells were taken as 5% of the maximal spike frequency.

3. Results

3.1 Beads injection leads to IOP increase

We used the microbeads injection method to induce the elevation of IOP in the mouse eye. The beads injected were stuck in corner of the iris-cornea and Schlemm's canal (**Fig 6.1 A**). The IOP was increased 3.28±1.41 mmHg 7 days after injection (**Fig 6.1 B**: 7 days Control eye: 15.37±0.82, Beads eye: 18.65±1.44; p=0.033, n=18), and could last to 28d after injection. The mice of which IOP increased over 30 mmHg or did not reach 15 mmHg during the 4 weeks were excluded, as the mice with IOP over 30 mmHg usually had chances to develop corneal pathologies like edema and inflammation. The mice with cornea edema, hemorrhage, inflammation of anterior segment, or eyeball atrophy were also excluded to eliminate the effect rather than IOP elevation.

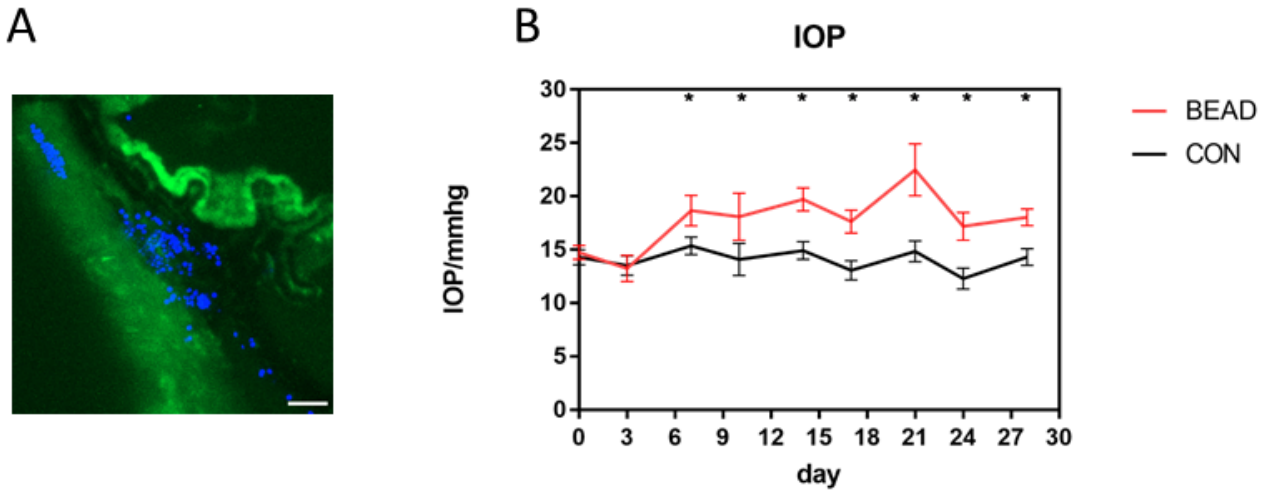

Figure 6.1 Microbeads injection induced IOP elevation in the mouse

[A] The microbeads injected were obstructed at the corner of iris-cornea, Schlemm's canal.

[B] IOP of microbeads-injected eyes (n=18) and control eye (n=18) in 28 days after injection. Day 0 is the injected day. The elevation was statistically significant from 7d to 28d.

* p<0.05 (paired t-test).

3.2 The RGCs number decreased after 4-week elevation of IOP

The retinas of the microbeads-injected eyes and control eyes were removed after 4 weeks and stained with Brn3a and DAPI for cell counting. All the cells in GCL were stained with DAPI, RGCs were labeled with Brn3a, ACs were indicated as DAPI-positive but Brn3a-negative cells (**Fig 6.2 A-C**). Two areas in 4 quadrants were taken by confocal and averaged in each retina (**Fig 6.2 D**). The peripheral number of RGCs in the bead retina showed significant decrease compared with the control retina (Bead: 18.96±4.06, Control: 21.05±3.53; p=0.01). The RGCs' number also decreased in central areas in IOP elevation (Bead: 23.03±4.88, Control: 25.75±4.50; p=0.03). ACs did not show a statistical decrease in central and peripheral retinas (**Fig 6.2 E-F**).

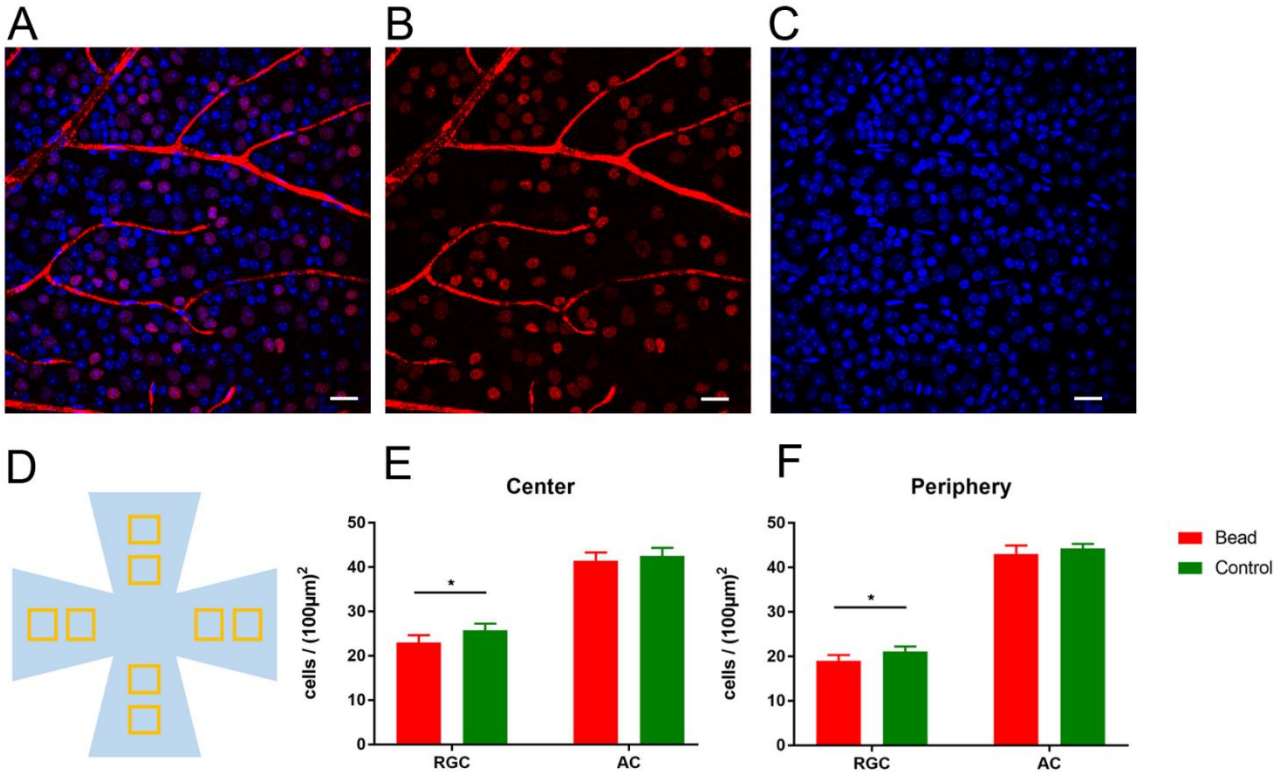

Figure 6.2 Number of RGCs and ACs under IOP elevation.

[A-C] Cells in GCL were stained with Brn-3a (red) and DAPI (blue). Brn3a-positive cells were indicated as RGCs. DAPI-positive and Brn3a-negative cells were indicated as ACs. Scale bar: 20μm.

[D] Two areas in 4 quadrants of the retina were taken by confocal. The central 4 areas were averaged as Center in F, peripheral 4 areas were averaged as Periphery in G.

[E] RGCs in central area showed significant decreased under IOP elevation (RGC: $p=0.03<0.05$, AC: $p=0.73$; Wilcoxon matched-pairs signed rank test).

[F] Peripheral RGCs showed significant decreased under IOP elevation (RGC: $p=0.01<0.05$, AC: $p=0.57$).

Scotopic and photopic ERG was conducted after 4 weeks. The scotopic threshold response (STR) reflected the responses of RGCs. The positive STR (pSTR) and negative STR (nSTR) usually elicited at around 120ms and 220ms, respectively (Bui & Fortune, 2004). Photopic negative response (PhNR) could also reflect the RGCs activity (Chrysostomou & Crowston, 2013). Photoreceptor function could be reflected by a wave, and b wave mainly indicated BCs function. The results showed no significant difference in amplitude of pSTR, nSTR (**Fig 6.3 A**, light intensity -4.32 cd*s/m^2), a wave, b wave (**Fig 6.3 B**, light intensity -0.29 cd*s/m^2), and PhNR (**Fig 6.3 C**) ($p>0.05$, $n=5$). Only the induce time of a wave was delayed in Beads eyes (**Fig 6.3 D**).

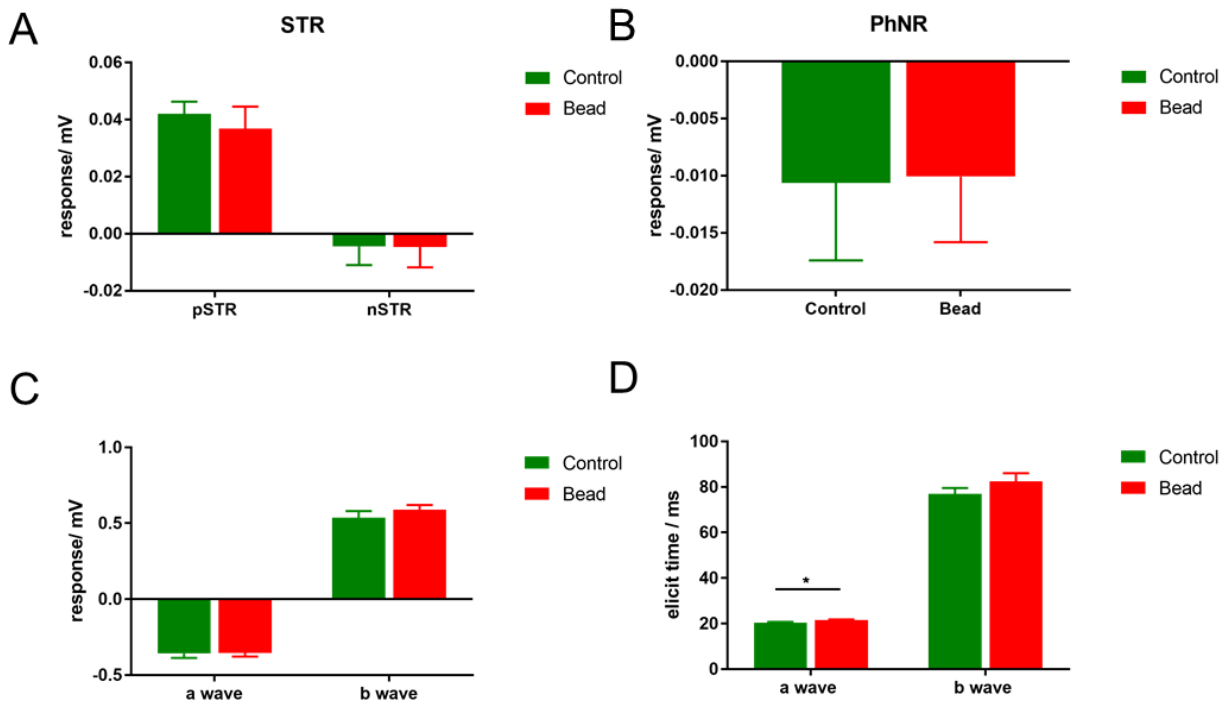

Figure 6.3 ERG results from the microbeads injected and control eyes.

[A-C] Amplitude of response of STR, PhNR, a wave, and b wave in Beads and Control eyes. There was no significant difference between the two groups.

[D] Only the elicit time of a-wave in Bead eyes was delayed compared with control eye (a wave time: 20.3±0.37 in Control, 21.5±0.31 in Bead; * p=0.03, paired t-test, n=5).

3.3 IOP elevated of 4 weeks increased light sensitivity of OFF RGCs

The spontaneous spike activity of single αRGC was recorded. The RGCs under IOP elevation had more frequent firing rates, but no statistical difference (**Fig 6.4 A**). Concerning the synchronous activity, among 31 pairs of αRGCs recorded in Bead retinas, 8 pairs spiking activity were synchronized. The percentage number in IOP elevation 26% (8/31) is higher than the number 22% (2/9) in control condition, but there was no significant difference (**Fig 6.4 B**, p=0.21).

According to the light sensitivity, the light response of a total of 26 αRGCs in the control group, 24 αRGCs in the IOP elevation group, and 6 αRGCs in the Cx36-knockout group were measure from low to high light intensity and fitted with the Hill equation. The light sensitivity threshold was calculated as 5% of the light intensity inducing the maximum light response. There was no significant difference in light sensitivity threshold of all the cells among the three groups (**Fig 6.4 C**). However, after separating the ON and OFF αRGCs, the OFF αRGCs in the Bead group had a significantly lower light sensitivity threshold than the control group (**Fig 6.4 D**), which suggested the higher sensitivity under IOP elevation.

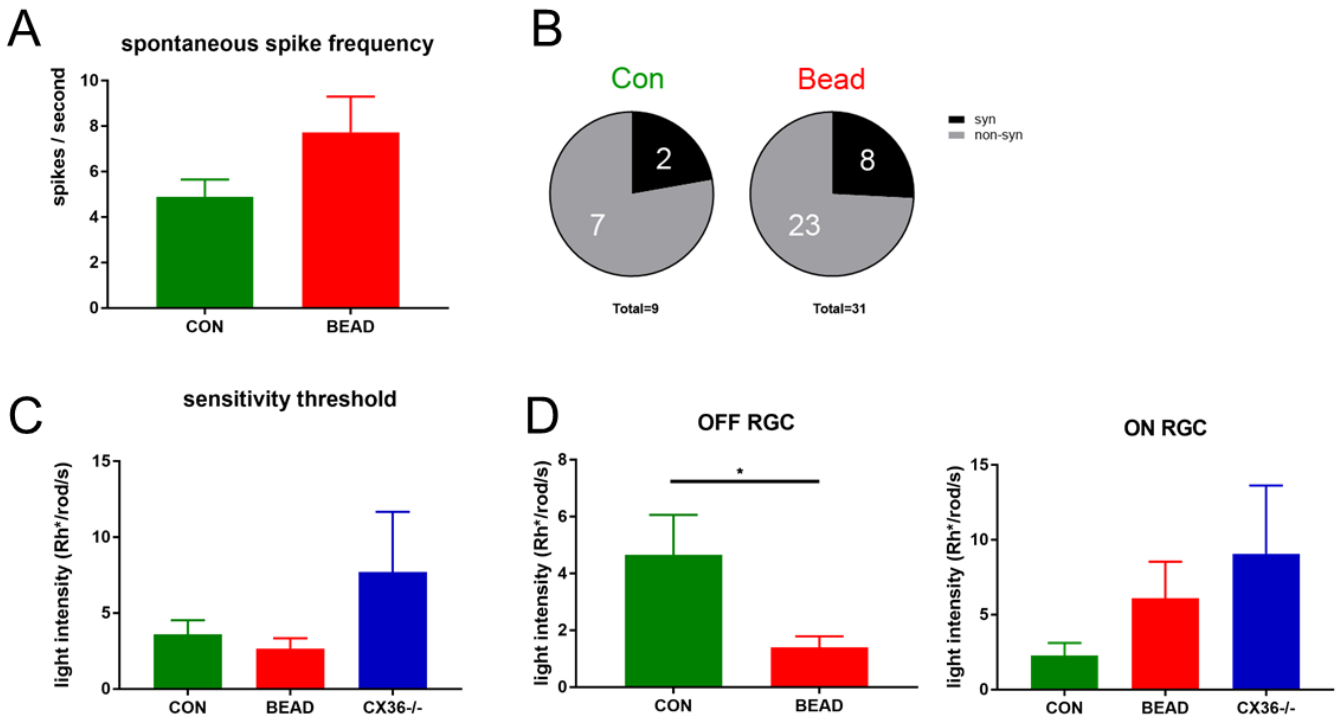

Figure 6.4 The electrical activity of αRGCs in the beads injected and control retinas

[A] The spontaneous spike frequency of αRGCs did not show significant difference between Bead and Control eyes (Bead: 7.73±1.57 spikes/s, n=45; Control: 4.88±0.77 spikes/s, n=24; p=0.20; unpaired t-test).

[B] The synchronous percentage of the αRGCs recorded in Control and Bead eyes were 22% (2/9) and 26% (8/31), respectively. There was no significant difference (p=0.21; chi-squared test).

[C] The light sensitivity threshold of αRGCs in Control eye (n=26), Beads eye (n=24), and Cx36-knockout mouse eye (n=6). No statistical difference among the groups (One-way ANOVA).

[D] Left: OFF αRGCs in the Bead eye had significantly lower light sensitivity threshold compared with the Control eye (Control: 4.56±1.4 Rh*/rod/s, n=16, Bead: 1.39±0.39 Rh*/rod/s, n=16; * p=0.032, t-test). Right: No significant differences were observed among the Control, Bead and $Cx36^{-/-}$ groups.

4. Discussion

The preliminary data showed the method of microbeads injection significantly increased the IOP of mouse eye in 7 days. This increase could last for at least 21 days. Results showed that 4-week mild IOP elevation induced overall 11% RGCs lost. Other studies also reported the RGCs and ACs loss after IOP elevation in mouse, but the lost percentage and time varied. One study reported the RGCs and ACs did not show a significant decrease until 4 weeks after IOP elevation (Akopian et al., 2016). While the other study reported 25% RGC loss at 2 weeks after IOP elevation (Chen et al., 2011). The ACs, especially ACs coupled to RGCs, were also reported to lost under IOP elevation (Akopian et al., 2016). However, we did not observe a significant loss of ACs in beads-injected retina, which may be due to relative low amplitude of the IOP elevated.

The ERG was demonstrated to have the potential to predict glaucoma. One study reported the increased b-wave and decreased pSTR before RGCs loss (Frankfort et al., 2013). The other studies reported decreased oscillatory potential amplitudes or STR in IOP elevated animals (Bayer et al., 2001a). The ERG also showed decreased amplitude in patients of glaucoma or ocular hypertension (Falsini et al., 2008; Horn et al., 2011; North et al., 2010). In this study, the ERG result at 4 weeks did not show any significant changes in the amplitude between high IOP and control group. The insignificant results may be due to the small samples or IOP elevated amplitude. Meantime, the fluorescent microbeads injected may affect the normal light reflection and absorption through ocular components, varying the accuracy of ERG to assess the retinal function.

There are discrepancies about the electrical activity of single RGCs under IOP elevation in other studies. It was reported increased (Ward et al., 2014) or decreased (Della Santina et al., 2013) spontaneous activity of RGCs in mice, decreased light sensitivity (Pang et al., 2015), and faster temporal kinetics of receptive field (Tao et al., 2019). In cortical neurodegenerative

diseases such as Alzheimer's disease and Parkinson's disease, a hyperexcitable status of neurons was usually observed (Branch et al., 2016; Busche & Konnerth, 2016; Saxena & Caroni, 2011; Wainger et al., 2014). Glaucoma shares lots of similarities with the cortical neurodegenerative diseases in the etiological and pathological processes. Thus, in the high IOP condition, we postulated the status of RGCs should have a similar process before the final degeneration.

The preliminary data showed that light sensitivity threshold of OFF αRGCs was lower than control group, indicating a hyper-excitable condition of OFF αRGCs. The other study also reported paradoxical enhanced excitability of RGCs. RGCs increased resting potential and firing rate after IOP elevation for 2 weeks and decreased subsequently at 4 weeks (Risner et al., 2018). The hyper-excitability only observed in OFF cells may underlie different sensitivity of ON and OFF cells. OFF cells may have higher sensitivity to detect IOP elevation and enter the hyper-excitable condition, or alternatively OFF cells keep a longer time in hyper-excitability than ON cells.

Previous literature suggested gap junction blockers provided neuroprotective effect to RGCs under high IOP, and RGCs of Cx36-knockout mouse had more resistance to IOP elevation. RGCs of Cx36-knockout mice are postulated to have lower light sensitivity than the wide type mice. Deficiency of rod pathway of Cx36-knockout mouse led to decrease of light sensitivity of ON RGCs (Deans et al., 2002), and substantial decreased glycinergic input affected light sensitivity of OFF RGCs (van Wyk et al., 2009). The 6 ON RGCs of Cx36-knockout mice had lower but insignificant light sensitivity than control group in this study. We suspected that elevated IOP increased the light sensitivity of RGCs at the beginning, and lower light sensitivity of RGCs in Cx36-knockout mice may underlie the protective effects.

5. Future work

Some of the preliminary data did not show statistically different results. The reason may underlie the relatively low amplitude of IOP elevation and small sample size. Therefore, the following experiments should be performed in the future study.

The first step is to improve and stabilize the IOP elevation in the microbeads mouse model. The mouse model in the preliminary data only showed an increase IOP of 3 mmHg at day 7 after beads injection. The amount of elevation might be not high enough to induce insults on the RGCs effectively. Meantime, the IOP showed unstable elevation which led to a high percentage of exclusion and high variation among the samples, which might be the major reason for the insignificant results. Thus, we need to modify the microbeads injecting procedure to increase and stabilize IOP elevation. Secondly, increase the sample size to verify the quantitative changes and insignificant differences in preliminary data. Thirdly, gap junction antagonists will be applied to RGCs in IOP elevation group. Gap junction blockers were demonstrated to protect the neuron under IOP elevation. We would like to investigate the mechanism by measuring electrical activity of RGCs.

Need to mention that, the mouse is shown to lack the lamina cribrosa, which is an important target of human glaucoma disease. The conclusions got from mice need to deal with caution when applying to humans in ocular hypertension disease.

Chapter 7 Overall conclusions

RGCs are the output neurons in the vertebrate retina to the brain. There are more than 40 types of RGCs in the mouse retina to detect and encode distinctive aspects of visual information.

This thesis firstly characterized the morphology of ACs coupled to RGCs, specifically the most studied ON and OFF αRGCs. ACs provide feedback inhibition to shape the visual signals such as computing local contrast in the circuit formed around RGCs. Wide-field or polyaxonal ACs are coupled to the ON and OFF αRGCs to different coupling extents. After the basic characterization of αRGCs and their circuitry with ACs, the signaling of RGCs was investigated under the pathological conditions, including myopia, retinitis pigmentosa, and glaucoma.

Defocus is an important factor of myopic etiology. As evidence shows that the retina could detect defocus during the visually guided refractive development period, RGC therefore becomes a strong candidate for mediating the retina to sclera signaling pathway leading to myopia. Both excitatory and inhibitory conductance of ON and OFF αRGCs decreased in defocused stimuli.

As atropine is used to control myopia progression in clinical trials, the effect of atropine on αRGCs was tested. Low-dose atropine did not change the morphological and firing patterns of most αRGCs. However, atropine unmasked ON response in certain OFF αRGCs possibly via the GABAergic pathway. This effect might disturb the accuracy of visual signaling transport to the CNS.

These two studies investigated the etiology and pharmaceutical therapy of myopia. We found that RGCs could sense the defocus in electrical activity. In addition, atropine also changed the RGCs spiking activities. The GABAergic pathway may involve in this process, probably via mACh receptors. Our further study will focus on a specific RGCs type, ON-OFF RGCs, as

their dendritic stratification and direction-selective function. We postulated to observe spiking activities responded to defocus in ON-OFF RGCs, probably in the function of directive selection. Since ACh and GABA are important neurotransmitters to modulate the directive selection of RGCs, it would be interesting to observe the defocus effect on ON-OFF RGCs and whether atropine would affect the process via ACh and GABA pathways.

Retinitis pigmentosa is a group of blinding eye diseases characterized by photoreceptors lost. Unmasking input signals under physiologic conditions is well documented in the brain and the retina. To take advantage of this pre-existing physiologic masking of input signals in the rd10 mouse retina, PTX was applied to unmask the signals of αRGCs to light stimuli from surviving cones. Behavioral measurement of visual acuity and ERG of rd10 mice showed vision improvement with PTX application. Thus, unmasking signals might provide a cost-effective method to limit the deterioration of the neurodegenerative disease.

Glaucoma is a leading cause of blindness worldwide. Electrical activities of αRGCs in IOP elevation were also investigated via microbeads injection. Preliminary data showed that 4-week elevation of IOP led to reduction of RGCs numbers and increased light sensitivity on certain RGCs. Changes in electrical activities of RGCs were postulated in an early stage of IOP elevation. However, some biophysical parameters did not show significant changes in preliminary data, suggesting further experiments are needed to optimize the animal models.

Overall, the observations of signaling of RGCs in different physiological and pathological conditions have important consequences for understanding neural information processing in the retina. Signaling of RGCs reflects very early pathological changes, provides biophysical mechanisms for exploring preventive strategies for eye diseases in early stage.

References

Aasen, T., Leithe, E., Graham, S. V., Kameritsch, P., Mayán, M. D., Mesnil, M., . . . Tabernero, A. (2019). Connexins in cancer: bridging the gap to the clinic. *Oncogene, 38*(23), 4429-4451. doi:10.1038/s41388-019-0741-6

Akopian, A., Atlasz, T., Pan, F., Wong, S., Zhang, Y., Volgyi, B., . . . Bloomfield, S. A. (2014). Gap junction-mediated death of retinal neurons is connexin and insult specific: a potential target for neuroprotection. *J Neurosci, 34*(32), 10582-10591. doi:10.1523/jneurosci.1912-14.2014

Akopian, A., Kumar, S., Ramakrishnan, H., Roy, K., Viswanathan, S., & Bloomfield, S. A. (2017). Targeting neuronal gap junctions in mouse retina offers neuroprotection in glaucoma. *J Clin Invest, 127*(7), 2647-2661. doi:10.1172/jci91948

Akopian, A., Kumar, S., Ramakrishnan, H., Viswanathan, S., & Bloomfield, S. (2016). Amacrine Cells Coupled to Ganglion Cells via Gap Junctions Are Highly Vulnerable in Glaucomatous Mouse Retinas: Amacrine cells are vulnerable in glaucoma. *Journal of Comparative Neurology, 527*. doi:10.1002/cne.24074

Ameri, H. (2018). Prospect of retinal gene therapy following commercialization of voretigene neparvovec-rzyl for retinal dystrophy mediated by RPE65 mutation. *Journal of current ophthalmology, 30*(1), 1-2. doi:10.1016/j.joco.2018.01.006

Amthor, F. R., Takahashi, E. S., & Oyster, C. W. (1989). Morphologies of rabbit retinal ganglion cells with concentric receptive fields. *J Comp Neurol, 280*(1), 72-96. doi:10.1002/cne.902800107

Anstice, N. S., & Phillips, J. R. (2011). Effect of Dual-Focus Soft Contact Lens Wear on Axial Myopia Progression in Children. *Ophthalmology, 118*(6), 1152-1161. doi:https://doi.org/10.1016/j.ophtha.2010.10.035

Applebury, M. L., Antoch, M. P., Baxter, L. C., Chun, L. L. Y., Falk, J. D., Farhangfar, F., . . . Robbins, J. T. (2000). The Murine Cone Photoreceptor: A Single Cone Type Expresses Both S and M Opsins with Retinal Spatial Patterning. *Neuron, 27*(3), 513-523. doi:https://doi.org/10.1016/S0896-6273(00)00062-3

Arman, A. C., & Sampath, A. P. (2012). Dark-adapted response threshold of OFF ganglion cells is not set by OFF bipolar cells in the mouse retina. *J Neurophysiol, 107*(10), 2649-2659. doi:10.1152/jn.01202.2011

Arumugam, B., Hung, L.-F., To, C.-h., Holden, B., & Smith, E. L., III. (2014). The Effects of Simultaneous Dual Focus Lenses on Refractive Development in Infant Monkeys. *Invest Ophthalmol Vis Sci, 55*(11), 7423-7432. doi:10.1167/iovs.14-14250

Arumugam, B., & McBrien, N. A. (2012). Muscarinic Antagonist Control of Myopia: Evidence for M4 and M1 Receptor-Based Pathways in the Inhibition of Experimentally-Induced Axial Myopia in the Tree Shrew. *Invest Ophthalmol Vis Sci, 53*(9), 5827-5837.

doi:10.1167/iovs.12-9943

Au - Ito, Y. A., Au - Belforte, N., Au - Cueva Vargas, J. L., & Au - Di Polo, A. (2016). A Magnetic Microbead Occlusion Model to Induce Ocular Hypertension-Dependent Glaucoma in Mice. *JoVE*(109), e53731. doi:doi:10.3791/53731

Auferkorte, O. N., Baden, T., Kaushalya, S. K., Zabouri, N., Rudolph, U., Haverkamp, S., & Euler, T. (2012). GABA(A) receptors containing the α2 subunit are critical for direction-selective inhibition in the retina. *PLoS One, 7*(4), e35109-e35109. doi:10.1371/journal.pone.0035109

Bach, M., & Poloschek, C. M. (2013). Electrophysiology and glaucoma: current status and future challenges. *Cell and Tissue Research, 353*(2), 287-296. doi:10.1007/s00441-013-1598-6

Bach, M., Unsoeld, A. S., Philippin, H., Staubach, F., Maier, P., Walter, H. S., . . . Funk, J. (2006). Pattern ERG as an Early Glaucoma Indicator in Ocular Hypertension: A Long-Term, Prospective Study. *Invest Ophthalmol Vis Sci, 47*(11), 4881-4887. doi:10.1167/iovs.05-0875

Baden, T., Berens, P., Franke, K., Roman Roson, M., Bethge, M., & Euler, T. (2016). The functional diversity of retinal ganglion cells in the mouse. *Nature, 529*(7586), 345-350. doi:10.1038/nature16468

Baden, T., Schaeffel, F., & Berens, P. (2017). Visual Neuroscience: A Retinal Ganglion Cell to Report Image Focus? *Current Biology, 27*(4), R139-R141. doi:https://doi.org/10.1016/j.cub.2016.12.022

Baldridge, W. H. (1996). Optical Recordings of the Effects of Cholinergic Ligands on Neurons in the Ganglion Cell Layer of Mammalian Retina. *The Journal of Neuroscience, 16*(16), 5060. doi:10.1523/JNEUROSCI.16-16-05060.1996

Banerjee, S., Wang, Q., So, C. H., & Pan, F. (2020). Defocused Images Change Multineuronal Firing Patterns in the Mouse Retina. *Cells, 9*(3). doi:10.3390/cells9030530

Barathi, V. A., Chaurasia, S. S., Poidinger, M., Koh, S. K., Tian, D., Ho, C., . . . Zhou, L. (2014). Involvement of GABA Transporters in Atropine-Treated Myopic Retina As Revealed by iTRAQ Quantitative Proteomics. *Journal of Proteome Research, 13*(11), 4647-4658. doi:10.1021/pr500558y

Barnett, M. W., & Larkman, P. M. (2007). The action potential. *Practical Neurology, 7*(3), 192.

Barron, H. C., Vogels, T. P., Emir, U. E., Makin, T. R., O'Shea, J., Clare, S., . . . Behrens, T. E. J. (2016). Unmasking Latent Inhibitory Connections in Human Cortex to Reveal Dormant Cortical Memories. *Neuron, 90*(1), 191-203. doi:https://doi.org/10.1016/j.neuron.2016.02.031

Bayer, A. U., Danias, J., Brodie, S., Maag, K. P., Chen, B., Shen, F., . . . Mittag, T. W. (2001a). Electroretinographic Abnormalities in a Rat Glaucoma Model with Chronic Elevated Intraocular Pressure. *Exp Eye Res, 72*(6), 667-677.

doi:https://doi.org/10.1006/exer.2001.1004

Bayer, A. U., Neuhardt, T., May, A. C., Martus, P., Maag, K.-P., Brodie, S., . . . Mittag, T. (2001b). Retinal Morphology and ERG Response in the DBA/2NNia Mouse Model of Angle-Closure Glaucoma. *Invest Ophthalmol Vis Sci, 42*(6), 1258-1265.

Beaulieu, J.-M., & Gainetdinov, R. R. (2011). The Physiology, Signaling, and Pharmacology of Dopamine Receptors. *Pharmacological Reviews, 63*(1), 182. doi:10.1124/pr.110.002642

Berntsen, D. A., Barr, C. D., Mutti, D. O., & Zadnik, K. (2013). Peripheral Defocus and Myopia Progression in Myopic Children Randomly Assigned to Wear Single Vision and Progressive Addition Lenses. *Invest Ophthalmol Vis Sci, 54*(8), 5761-5770. doi:10.1167/iovs.13-11904

Birch, D. G., Bennett, L. D., Duncan, J. L., Weleber, R. G., & Pennesi, M. E. (2016). Long-term Follow-up of Patients With Retinitis Pigmentosa Receiving Intraocular Ciliary Neurotrophic Factor Implants. *Am J Ophthalmol, 170*, 10-14. doi:10.1016/j.ajo.2016.07.013

Bitzer, M., & Schaeffel, F. (2006). ZENK expression of retinal glucagon amacrine cells in chicks: the effect of defocus presented in vivo, in vitro and under anesthesia. *Vision Res, 46*(6-7), 848-859. doi:10.1016/j.visres.2005.09.038

Bloomfield, S. A., & Miller, R. F. (1982). A physiological and morphological study of the horizontal cell types of the rabbit retina. *Journal of Comparative Neurology, 208*(3), 288-303. doi:10.1002/cne.902080306

Bloomfield, S. A., & Volgyi, B. (2009). The diverse functional roles and regulation of neuronal gap junctions in the retina. *Nat Rev Neurosci, 10*(7), 495-506. doi:10.1038/nrn2636

Borghuis, B. G., Marvin, J. S., Looger, L. L., & Demb, J. B. (2013). Two-Photon Imaging of Nonlinear Glutamate Release Dynamics at Bipolar Cell Synapses in the Mouse Retina. *The Journal of Neuroscience, 33*(27), 10972. doi:10.1523/JNEUROSCI.1241-13.2013

Borowska, J., Trenholm, S., & Awatramani, G. B. (2011). An intrinsic neural oscillator in the degenerating mouse retina. *J Neurosci, 31*(13), 5000-5012. doi:10.1523/jneurosci.5800-10.2011

Boycott, B. B., & Wassle, H. (1974). The morphological types of ganglion cells of the domestic cat's retina. *J Physiol, 240*(2), 397-419.

Boycott, B. B., & Wassle, H. (1991). Morphological Classification of Bipolar Cells of the Primate Retina. *Eur J Neurosci, 3*(11), 1069-1088. doi:10.1111/j.1460-9568.1991.tb00043.x

Branch, S. Y., Chen, C., Sharma, R., Lechleiter, J. D., Li, S., & Beckstead, M. J. (2016). Dopaminergic Neurons Exhibit an Age-Dependent Decline in Electrophysiological Parameters in the MitoPark Mouse Model of Parkinson's Disease. *J Neurosci, 36*(14), 4026-4037. doi:10.1523/JNEUROSCI.1395-15.2016

Bui, B. V., Edmunds, B., Cioffi, G. A., & Fortune, B. (2005). The gradient of retinal functional

changes during acute intraocular pressure elevation. *Invest Ophthalmol Vis Sci, 46*(1), 202-213. doi:10.1167/iovs.04-0421

Bui, B. V., & Fortune, B. (2004). Ganglion cell contributions to the rat full-field electroretinogram. *J Physiol, 555*(Pt 1), 153-173. doi:10.1113/jphysiol.2003.052738

Burge, J., & Geisler, W. S. (2011). Optimal defocus estimation in individual natural images. *Proceedings of the National Academy of Sciences, 108*(40), 16849. doi:10.1073/pnas.1108491108

Busche, M. A., & Konnerth, A. (2016). Impairments of neural circuit function in Alzheimer's disease. *Philos Trans R Soc Lond B Biol Sci, 371*(1700). doi:10.1098/rstb.2015.0429

Campochiaro, P. A., & Mir, T. A. (2018). The mechanism of cone cell death in Retinitis Pigmentosa. *Prog Retin Eye Res, 62*, 24-37. doi:10.1016/j.preteyeres.2017.08.004

Carr, B. J., & Stell, W. K. (2016). Nitric Oxide (NO) Mediates the Inhibition of Form-Deprivation Myopia by Atropine in Chicks. *Scientific Reports, 6*(1), 9. doi:10.1038/s41598-016-0002-7

Chakraborty, R., Park, H. N., Hanif, A. M., Sidhu, C. S., Iuvone, P. M., & Pardue, M. T. (2015). ON pathway mutations increase susceptibility to form-deprivation myopia. *Exp Eye Res, 137*, 79-83. doi:10.1016/j.exer.2015.06.009

Chan, H. L., & Brown, B. (1999). Multifocal ERG changes in glaucoma. *Ophthalmic and Physiological Optics, 19*(4), 306-316. doi:10.1111/j.1475-1313.1999.00439.x

Chang, B., Hawes, N. L., Hurd, R. E., Davisson, M. T., Nusinowitz, S., & Heckenlively, J. R. (2002). Retinal degeneration mutants in the mouse. *Vision Res, 42*(4), 517-525. doi:https://doi.org/10.1016/S0042-6989(01)00146-8

Chen, H., Wei, X., Cho, K. S., Chen, G., Sappington, R., Calkins, D. J., & Chen, D. F. (2011). Optic neuropathy due to microbead-induced elevated intraocular pressure in the mouse. *Invest Ophthalmol Vis Sci, 52*(1), 36-44. doi:10.1167/iovs.09-5115

Chen, M., Wang, K., & Lin, B. (2012). Development and degeneration of cone bipolar cells are independent of cone photoreceptors in a mouse model of retinitis pigmentosa. *PLoS One, 7*(8), e44036-e44036. doi:10.1371/journal.pone.0044036

Chia, A., Chua, W. H., Cheung, Y. B., Wong, W. L., Lingham, A., Fong, A., & Tan, D. (2012). Atropine for the treatment of childhood myopia: safety and efficacy of 0.5%, 0.1%, and 0.01% doses (Atropine for the Treatment of Myopia 2). *Ophthalmology, 119*(2), 347-354. doi:10.1016/j.ophtha.2011.07.031

Chia, A., Li, W., Tan, D., & Luu, C. D. (2013). Full-field electroretinogram findings in children in the atropine treatment for myopia (ATOM2) study. *Documenta ophthalmologica, 126*(3), 177-186. doi:10.1007/s10633-012-9372-8

Chiang, S. T., Chen, T. L., & Phillips, J. R. (2018). Effect of Optical Defocus on Choroidal Thickness in Healthy Adults With Presbyopia. *Invest Ophthalmol Vis Sci, 59*(12), 5188-5193. doi:10.1167/iovs.18-24815

Chin, M. P., Chu, P. H. W., Cheong, A. M. Y., & Chan, H. H. L. (2015). Human Electroretinal Responses to Grating Patterns and Defocus Changes by Global Flash Multifocal Electroretinogram. *PLoS One, 10*(4), e0123480. doi:10.1371/journal.pone.0123480

Chrysostomou, V., & Crowston, J. G. (2013). The photopic negative response of the mouse electroretinogram: reduction by acute elevation of intraocular pressure. *Invest Ophthalmol Vis Sci, 54*(7), 4691-4697. doi:10.1167/iovs.13-12415

Chua, W.-H., Balakrishnan, V., Chan, Y.-H., Tong, L., Ling, Y., Quah, B.-L., & Tan, D. (2006). Atropine for the Treatment of Childhood Myopia. *Ophthalmology, 113*(12), 2285-2291. doi:https://doi.org/10.1016/j.ophtha.2006.05.062

Chung, K., Mohidin, N., & O'Leary, D. J. (2002). Undercorrection of myopia enhances rather than inhibits myopia progression. *Vision Res, 42*(22), 2555-2559. doi:https://doi.org/10.1016/S0042-6989(02)00258-4

Conn, P. J., & Pin, J. P. (1997). Pharmacology and functions of metabotropic glutamate receptors. *Annu Rev Pharmacol Toxicol, 37*, 205-237. doi:10.1146/annurev.pharmtox.37.1.205

Contini, M., & Raviola, E. (2003). GABAergic synapses made by a retinal dopaminergic neuron. *Proc Natl Acad Sci U S A, 100*(3), 1358-1363. doi:10.1073/pnas.0337681100

Cooper, J., Eisenberg, N., Schulman, E., & Wang, F. M. (2013). Maximum atropine dose without clinical signs or symptoms. *Optometry and vision science : official publication of the American Academy of Optometry, 90*(12), 1467-1472. doi:10.1097/opx.0000000000000037

Cooper, J., & Tkatchenko, A. V. (2018). A Review of Current Concepts of the Etiology and Treatment of Myopia. *Eye & contact lens, 44*(4), 231-247. doi:10.1097/ICL.0000000000000499

Correction of Myopia Evaluation Trial 2 Study Group for the Pediatric Eye Disease Investigator, G. (2011). Progressive-Addition Lenses versus Single-Vision Lenses for Slowing Progression of Myopia in Children with High Accommodative Lag and Near Esophoria. *Invest Ophthalmol Vis Sci, 52*(5), 2749-2757. doi:10.1167/iovs.10-6631

Crewther, S. G., & Crewther, D. P. (2003). Inhibition of retinal ON/OFF systems differentially affects refractive compensation to defocus. *Neuroreport, 14*(9), 1233-1237. doi:10.1097/00001756-200307010-00009

Cueva, J. G., Haverkamp, S., Reimer, R. J., Edwards, R., Wässle, H., & Brecha, N. C. (2002). Vesicular gamma-aminobutyric acid transporter expression in amacrine and horizontal cells. *J Comp Neurol, 445*(3), 227-237. doi:10.1002/cne.10166

Dacey, D. M. (1990). The dopaminergic amacrine cell. *Journal of Comparative Neurology, 301*(3), 461-489. doi:https://doi.org/10.1002/cne.903010310

Deans, M. R., Volgyi, B., Goodenough, D. A., Bloomfield, S. A., & Paul, D. L. (2002). Connexin36 is essential for transmission of rod-mediated visual signals in the mammalian retina.

Neuron, 36(4), 703-712. doi:10.1016/s0896-6273(02)01046-2

Della Santina, L., Inman, D. M., Lupien, C. B., Horner, P. J., & Wong, R. O. (2013). Differential progression of structural and functional alterations in distinct retinal ganglion cell types in a mouse model of glaucoma. *J Neurosci, 33*(44), 17444-17457. doi:10.1523/JNEUROSCI.5461-12.2013

Demb, J. B., & Singer, J. H. (2015). Functional Circuitry of the Retina. *Annu Rev Vis Sci, 1*, 263-289. doi:10.1146/annurev-vision-082114-035334

DeVries, S. H., & Baylor, D. A. (1995). An alternative pathway for signal flow from rod photoreceptors to ganglion cells in mammalian retina. *Proceedings of the National Academy of Sciences, 92*(23), 10658-10662.

Djamgoz, M. B. A., Hankins, M. W., Hirano, J., & Archer, S. N. (1997). Neurobiology of retinal dopamine in relation to degenerative states of the tissue. *Vision Res, 37*(24), 3509-3529. doi:https://doi.org/10.1016/S0042-6989(97)00129-6

Dong, A., Liu, S., & Li, Y. (2018). Gap Junctions in the Nervous System: Probing Functional Connections Using New Imaging Approaches. *Frontiers in Cellular Neuroscience, 12*(320). doi:10.3389/fncel.2018.00320

Dong, C. J., Picaud, S. A., & Werblin, F. S. (1994). GABA transporters and GABAC-like receptors on catfish cone- but not rod- driven horizontal cells. *The Journal of Neuroscience, 14*(5), 2648. doi:10.1523/JNEUROSCI.14-05-02648.1994

Dostrovsky, J. O., Millar, J., & Wall, P. D. (1976). The immediate shift of afferent drive of dorsal column nucleus cells following deafferentation: A comparison of acute and chronic deafferentation in gracile nucleus and spinal cord. *Experimental Neurology, 52*(3), 480-495. doi:https://doi.org/10.1016/0014-4886(76)90219-3

Drasdo, N., Aldebasi, Y. H., Chiti, Z., Mortlock, K. E., Morgan, J. E., & North, R. V. (2001). The S-Cone PhNR and Pattern ERG in Primary Open Angle Glaucoma. *Invest Ophthalmol Vis Sci, 42*(6), 1266-1272.

Duan, X., Qiao, M., Bei, F., Kim, I. J., He, Z., & Sanes, J. R. (2015). Subtype-specific regeneration of retinal ganglion cells following axotomy: effects of osteopontin and mTOR signaling. *Neuron, 85*(6), 1244-1256. doi:10.1016/j.neuron.2015.02.017

Duvoisin, R. M., Zhang, C., & Ramonell, K. (1995). A novel metabotropic glutamate receptor expressed in the retina and olfactory bulb. *J Neurosci, 15*(4), 3075-3083. doi:10.1523/jneurosci.15-04-03075.1995

Elgueta, C., Vielma, A. H., Palacios, A. G., & Schmachtenberg, O. (2015). Acetylcholine induces GABA release onto rod bipolar cells through heteromeric nicotinic receptors expressed in A17 amacrine cells. *Front Cell Neurosci, 9*, 6. doi:10.3389/fncel.2015.00006

Falsini, B., Marangoni, D., Salgarello, T., Stifano, G., Montrone, L., Campagna, F., . . . Colotto, A. (2008). Structure–function relationship in ocular hypertension and glaucoma: interindividual and interocular analysis by OCT and pattern ERG. *Graefe's Archive for*

Clinical and Experimental Ophthalmology, 246(8), 1153-1162. doi:10.1007/s00417-008-0808-5

Famiglietti, E. V., Jr., & Kolb, H. (1976). Structural basis for ON-and OFF-center responses in retinal ganglion cells. *Science, 194*(4261), 193-195. doi:10.1126/science.959847

Farajian, R., Pan, F., Akopian, A., Volgyi, B., & Bloomfield, S. A. (2011). Masked excitatory crosstalk between the ON and OFF visual pathways in the mammalian retina. *J Physiol, 589*(Pt 18), 4473-4489. doi:10.1113/jphysiol.2011.213371

Feldkaemper, M., & Schaeffel, F. (2013). An updated view on the role of dopamine in myopia. *Exp Eye Res, 114*, 106-119. doi:https://doi.org/10.1016/j.exer.2013.02.007

Ferraguti, F., & Shigemoto, R. (2006). Metabotropic glutamate receptors. *Cell Tissue Res, 326*(2), 483-504. doi:10.1007/s00441-006-0266-5

Ferrari, S., Di Iorio, E., Barbaro, V., Ponzin, D., Sorrentino, F. S., & Parmeggiani, F. (2011). Retinitis pigmentosa: genes and disease mechanisms. *Current genomics, 12*(4), 238-249. doi:10.2174/138920211795860107

Flores-Herr, N., Protti, D. A., & Wässle, H. (2001). Synaptic currents generating the inhibitory surround of ganglion cells in the mammalian retina. *J Neurosci, 21*(13), 4852-4863. doi:10.1523/jneurosci.21-13-04852.2001

Fortune, B., Bearse, M. A., Jr, Cioffi, G. A., & Johnson, C. A. (2002). Selective Loss of an Oscillatory Component from Temporal Retinal Multifocal ERG Responses in Glaucoma. *Invest Ophthalmol Vis Sci, 43*(8), 2638-2647.

Frankfort, B. J., Khan, A. K., Tse, D. Y., Chung, I., Pang, J.-J., Yang, Z., . . . Wu, S. M. (2013). Elevated Intraocular Pressure Causes Inner Retinal Dysfunction Before Cell Loss in a Mouse Model of Experimental Glaucoma. *Invest Ophthalmol Vis Sci, 54*(1), 762-770. doi:10.1167/iovs.12-10581

Ganesan, P., & Wildsoet, C. F. (2010). Pharmaceutical intervention for myopia control. *Expert review of ophthalmology, 5*(6), 759-787. doi:10.1586/eop.10.67

Gargini, C., Terzibasi, E., Mazzoni, F., & Strettoi, E. (2007). Retinal organization in the retinal degeneration 10 (rd10) mutant mouse: a morphological and ERG study. *J Comp Neurol, 500*(2), 222-238. doi:10.1002/cne.21144

Gaudana, R., Ananthula, H. K., Parenky, A., & Mitra, A. K. (2010). Ocular Drug Delivery. *The AAPS Journal, 12*(3), 348-360. doi:10.1208/s12248-010-9183-3

Geffen, M. N., de Vries, S. E., & Meister, M. (2007). Retinal ganglion cells can rapidly change polarity from Off to On. *PLoS Biol, 5*(3), e65. doi:10.1371/journal.pbio.0050065

Gong, Q., Janowski, M., Luo, M., Wei, H., Chen, B., Yang, G., & Liu, L. (2017). Efficacy and Adverse Effects of Atropine in Childhood Myopia: A Meta-analysis. *JAMA Ophthalmology, 135*(6), 624-630. doi:10.1001/jamaophthalmol.2017.1091

Grzybowski, A., Kanclerz, P., Tsubota, K., Lanca, C., & Saw, S.-M. (2020). A review on the epidemiology of myopia in school children worldwide. *BMC Ophthalmology, 20*(1), 27.

doi:10.1186/s12886-019-1220-0

Haarman, A. E. G., Enthoven, C. A., Tideman, J. W. L., Tedja, M. S., Verhoeven, V. J. M., & Klaver, C. C. W. (2020). The Complications of Myopia: A Review and Meta-Analysis. *Invest Ophthalmol Vis Sci, 61*(4), 49-49. doi:10.1167/iovs.61.4.49

Hartline, H. K. (1938). The response of single optic nerve fibers of the vertebrate eye to illumination of the retina. *American Journal of Physiology, 121*, 400-415.

Herrmann, R., Heflin, S. J., Hammond, T., Lee, B., Wang, J., Gainetdinov, R. R., . . . Arshavsky, V. Y. (2011). Rod vision is controlled by dopamine-dependent sensitization of rod bipolar cells by GABA. *Neuron, 72*(1), 101-110. doi:10.1016/j.neuron.2011.07.030

Ho, W. C., Wong, O. Y., Chan, Y. C., Wong, S. W., Kee, C. S., & Chan, H. H. (2012). Sign-dependent changes in retinal electrical activity with positive and negative defocus in the human eye. *Vision Res, 52*(1), 47-53. doi:10.1016/j.visres.2011.10.017

Hodgkin, A. L., & Huxley, A. F. (1952). A quantitative description of membrane current and its application to conduction and excitation in nerve. *The Journal of Physiology, 117*(4), 500-544. doi:10.1113/jphysiol.1952.sp004764

Holcombe, D. J., Lengefeld, N., Gole, G. A., & Barnett, N. L. (2008). Selective inner retinal dysfunction precedes ganglion cell loss in a mouse glaucoma model. *Br J Ophthalmol, 92*(5), 683-688. doi:10.1136/bjo.2007.133223

Horn, F. K., Gottschalk, K., Mardin, C. Y., Pangeni, G., Jünemann, A. G., & Kremers, J. (2011). On and off responses of the photopic fullfield ERG in normal subjects and glaucoma patients. *Documenta ophthalmologica, 122*(1), 53-62.

Hoseini-Yazdi, H., Vincent, S. J., Collins, M. J., & Read, S. A. (2019). Regional alterations in human choroidal thickness in response to short-term monocular hemifield myopic defocus. *Ophthalmic Physiol Opt, 39*(3), 172-182. doi:10.1111/opo.12609

Hoshi, H., Liu, W. L., Massey, S. C., & Mills, S. L. (2009). ON inputs to the OFF layer: bipolar cells that break the stratification rules of the retina. *J Neurosci, 29*(28), 8875-8883. doi:10.1523/jneurosci.0912-09.2009

Huang, J., Wen, D., Wang, Q., McAlinden, C., Flitcroft, I., Chen, H., . . . Qu, J. (2016). Efficacy Comparison of 16 Interventions for Myopia Control in Children: A Network Meta-analysis. *Ophthalmology, 123*(4), 697-708. doi:https://doi.org/10.1016/j.ophtha.2015.11.010

Hung, G. K., & Ciuffreda, K. J. (2007). Incremental retinal-defocus theory of myopia development--schematic analysis and computer simulation. *Comput Biol Med, 37*(7), 930-946. doi:10.1016/j.compbiomed.2006.10.004

Isayama, T., O'Brien, B. J., Ugalde, I., Muller, J. F., Frenz, A., Aurora, V., . . . Berson, D. M. (2009). Morphology of retinal ganglion cells in the ferret (Mustela putorius furo). *J Comp Neurol, 517*(4), 459-480. doi:10.1002/cne.22145

Jacobs, K. M., & Donoghue, J. P. (1991). Reshaping the cortical motor map by unmasking latent

intracortical connections. *Science, 251*(4996), 944-947. doi:10.1126/science.2000496

Jensen, R. J. (2012). Blocking GABAC receptors increases light responsiveness of retinal ganglion cells in a rat model of retinitis pigmentosa. *Exp Eye Res, 105*, 21-26. doi:https://doi.org/10.1016/j.exer.2012.10.005

Jeon, C.-J., Strettoi, E., & Masland, R. H. (1998a). The Major Cell Populations of the Mouse Retina. *The Journal of Neuroscience, 18*(21), 8936. doi:10.1523/JNEUROSCI.18-21-08936.1998

Jeon, C.-J., Strettoi, E., & Masland, R. H. (1998b). The major cell populations of the mouse retina. *Journal of Neuroscience, 18*(21), 8936-8946.

Johnson, T. V., & Tomarev, S. I. (2016). Animal Models of Glaucoma. In *Animal Models of Ophthalmic Diseases* (pp. 31-50).

Jonas, J. B., Aung, T., Bourne, R. R., Bron, A. M., Ritch, R., & Panda-Jonas, S. (2017). Glaucoma. *Lancet, 390*(10108), 2183-2193. doi:10.1016/s0140-6736(17)31469-1

Jones, B. W., Pfeiffer, R. L., Ferrell, W. D., Watt, C. B., Marmor, M., & Marc, R. E. (2016). Retinal remodeling in human retinitis pigmentosa. *Exp Eye Res, 150*, 149-165. doi:https://doi.org/10.1016/j.exer.2016.03.018

Khan, A. K., Tse, D. Y., van der Heijden, M. E., Shah, P., Nusbaum, D. M., Yang, Z., . . . Frankfort, B. J. (2015). Prolonged elevation of intraocular pressure results in retinal ganglion cell loss and abnormal retinal function in mice. *Exp Eye Res, 130*, 29-37. doi:10.1016/j.exer.2014.11.007

Khanal, S., Turnbull, P. R. K., Lee, N., & Phillips, J. R. (2019). The Effect of Atropine on Human Global Flash mfERG Responses to Retinal Defocus. *Invest Ophthalmol Vis Sci, 60*(1), 218-225. doi:10.1167/iovs.18-24600

Kinoshita, N., Konno, Y., Hamada, N., Kanda, Y., Shimmura-Tomita, M., Kaburaki, T., & Kakehashi, A. (2020). Efficacy of combined orthokeratology and 0.01% atropine solution for slowing axial elongation in children with myopia: a 2-year randomised trial. *Scientific Reports, 10*(1), 12750. doi:10.1038/s41598-020-69710-8

Kolb, H., Nelson, R., & Mariani, A. (1981). Amacrine cells, bipolar cells and ganglion cells of the cat retina: a Golgi study. *Vision Res, 21*(7), 1081-1114. doi:10.1016/0042-6989(81)90013-4

Kothmann, W. W., Li, X., Burr, G. S., & O'Brien, J. (2007). Connexin 35/36 is phosphorylated at regulatory sites in the retina. *Vis Neurosci, 24*(3), 363-375. doi:10.1017/S095252380707037X

Krieger, B., Qiao, M., Rousso, D. L., Sanes, J. R., & Meister, M. (2017). Four alpha ganglion cell types in mouse retina: Function, structure, and molecular signatures. *PLoS One, 12*(7), e0180091. doi:10.1371/journal.pone.0180091

Lagnado, L. (1998). Retinal processing: amacrine cells keep it short and sweet. *Curr Biol, 8*(17), R598-600. doi:10.1016/s0960-9822(98)70385-9

Lakshmanan, Y., Wong, F. S., Yu, W. Y., Li, S. Z., Choi, K. Y., So, K. F., & Chan, H. H. (2019). Lycium Barbarum Polysaccharides Rescue Neurodegeneration in an Acute Ocular Hypertension Rat Model Under Pre- and Posttreatment Conditions. *Invest Ophthalmol Vis Sci, 60*(6), 2023-2033. doi:10.1167/iovs.19-26752

Lam, C. S. Y., Tang, W. C., Tse, D. Y.-y., Lee, R. P. K., Chun, R. K. M., Hasegawa, K., . . . To, C. H. (2020). Defocus Incorporated Multiple Segments (DIMS) spectacle lenses slow myopia progression: a 2-year randomised clinical trial. *British Journal of Ophthalmology, 104*(3), 363. doi:10.1136/bjophthalmol-2018-313739

Lam, C. S. Y., Tang, W. C., Tse, D. Y.-Y., Tang, Y. Y., & To, C. H. (2014). Defocus Incorporated Soft Contact (DISC) lens slows myopia progression in Hong Kong Chinese schoolchildren: a 2-year randomised clinical trial. *British Journal of Ophthalmology, 98*(1), 40. doi:10.1136/bjophthalmol-2013-303914

Lee, T.-T., & Cho, P. (2010). Discontinuation of orthokeratology and myopic progression. *Optometry and Vision Science, 87*(12), 1053-1056.

Lettvin, J. Y., Maturana, H. R., McCulloch, W. S., & Pitts, W. H. (1959). What the frog's eye tells the frog's brain. *Proceedings of the IRE, 47*(11), 1940-1951.

Li, L., & Dowling, J. E. (2000). Effects of Dopamine Depletion on Visual Sensitivity of Zebrafish. *The Journal of Neuroscience, 20*(5), 1893. doi:10.1523/JNEUROSCI.20-05-01893.2000

Li, S., Woodfin, M., Long, S. S., & Fuerst, P. G. (2016). IPLaminator: an ImageJ plugin for automated binning and quantification of retinal lamination. *BMC Bioinformatics, 17*, 36. doi:10.1186/s12859-016-0876-1

Li, S. Z.-C., Yu, W.-Y., Choi, K.-Y., Lam, C. H.-I., Lakshmanan, Y., Wong, F. S.-Y., & Chan, H. H.-L. (2017). Subclinical Decrease in Central Inner Retinal Activity Is Associated With Myopia Development in Children. *Invest Ophthalmol Vis Sci, 58*(10), 4399-4406. doi:10.1167/iovs.16-21279

Lin, B., & Masland, R. H. (2006). Populations of wide-field amacrine cells in the mouse retina. *J Comp Neurol, 499*(5), 797-809. doi:10.1002/cne.21126

Lin, B., & Peng, E. B. (2013). Retinal ganglion cells are resistant to photoreceptor loss in retinal degeneration. *PLoS One, 8*(6), e68084. doi:10.1371/journal.pone.0068084

Liu, J., McGlinn, A. M., Fernandes, A., Milam, A. H., Strang, C. E., Andison, M. E., . . . Stone, R. A. (2009). Nicotinic Acetylcholine Receptor Subunits in Rhesus Monkey Retina. *Invest Ophthalmol Vis Sci, 50*(3), 1408-1415. doi:10.1167/iovs.08-2398

Liu, K., Wang, Y., Yin, Z., Weng, C., & Zeng, Y. (2013). Changes in glutamate homeostasis cause retinal degeneration in Royal College of Surgeons rats. *Int J Mol Med, 31*(5), 1075-1080. doi:10.3892/ijmm.2013.1297

Luu, C. D., Lau, A. M. I., Koh, A. H. C., & Tan, D. (2005). Multifocal electroretinogram in children on atropine treatment for myopia. *British Journal of Ophthalmology, 89*(2), 151-153. doi:10.1136/bjo.2004.045526

Ma, X., Congdon, N., Yi, H., Zhou, Z., Pang, X., Meltzer, M. E., . . . Rozelle, S. (2015). Safety of Spectacles for Children's Vision: A Cluster-Randomized Controlled Trial. *Am J Ophthalmol, 160*(5), 897-904. doi:10.1016/j.ajo.2015.08.013

Majumdar, S., Heinze, L., Haverkamp, S., Ivanova, E., & Wässle, H. (2007). Glycine receptors of A-type ganglion cells of the mouse retina. *Vis Neurosci, 24*(4), 471-487. doi:10.1017/s0952523807070174

Mangrum, W. I., Dowling, J. E., & Cohen, E. D. (2002). A morphological classification of ganglion cells in the zebrafish retina. *Vis Neurosci, 19*(6), 767-779. doi:10.1017/s0952523802196076

Mani, A., & Schwartz, G. W. (2017). Circuit Mechanisms of a Retinal Ganglion Cell with Stimulus-Dependent Response Latency and Activation Beyond Its Dendrites. *Current Biology, 27*(4), 471-482. doi:https://doi.org/10.1016/j.cub.2016.12.033

Marc, R., Marc, R., & Neurotransmitters, R. (2004). Retinal neurotransmitters. *Vis. Neurosci.*

Marc, R. E., & Jones, B. W. (2003). Retinal remodeling in inherited photoreceptor degenerations. *Molecular Neurobiology, 28*(2), 139-147. doi:10.1385/MN:28:2:139

Martersteck, E. M., Hirokawa, K. E., Evarts, M., Bernard, A., Duan, X., Li, Y., . . . Harris, J. A. (2017). Diverse Central Projection Patterns of Retinal Ganglion Cells. *Cell Rep, 18*(8), 2058-2072. doi:10.1016/j.celrep.2017.01.075

Masland, R. H. (2012a). The neuronal organization of the retina. *Neuron, 76*(2), 266-280. doi:10.1016/j.neuron.2012.10.002

Masland, R. H. (2012b). The tasks of amacrine cells. *Vis Neurosci, 29*(1), 3-9. doi:10.1017/s0952523811000344

Massey, S. C., Linn, D. M., Kittila, C. A., & Mirza, W. (1997). Contributions of GABAA receptors and GABAC receptors to acetylcholine release and directional selectivity in the rabbit retina. *Vis Neurosci, 14*(5), 939-948. doi:10.1017/s0952523800011652

Mazzoni, F., Novelli, E., & Strettoi, E. (2008a). Retinal ganglion cells survive and maintain normal dendritic morphology in a mouse model of inherited photoreceptor degeneration. *J Neurosci, 28*(52), 14282-14292. doi:10.1523/jneurosci.4968-08.2008

Mazzoni, F., Novelli, E., & Strettoi, E. (2008b). Retinal ganglion cells survive and maintain normal dendritic morphology in a mouse model of inherited photoreceptor degeneration. *Journal of Neuroscience, 28*(52), 14282-14292.

McBrien, N. A., Arumugam, B., Gentle, A., Chow, A., & Sahebjada, S. (2011). The M4 muscarinic antagonist MT-3 inhibits myopia in chick: evidence for site of action. *Ophthalmic Physiol Opt, 31*(5), 529-539. doi:10.1111/j.1475-1313.2011.00841.x

McBrien, N. A., Moghaddam, H. O., & Reeder, A. P. (1993). Atropine reduces experimental myopia and eye enlargement via a nonaccommodative mechanism. *Invest Ophthalmol Vis Sci, 34*(1), 205-215.

McFadden, S. A., Tse, D. Y., Bowrey, H. E., Leotta, A. J., Lam, C. S., Wildsoet, C. F., & To, C.-H.

(2014). Integration of Defocus by Dual Power Fresnel Lenses Inhibits Myopia in the Mammalian Eye. *Invest Ophthalmol Vis Sci, 55*(2), 908-917. doi:10.1167/iovs.13-11724

Meister, M., Lagnado, L., & Baylor, D. A. (1995). Concerted signaling by retinal ganglion cells. *Science, 270*(5239), 1207-1210. doi:10.1126/science.270.5239.1207

Mertz, J. R., & Wallman, J. (2000). Choroidal retinoic acid synthesis: a possible mediator between refractive error and compensatory eye growth. *Exp Eye Res, 70*(4), 519-527. doi:10.1006/exer.1999.0813

Mills, S. L., & Massey, S. C. (1995). Differential properties of two gap junctional pathways made by AII amacrine cells. *Nature, 377*(6551), 734-737. doi:10.1038/377734a0

Mills, S. L., Xia, X.-B., Hoshi, H., Firth, S. I., Rice, M. E., Frishman, L. J., & Marshak, D. W. (2007). Dopaminergic modulation of tracer coupling in a ganglion-amacrine cell network. *Vis Neurosci, 24*(4), 593-608. doi:10.1017/S0952523807070575

Monaghan, D. T., Bridges, R. J., & Cotman, C. W. (1989). The excitatory amino acid receptors: their classes, pharmacology, and distinct properties in the function of the central nervous system. *Annu Rev Pharmacol Toxicol, 29*, 365-402. doi:10.1146/annurev.pa.29.040189.002053

Moreno, M. C., de Zavalía, N., Sande, P., Jaliffa, C. O., Fernandez, D. C., Keller Sarmiento, M. I., & Rosenstein, R. E. (2008). Effect of ocular hypertension on retinal GABAergic activity. *Neurochem Int, 52*(4-5), 675-682. doi:10.1016/j.neuint.2007.08.014

Morgan, I. G., Ohno-Matsui, K., & Saw, S.-M. (2012). Myopia. *The Lancet, 379*(9827), 1739-1748.

Nakase, T., & Naus, C. C. (2004). Gap junctions and neurological disorders of the central nervous system. *Biochim Biophys Acta, 1662*(1-2), 149-158. doi:10.1016/j.bbamem.2004.01.009

Nanou, E., Lee, A., & Catterall, W. A. (2018). Control of Excitation/Inhibition Balance in a Hippocampal Circuit by Calcium Sensor Protein Regulation of Presynaptic Calcium Channels. *J Neurosci, 38*(18), 4430-4440. doi:10.1523/jneurosci.0022-18.2018

Nelson, R., Famiglietti, E. V., Jr., & Kolb, H. (1978). Intracellular staining reveals different levels of stratification for on- and off-center ganglion cells in cat retina. *J Neurophysiol, 41*(2), 472-483. doi:10.1152/jn.1978.41.2.472

Nielsen, M. S., Axelsen, L. N., Sorgen, P. L., Verma, V., Delmar, M., & Holstein-Rathlou, N.-H. (2012). Gap junctions. *Comprehensive Physiology, 2*(3), 1981-2035. doi:10.1002/cphy.c110051

North, R. V., Jones, A. L., Drasdo, N., Wild, J. M., & Morgan, J. E. (2010). Electrophysiological Evidence of Early Functional Damage in Glaucoma and Ocular Hypertension. *Invest Ophthalmol Vis Sci, 51*(2), 1216-1222. doi:10.1167/iovs.09-3409

O'Brien, J., & Bloomfield, S. A. (2018). Plasticity of Retinal Gap Junctions: Roles in Synaptic Physiology and Disease. *Annu Rev Vis Sci, 4*, 79-100. doi:10.1146/annurev-vision-

091517-034133

Ostrin, L. A., Choh, V., & Wildsoet, C. F. (2016). The pattern ERG in chicks - Stimulus dependence and optic nerve section. *Vision Res, 128*, 45-52. doi:10.1016/j.visres.2016.09.009

Ou, Y., Jo, R. E., Ullian, E. M., Wong, R. O., & Della Santina, L. (2016). Selective Vulnerability of Specific Retinal Ganglion Cell Types and Synapses after Transient Ocular Hypertension. *J Neurosci, 36*(35), 9240-9252. doi:10.1523/JNEUROSCI.0940-16.2016

Paik, S.-S., Park, N.-G., Lee, S.-J., Han, H.-K., Jung, C.-S., Bai, S.-H., & Chun, M.-H. (2003). GABA receptors on horizontal cells in the goldfish retina. *Vision Res, 43*(20), 2101-2106. doi:https://doi.org/10.1016/S0042-6989(03)00335-3

Pan, F. (2019). Defocused Image Changes Signaling of Ganglion Cells in the Mouse Retina. *Cells, 8*(7). doi:10.3390/cells8070640

Pan, F., Paul, D. L., Bloomfield, S. A., & Volgyi, B. (2010). Connexin36 is required for gap junctional coupling of most ganglion cell subtypes in the mouse retina. *J Comp Neurol, 518*(6), 911-927. doi:10.1002/cne.22254

Pan, F., Toychiev, A., Zhang, Y., Atlasz, T., Ramakrishnan, H., Roy, K., . . . Bloomfield, S. A. (2016). Inhibitory masking controls the threshold sensitivity of retinal ganglion cells. *J Physiol, 594*(22), 6679-6699. doi:10.1113/jp272267

Pang, J.-J., Gao, F., & Wu, S. M. (2002). Relative contributions of bipolar cell and amacrine cell inputs to light responses of ON, OFF and ON–OFF retinal ganglion cells. *Vision Res, 42*(1), 19-27. doi:https://doi.org/10.1016/S0042-6989(01)00258-9

Pang, J. J., Frankfort, B. J., Gross, R. L., & Wu, S. M. (2015). Elevated intraocular pressure decreases response sensitivity of inner retinal neurons in experimental glaucoma mice. *Proc Natl Acad Sci U S A, 112*(8), 2593-2598. doi:10.1073/pnas.1419921112

Pang, J. J., Gao, F., & Wu, S. M. (2004). Light-evoked current responses in rod bipolar cells, cone depolarizing bipolar cells and AII amacrine cells in dark-adapted mouse retina. *J Physiol, 558*(Pt 3), 897-912. doi:10.1113/jphysiol.2003.059543

Pang, J. J., Paul, D. L., & Wu, S. M. (2013). Survey on amacrine cells coupling to retrograde-identified ganglion cells in the mouse retina. *Invest Ophthalmol Vis Sci, 54*(8), 5151-5162. doi:10.1167/iovs.13-11774

Peichl, L. (1991). Alpha ganglion cells in mammalian retinae: Common properties, species differences, and some comments on other ganglion cells. *Vis Neurosci, 7*(1-2), 155-169. doi:10.1017/S0952523800011020

Peichl, L., & Wassle, H. (1981). Morphological identification of on- and off-centre brisk transient (Y) cells in the cat retina. *Proc R Soc Lond B Biol Sci, 212*(1187), 139-153. doi:10.1098/rspb.1981.0030

Peirce, J. (2007). PsychoPy—Psychophysics software in Python. *Journal of neuroscience methods, 162*, 8-13. doi:10.1016/j.jneumeth.2006.11.017

Penn, J. S., & Williams, T. P. (1984). A new microspectrophotometric method for measuring absorbance of rat photoreceptors. *Vision Res, 24*(11), 1673-1676.

Phillips, J. R. (2005). Monovision slows juvenile myopia progression unilaterally. *Br J Ophthalmol, 89*(9), 1196-1200. doi:10.1136/bjo.2004.064212

Picaud, S., Pattnaik, B., Hicks, D., Forster, V., Fontaine, V., Sahel, J., & Dreyfus, H. (1998). GABAA and GABAC receptors in adult porcine cones: evidence from a photoreceptor-glia co-culture model. *The Journal of Physiology, 513*(1), 33-42. doi:https://doi.org/10.1111/j.1469-7793.1998.033by.x

Picciotto, M. R., Higley, M. J., & Mineur, Y. S. (2012). Acetylcholine as a neuromodulator: cholinergic signaling shapes nervous system function and behavior. *Neuron, 76*(1), 116-129. doi:10.1016/j.neuron.2012.08.036

Pillow, J. W., Shlens, J., Paninski, L., Sher, A., Litke, A. M., Chichilnisky, E. J., & Simoncelli, E. P. (2008). Spatio-temporal correlations and visual signalling in a complete neuronal population. *Nature, 454*(7207), 995-999. doi:10.1038/nature07140

Popova, E. (1995). Role of Dopamine in Retinal Function. In H. Kolb, E. Fernandez, & R. Nelson (Eds.), *Webvision: The Organization of the Retina and Visual System*. Salt Lake City (UT): University of Utah Health Sciences Center

Popova, E. (2014). ON-OFF Interactions in the Retina: Role of Glycine and GABA. *Current neuropharmacology, 12*(6), 509-526. doi:10.2174/1570159X13999150122165018

Popova, E. (2015). GABAergic neurotransmission and retinal ganglion cell function. *Journal of Comparative Physiology A, 201*(3), 261-283. doi:10.1007/s00359-015-0981-z

Porciatti, V. (2015). Electrophysiological assessment of retinal ganglion cell function. *Exp Eye Res, 141*, 164-170. doi:10.1016/j.exer.2015.05.008

. Postsynaptic Currents (EPSCs and IPSCs) or Potentials (EPSPs and IPSPs). (2009). In M. D. Binder, N. Hirokawa, & U. Windhorst (Eds.), *Encyclopedia of Neuroscience* (pp. 3208-3208). Berlin, Heidelberg: Springer Berlin Heidelberg.

Potapenko, E. S., Biancardi, V. C., Florschutz, R. M., Ryu, P. D., & Stern, J. E. (2011). Inhibitory-excitatory synaptic balance is shifted toward increased excitation in magnocellular neurosecretory cells of heart failure rats. *J Neurophysiol, 106*(3), 1545-1557. doi:10.1152/jn.00218.2011

Pribilla, I., Takagi, T., Langosch, D., Bormann, J., & Betz, H. (1992). The atypical M2 segment of the beta subunit confers picrotoxinin resistance to inhibitory glycine receptor channels. *The EMBO journal, 11*(12), 4305-4311.

Qiao, S.-N., Zhang, Z., Ribelayga, C. P., Zhong, Y.-M., & Zhang, D.-Q. (2016). Multiple cone pathways are involved in photic regulation of retinal dopamine. *Scientific Reports, 6*(1), 28916. doi:10.1038/srep28916

Quraishi, S., Gayet, J., Morgans, C. W., & Duvoisin, R. M. (2007). Distribution of group-III

metabotropic glutamate receptors in the retina. *J Comp Neurol, 501*(6), 931-943. doi:10.1002/cne.21274

Rada, J. A., Shelton, S., & Norton, T. T. (2006). The sclera and myopia. *Exp Eye Res, 82*(2), 185-200. doi:10.1016/j.exer.2005.08.009

Rajan, R. (2001). Plasticity of excitation and inhibition in the receptive field of primary auditory cortical neurons after limited receptor organ damage. *Cereb Cortex, 11*(2), 171-182. doi:10.1093/cercor/11.2.171

Ramon y Cajal, S. (1933). The structure of the retina (Translated by SA Thorpe and M. Glickstein). *Springfield, III.: Charles C. Thomas*.

Read, S. A., Collins, M. J., & Sander, B. P. (2010). Human optical axial length and defocus. *Invest Ophthalmol Vis Sci, 51*(12), 6262-6269. doi:10.1167/iovs.10-5457

Reed, B. T., Amthor, F. R., & Keyser, K. T. (2002). Rabbit retinal ganglion cell responses mediated by α-bungarotoxin-sensitive nicotinic acetylcholine receptors. *Vis Neurosci, 19*(4), 427-438. doi:10.1017/S0952523802194053

Ren, Y.-M., Weng, C.-H., Zhao, C.-J., & Yin, Z.-Q. (2018). Changes in intrinsic excitability of ganglion cells in degenerated retinas of RCS rats. *International journal of ophthalmology, 11*(5), 756-765. doi:10.18240/ijo.2018.05.07

Rheaume, B. A., Jereen, A., Bolisetty, M., Sajid, M. S., Yang, Y., Renna, K., . . . Trakhtenberg, E. F. (2018). Single cell transcriptome profiling of retinal ganglion cells identifies cellular subtypes. *Nature Communications, 9*(1), 2759. doi:10.1038/s41467-018-05134-3

Ripps, H. (2002). Cell death in retinitis pigmentosa: gap junctions and the 'bystander' effect. *Exp Eye Res, 74*(3), 327-336. doi:10.1006/exer.2002.1155

Risner, M. L., Pasini, S., Cooper, M. L., Lambert, W. S., & Calkins, D. J. (2018). Axogenic mechanism enhances retinal ganglion cell excitability during early progression in glaucoma. *Proc Natl Acad Sci U S A, 115*(10), E2393-e2402. doi:10.1073/pnas.1714888115

Rockhill, R. L., Daly, F. J., MacNeil, M. A., Brown, S. P., & Masland, R. H. (2002). The diversity of ganglion cells in a mammalian retina. *J Neurosci, 22*(9), 3831-3843. doi:20026369

Rose, K. A., French, A. N., & Morgan, I. G. (2016). Environmental Factors and Myopia: Paradoxes and Prospects for Prevention. *The Asia-Pacific Journal of Ophthalmology, 5*(6).

Roy, K., Kumar, S., & Bloomfield, S. A. (2017). Gap junctional coupling between retinal amacrine and ganglion cells underlies coherent activity integral to global object perception. *Proc Natl Acad Sci U S A, 114*(48), E10484-E10493. doi:10.1073/pnas.1708261114

Saha, S., Greferath, U., Vessey, K. A., Grayden, D. B., Burkitt, A. N., & Fletcher, E. L. (2016). Changes in ganglion cells during retinal degeneration. *Neuroscience, 329*, 1-11. doi:10.1016/j.neuroscience.2016.04.032

Sanes, J. R., & Masland, R. H. (2015). The types of retinal ganglion cells: current status and implications for neuronal classification. *Annu Rev Neurosci, 38*, 221-246. doi:10.1146/annurev-neuro-071714-034120

Sankaridurg, P., Donovan, L., Varnas, S., Ho, A., Chen, X., Martinez, A., . . . Holden, B. (2010). Spectacle lenses designed to reduce progression of myopia: 12-month results. *Optometry and vision science : official publication of the American Academy of Optometry, 87*(9), 631-641. doi:10.1097/OPX.0b013e3181ea19c7

Santodomingo-Rubido, J., Villa-Collar, C., Gilmartin, B., & Gutiérrez-Ortega, R. (2012). Myopia Control with Orthokeratology Contact Lenses in Spain: Refractive and Biometric Changes. *Invest Ophthalmol Vis Sci, 53*(8), 5060-5065. doi:10.1167/iovs.11-8005

Sappington, R. M., Carlson, B. J., Crish, S. D., & Calkins, D. J. (2010). The microbead occlusion model: a paradigm for induced ocular hypertension in rats and mice. *Invest Ophthalmol Vis Sci, 51*(1), 207-216. doi:10.1167/iovs.09-3947

Saszik, S. M., Robson, J. G., & Frishman, L. J. (2002). The Scotopic Threshold Response of the Dark-Adapted Electroretinogram of the Mouse. *The Journal of Physiology, 543*(3), 899-916. doi:https://doi.org/10.1113/jphysiol.2002.019703

Saxena, S., & Caroni, P. (2011). Selective neuronal vulnerability in neurodegenerative diseases: from stressor thresholds to degeneration. *Neuron, 71*(1), 35-48. doi:10.1016/j.neuron.2011.06.031

Schaeffel, F., Troilo, D., Wallman, J., & Howland, H. C. (1990). Developing eyes that lack accommodation grow to compensate for imposed defocus. *Vis Neurosci, 4*(2), 177-183. doi:10.1017/s0952523800002327

Schaeffel, F., & Wildsoet, C. (2013). Can the retina alone detect the sign of defocus? *Ophthalmic Physiol Opt, 33*(3), 362-367. doi:10.1111/opo.12058

Schmucker, C., & Schaeffel, F. (2004). A paraxial schematic eye model for the growing C57BL/6 mouse. *Invest Ophthalmol Vis Sci, 45*(13), 4279-4279.

Schubert, T., Degen, J., Willecke, K., Hormuzdi, S. G., Monyer, H., & Weiler, R. (2005a). Connexin36 mediates gap junctional coupling of alpha-ganglion cells in mouse retina. *J Comp Neurol, 485*(3), 191-201. doi:10.1002/cne.20510

Schubert, T., Maxeiner, S., Kruger, O., Willecke, K., & Weiler, R. (2005b). Connexin45 mediates gap junctional coupling of bistratified ganglion cells in the mouse retina. *J Comp Neurol, 490*(1), 29-39. doi:10.1002/cne.20621

Schwahn, H. N., Kaymak, H., & Schaeffel, F. (2000). Effects of atropine on refractive development, dopamine release, and slow retinal potentials in the chick. *Vis Neurosci, 17*(2), 165-176. doi:10.1017/S0952523800171184

Sethuramanujam, S., McLaughlin, A. J., deRosenroll, G., Hoggarth, A., Schwab, D. J., & Awatramani, G. B. (2016). A Central Role for Mixed Acetylcholine/GABA Transmission in Direction Coding in the Retina. *Neuron, 90*(6), 1243-1256.

doi:10.1016/j.neuron.2016.04.041

Shen, W., & Jiang, Z. (2007). Characterization of glycinergic synapses in vertebrate retinas. *J Biomed Sci, 14*(1), 5-13. doi:10.1007/s11373-006-9118-2

Shields, C. R., Tran, M. N., Wong, R. O., & Lukasiewicz, P. D. (2000). Distinct ionotropic GABA receptors mediate presynaptic and postsynaptic inhibition in retinal bipolar cells. *J Neurosci, 20*(7), 2673-2682. doi:10.1523/jneurosci.20-07-02673.2000

Shih, Y. F., Chen, C. H., Chou, A. C., Ho, T. C., Lin, L. L., & Hung, P. T. (1999). Effects of different concentrations of atropine on controlling myopia in myopic children. *J Ocul Pharmacol Ther, 15*(1), 85-90. doi:10.1089/jop.1999.15.85

Shlens, J., Field, G. D., Gauthier, J. L., Greschner, M., Sher, A., Litke, A. M., & Chichilnisky, E. J. (2009). The Structure of Large-Scale Synchronized Firing in Primate Retina. *The Journal of Neuroscience, 29*(15), 5022. doi:10.1523/JNEUROSCI.5187-08.2009

Shlens, J., Rieke, F., & Chichilnisky, E. J. (2008). Synchronized firing in the retina. *Current Opinion in Neurobiology, 18*(4), 396-402. doi:https://doi.org/10.1016/j.conb.2008.09.010

Slaughter, M. M., & Miller, R. F. (1981). 2-amino-4-phosphonobutyric acid: a new pharmacological tool for retina research. *Science, 211*(4478), 182-185. doi:10.1126/science.6255566

Smith, B. J., Wang, X., Chauhan, B. C., Côté, P. D., & Tremblay, F. (2014). Contribution of retinal ganglion cells to the mouse electroretinogram. *Doc Ophthalmol, 128*(3), 155-168. doi:10.1007/s10633-014-9433-2

Smith, E. L., 3rd, Hung, L.-F., Huang, J., Blasdel, T. L., Humbird, T. L., & Bockhorst, K. H. (2010). Effects of optical defocus on refractive development in monkeys: evidence for local, regionally selective mechanisms. *Invest Ophthalmol Vis Sci, 51*(8), 3864-3873. doi:10.1167/iovs.09-4969

Smith Iii, E. L., & Hung, L.-F. (1999). The role of optical defocus in regulating refractive development in infant monkeys. *Vision Res, 39*(8), 1415-1435. doi:https://doi.org/10.1016/S0042-6989(98)00229-6

Song, Y. Y., Wang, H., Wang, B. S., Qi, H., Rong, Z. X., & Chen, H. Z. (2011). Atropine in ameliorating the progression of myopia in children with mild to moderate myopia: a meta-analysis of controlled clinical trials. *J Ocul Pharmacol Ther, 27*(4), 361-368. doi:10.1089/jop.2011.0017

Sridhar, S., Landis, E., Hutson, L., & Pardue, M. (2020). Electroretinogram (ERG) recordings unaltered in mice with form deprivation myopia. *Invest Ophthalmol Vis Sci, 61*(7), 3409-3409.

Stacy, R. C., Demas, J., Burgess, R. W., Sanes, J. R., & Wong, R. O. L. (2005). Disruption and Recovery of Patterned Retinal Activity in the Absence of Acetylcholine. *The Journal of Neuroscience, 25*(41), 9347. doi:10.1523/JNEUROSCI.1800-05.2005

Stasheff, S. F., Shankar, M., & Andrews, M. P. (2011a). Developmental time course distinguishes changes in spontaneous and light-evoked retinal ganglion cell activity in rd1 and rd10 mice. *J Neurophysiol, 105*(6), 3002-3009. doi:10.1152/jn.00704.2010

Stasheff, S. F., Shankar, M., & Andrews, M. P. (2011b). Developmental time course distinguishes changes in spontaneous and light-evoked retinal ganglion cell activity in rd1 and rd10 mice. *J Neurophysiol, 105*(6), 3002-3009. doi:10.1152/jn.00704.2010

Stone, R. A., Laties, A. M., Raviola, E., & Wiesel, T. N. (1988). Increase in retinal vasoactive intestinal polypeptide after eyelid fusion in primates. *Proc Natl Acad Sci U S A, 85*(1), 257-260. doi:10.1073/pnas.85.1.257

Stone, R. A., Lin, T., Laties, A. M., & Iuvone, P. M. (1989). Retinal dopamine and form-deprivation myopia. *Proceedings of the National Academy of Sciences of the United States of America, 86*(2), 704-706. doi:10.1073/pnas.86.2.704

Stone, R. A., Liu, J., Sugimoto, R., Capehart, C., Zhu, X., & Pendrak, K. (2003). GABA, Experimental Myopia, and Ocular Growth in Chick. *Invest Ophthalmol Vis Sci, 44*(9), 3933-3946. doi:10.1167/iovs.02-0774

Strang, C. E., Renna, J. M., Amthor, F. R., & Keyser, K. T. (2010). Muscarinic acetylcholine receptor localization and activation effects on ganglion response properties. *Invest Ophthalmol Vis Sci, 51*(5), 2778-2789. doi:10.1167/iovs.09-4771

Sucher, N. J., Lipton, S. A., & Dreyer, E. B. (1997). Molecular basis of glutamate toxicity in retinal ganglion cells. *Vision Res, 37*(24), 3483-3493. doi:https://doi.org/10.1016/S0042-6989(97)00047-3

Sun, W., Li, N., & He, S. (2002). Large-scale morophological survey of rat retinal ganglion cells. *Vis Neurosci, 19*(4), 483-493. doi:10.1017/s0952523802194107

Takeuchi, H., & Suzumura, A. (2014). Gap junctions and hemichannels composed of connexins: potential therapeutic targets for neurodegenerative diseases. *Front Cell Neurosci, 8*, 189. doi:10.3389/fncel.2014.00189

Tan, Q., Ng, A. L., Choy, B. N., Cheng, G. P., Woo, V. C., & Cho, P. (2020). One-year results of 0.01% atropine with orthokeratology (AOK) study: a randomised clinical trial. *Ophthalmic Physiol Opt, 40*(5), 557-566. doi:10.1111/opo.12722

Tao, X., Sabharwal, J., Seilheimer, R. L., Wu, S. M., & Frankfort, B. J. (2019). Mild Intraocular Pressure Elevation in Mice Reveals Distinct Retinal Ganglion Cell Functional Thresholds and Pressure-Dependent Properties. *J Neurosci, 39*(10), 1881-1891. doi:10.1523/JNEUROSCI.2085-18.2019

Telias, M., Denlinger, B., Helft, Z., Thornton, C., Beckwith-Cohen, B., & Kramer, R. H. (2019). Retinoic Acid Induces Hyperactivity, and Blocking Its Receptor Unmasks Light Responses and Augments Vision in Retinal Degeneration. *Neuron, 102*(3), 574-586.e575. doi:10.1016/j.neuron.2019.02.015

Tengölics, Á. J., Szarka, G., Ganczer, A., Szabó-Meleg, E., Nyitrai, M., Kovács-Öller, T., & Völgyi,

B. (2019). Response Latency Tuning by Retinal Circuits Modulates Signal Efficiency. *Scientific Reports, 9*(1), 15110. doi:10.1038/s41598-019-51756-y

Thibos, L. N., & Werblin, F. S. (1978). The properties of surround antagonism elicited by spinning windmill patterns in the mudpuppy retina. *The Journal of Physiology, 278*, 101-116. doi:10.1113/jphysiol.1978.sp012295

Tian, N. (2011). Developmental mechanisms that regulate retinal ganglion cell dendritic morphology. *Dev Neurobiol, 71*(12), 1297-1309. doi:10.1002/dneu.20900

Tikidji-Hamburyan, A., Reinhard, K., Seitter, H., Hovhannisyan, A., Procyk, C. A., Allen, A. E., . . . Münch, T. A. (2015). Retinal output changes qualitatively with every change in ambient illuminance. *Nat Neurosci, 18*(1), 66-74. doi:10.1038/nn.3891

Toychiev, A. H., Ivanova, E., Yee, C. W., & Sagdullaev, B. T. (2013). Block of gap junctions eliminates aberrant activity and restores light responses during retinal degeneration. *The Journal of neuroscience : the official journal of the Society for Neuroscience, 33*(35), 13972-13977. doi:10.1523/JNEUROSCI.2399-13.2013

Travis, A. M., Heflin, S. J., Hirano, A. A., Brecha, N. C., & Arshavsky, V. Y. (2018). Dopamine-Dependent Sensitization of Rod Bipolar Cells by GABA Is Conveyed through Wide-Field Amacrine Cells. *The Journal of Neuroscience, 38*(3), 723. doi:10.1523/JNEUROSCI.1994-17.2017

Troilo, D., Gottlieb, M. D., & Wallman, J. (1987). Visual deprivation causes myopia in chicks with optic nerve section. *Curr Eye Res, 6*(8), 993-999. doi:10.3109/02713688709034870

Tse, D. Y., & To, C.-h. (2011). Graded Competing Regional Myopic and Hyperopic Defocus Produce Summated Emmetropization Set Points in Chick. *Invest Ophthalmol Vis Sci, 52*(11), 8056-8062. doi:10.1167/iovs.10-5207

Turner, A. J., Vander Wall, R., Gupta, V., Klistorner, A., & Graham, S. L. (2017). DBA/2J mouse model for experimental glaucoma: pitfalls and problems. *Clin Exp Ophthalmol, 45*(9), 911-922. doi:10.1111/ceo.12992

Upadhyay, A., & Beuerman, R. W. (2020). Biological Mechanisms of Atropine Control of Myopia. *Eye & contact lens, 46*(3), 129-135. doi:10.1097/ICL.0000000000000677

Usrey, W. M., & Reid, R. C. (1999). SYNCHRONOUS ACTIVITY IN THE VISUAL SYSTEM. *Annual Review of Physiology, 61*(1), 435-456. doi:10.1146/annurev.physiol.61.1.435

van Wyk, M., Wässle, H., & Taylor, W. R. (2009). Receptive field properties of ON- and OFF-ganglion cells in the mouse retina. *Vis Neurosci, 26*(3), 297-308. doi:10.1017/S0952523809990137

Varela, C., Igartua, I., De la Rosa, E. J., & De la Villa, P. (2003). Functional modifications in rod bipolar cells in a mouse model of retinitis pigmentosa. *Vision Res, 43*(8), 879-885. doi:https://doi.org/10.1016/S0042-6989(02)00493-5

Viswanathan, S., Frishman, L. J., & Robson, J. G. (2000). The Uniform Field and Pattern ERG in

Macaques with Experimental Glaucoma: Removal of Spiking Activity. *Invest Ophthalmol Vis Sci, 41*(9), 2797-2810.

Volgyi, B., Abrams, J., Paul, D. L., & Bloomfield, S. A. (2005). Morphology and tracer coupling pattern of alpha ganglion cells in the mouse retina. *J Comp Neurol, 492*(1), 66-77. doi:10.1002/cne.20700

Volgyi, B., Chheda, S., & Bloomfield, S. A. (2009). Tracer coupling patterns of the ganglion cell subtypes in the mouse retina. *J Comp Neurol, 512*(5), 664-687. doi:10.1002/cne.21912

Volgyi, B., Pan, F., Paul, D. L., Wang, J. T., Huberman, A. D., & Bloomfield, S. A. (2013). Gap junctions are essential for generating the correlated spike activity of neighboring retinal ganglion cells. *PLoS One, 8*(7), e69426. doi:10.1371/journal.pone.0069426

Wainger, B. J., Kiskinis, E., Mellin, C., Wiskow, O., Han, S. S., Sandoe, J., . . . Woolf, C. J. (2014). Intrinsic membrane hyperexcitability of amyotrophic lateral sclerosis patient-derived motor neurons. *Cell Rep, 7*(1), 1-11. doi:10.1016/j.celrep.2014.03.019

Wang, J., Jacoby, R., & Wu, S. M. (2016). Physiological and morphological characterization of ganglion cells in the salamander retina. *Vision Res, 119*, 60-72. doi:10.1016/j.visres.2015.12.007

Wang, K., Xiao, J., Peng, B., Xing, F., So, K. F., Tipoe, G. L., & Lin, B. (2014). Retinal structure and function preservation by polysaccharides of wolfberry in a mouse model of retinal degeneration. *Sci Rep, 4*, 7601. doi:10.1038/srep07601

Wang, L. Z., Syn, N., Li, S., Barathi, V. A., Tong, L., Neo, J., . . . Zhou, L. (2019). The penetration and distribution of topical atropine in animal ocular tissues. *Acta Ophthalmologica, 97*(2), e238-e247. doi:https://doi.org/10.1111/aos.13889

Wang, P., & Slaughter, M. M. (2005). Effects of GABA receptor antagonists on retinal glycine receptors and on homomeric glycine receptor alpha subunits. *J Neurophysiol, 93*(6), 3120-3126. doi:10.1152/jn.01228.2004

Wang, Q., Banerjee, S., So, C., Qiu, C., Lam, H. C., Tse, D., . . . Pan, F. (2020). Unmasking inhibition prolongs neuronal function in retinal degeneration mouse model. *FASEB J, 34*(11), 15282-15299. doi:10.1096/fj.202001315RR

Ward, N. J., Ho, K. W., Lambert, W. S., Weitlauf, C., & Calkins, D. J. (2014). Absence of transient receptor potential vanilloid-1 accelerates stress-induced axonopathy in the optic projection. *J Neurosci, 34*(9), 3161-3170. doi:10.1523/JNEUROSCI.4089-13.2014

Wässle, H., Heinze, L., Ivanova, E., Majumdar, S., Weiss, J., Harvey, R. J., & Haverkamp, S. (2009). Glycinergic transmission in the Mammalian retina. *Frontiers in molecular neuroscience, 2*, 6-6. doi:10.3389/neuro.02.006.2009

Weinreb, R. N., Aung, T., & Medeiros, F. A. (2014). The pathophysiology and treatment of glaucoma: a review. *Jama, 311*(18), 1901-1911. doi:10.1001/jama.2014.3192

Weng, S., Sun, W., & He, S. (2005). Identification of ON-OFF direction-selective ganglion cells in the mouse retina. *J Physiol, 562*(Pt 3), 915-923. doi:10.1113/jphysiol.2004.076695

Wildsoet, C. (2003). Neural pathways subserving negative lens-induced emmetropization in chicks--insights from selective lesions of the optic nerve and ciliary nerve. *Curr Eye Res, 27*(6), 371-385. doi:10.1076/ceyr.27.6.371.18188

Witkovsky, P. (2004). Dopamine and retinal function. *Documenta ophthalmologica, 108*(1), 17-39. doi:10.1023/B:DOOP.0000019487.88486.0a

Wu, P.-C., Chuang, M.-N., Choi, J., Chen, H., Wu, G., Ohno-Matsui, K., . . . Cheung, C. M. G. (2019). Update in myopia and treatment strategy of atropine use in myopia control. *Eye (Lond), 33*(1), 3-13. doi:10.1038/s41433-018-0139-7

Wu, S. M. (2010). Synaptic organization of the vertebrate retina: general principles and species-specific variations: the Friedenwald lecture. *Invest Ophthalmol Vis Sci, 51*(3), 1263-1274. doi:10.1167/iovs.09-4396

Xu, M.-y., & Wong, A. H. C. (2018). GABAergic inhibitory neurons as therapeutic targets for cognitive impairment in schizophrenia. *Acta Pharmacologica Sinica, 39*(5), 733-753. doi:10.1038/aps.2017.172

Xue, M., Atallah, B. V., & Scanziani, M. (2014). Equalizing excitation–inhibition ratios across visual cortical neurons. *Nature, 511*(7511), 596-600. doi:10.1038/nature13321

Yan, W., Laboulaye, M. A., Tran, N. M., Whitney, I. E., Benhar, I., & Sanes, J. R. (2020). Mouse Retinal Cell Atlas: Molecular Identification of over Sixty Amacrine Cell Types. *The Journal of neuroscience : the official journal of the Society for Neuroscience, 40*(27), 5177-5195. doi:10.1523/JNEUROSCI.0471-20.2020

Yang, X. L. (2004). Characterization of receptors for glutamate and GABA in retinal neurons. *Prog Neurobiol, 73*(2), 127-150. doi:10.1016/j.pneurobio.2004.04.002

Yazulla, S., Studholme, K. M., & Pinto, L. H. (1997). Differences in the retinal GABA system among control, spastic mutant and retinal degeneration mutant mice. *Vision Res, 37*(24), 3471-3482. doi:https://doi.org/10.1016/S0042-6989(96)00223-4

Zeck, G. M., & Masland, R. H. (2007). Spike train signatures of retinal ganglion cell types. *Eur J Neurosci, 26*(2), 367-380. doi:10.1111/j.1460-9568.2007.05670.x

Zhang, D.-Q., Stone, J. F., Zhou, T., Ohta, H., & McMahon, D. G. (2004). Characterization of genetically labeled catecholamine neurons in the mouse retina. *Neuroreport, 15*(11), 1761-1765. doi:10.1097/01.wnr.0000135699.75775.41

Zhang, D.-Q., Zhou, T.-R., & McMahon, D. G. (2007). Functional Heterogeneity of Retinal Dopaminergic Neurons Underlying Their Multiple Roles in Vision. *The Journal of Neuroscience, 27*(3), 692. doi:10.1523/JNEUROSCI.4478-06.2007

Zhou, X., Pardue, M. T., Iuvone, P. M., & Qu, J. (2017). Dopamine signaling and myopia development: What are the key challenges. *Progress in retinal and eye research, 61*, 60-71. doi:10.1016/j.preteyeres.2017.06.003